UNIVERSITY OF CALIFORNIA, SAN DIEGO

Flame spread Analysis using a Variable B-Number

A dissertation submitted in partial satisfaction of the

requirements for the degree Doctor of Philosophy

in

Engineering Sciences (Mechanical Engineering)

by

Ali S. Rangwala

Committee in charge:

Professor Steven Buckley G., Chair
Professor Massimo Franceschetti
Professor Alex Groisman
Professor Kalyanasundaram Seshadri
Professor Forman A.Williams

2006

The dissertation of Ali S. Rangwala is approved, and it is acceptable in quality and form for publication on microfilm:

_____

_____

_____

_____

_____

Chair

University of California, San Diego

2006

TABLE OF CONTENTS

LIST OF FIGURES

LIST OF TABLES

NOMENCLATURE

A	=	An integral constant
A_{free}, A_{forced}	=	Integral constants based on natural / forced convection
B	=	Mass-transfer number, Spalding B-number
C	=	A constant
C_p	=	Specific heat at constant pressure (J / gK)
D	=	Diffusivity (cm^2 / s)
d	=	Solid fuel width (cm)
E	=	Activation energy (J / mol)
R	=	Universal gas constant ($J / mol\ K$)
F_e	=	Excess fuel fraction
g	=	Acceleration due to gravity (cm / s^2)
h_{vap}	=	$\int_{T_\infty}^{T_{vap}} C_p dT$ (Energy needed to raise temperature of fuel from ambient to its vaporization temperature) (J / g)
F	=	Mixture fraction
L	=	Latent heat of vaporization (J / g)
ΔH_p	=	Heat of gasification ($L + C_p(T_{ig} - T_\infty)$) ($J / g$)
$\dot{M}'$	=	Effective burning rate, taking lateral diffusion into account ($g / cm\ s$)
$\dot{M}_z'$	=	Lateral diffusion fuel loss ($g / cm\ s$)

$\dot{M}_f'$	=	Rate of fuel vaporization ($g / cm\,s$)
$\dot{m}_F''$	=	Mass burning rate per unit area ($g / cm^2 s$)
$\dot{m}_i'''$	=	Mass of species *i* generated per unit volume per unit time ($g / cm^3 s$)
Q	=	Losses at the fuel surface (J / g)
$\dot{Q}'$	=	Rate of heat release per unit width ($J / m - s$)
$\dot{q}_{s,c}''$	=	In-depth conduction ($J / gm^2 s$)
$\dot{q}_{s,r}''$	=	Surface re-radiation ($J / gm^2 s$)
$\dot{q}_{f,r}''$	=	Radiative feedback from the flame ($J / gm^2 s$)
r	=	$\frac{Y_{O,\infty}}{\upsilon_s}$ where υ_s = oxygen-fuel stoichiometric ratio
T	=	Temperature (*K*)
T_{ig}	=	Pyrolysis temperature of the solid fuel (*K*)
u	=	Velocity (Streamwise direction or X-axis) (*cm/s*)
V_Z	=	Diffusion velocity in the Z-direction (*cm/s*)
x_p	=	Pyrolysis length (length of fuel that's gasifying at a given instant of time) (*cm*)
x_f	=	Flame length (*cm*)
Y_i	=	Mass fraction

Greek symbols

η	=	Similarity variable
ν	=	Kinematic viscosity (cm^2/s)
ρ	=	Density (g/cm^3)
f	=	Function obtained when the momentum equation is transformed using boundary layer analysis
τ	=	$\frac{h_{vap}}{L}$
χ	=	Fraction of flame radiation that does not impinge on the fuel surface
y_f	=	Flame standoff distance (cm)
δ_D	=	Diffusion thickness (cm)

Subscripts

s	=	Solid
∞	=	Ambient
f	=	Flame
w	=	Wall

ACKNOWLEDGEMENTS

I have been very fortunate to learn about Combustion and Fire from wonderful teachers like Steven Buckley, Jose Torero, and James Quintiere. My deepest appreciation goes to my advisor, Steven Buckley. He has been my "beacon of hope" by giving me constant encouragement during the course of my Ph.D.

I would like to thank my committee members, especially Forman Williams and Kalyanasundaram Seshadri, for many helpful discussions and valuable feedback that has helped shape my dissertation. I also thank Professors Carlos Fernandez Pello at UC Berkeley and Joe Goddard at UC San Diego for their expert comments.

I thank Timothy Myers and Harri Kytomaa at Exponent for helping me through and beyond my internship.

I am grateful to the University of Maryland, College Park, the University of California, San Diego, and NASA that have funded my stint in grad school. I also thank Gary Ruff and Fletcher Miller at NASA for providing insightful discussions.

I thank my friends who helped me preserve my sanity – Purba Mukerji, the Pithoo gang, Rajeev Balasubramonian (Da Ronz) and Deepti, Pushkar Khair – my classmates at UCSD – Anish Karandikar, Gregg Lithgow, Zuhair Ibrahim, Reza Gharavi, Francesco Ferioli, Priyank Saxena, Gonzalo Del Alamo, Diogo Bolster, Alex Telengator, presentation gurus – Craig Wildman, Melanie Zauscher, Morris Flynn, software guru – Satya Mallick, Microsoft Word guru – Nancy Bastian … Himanshu Bal, Pratik Mukhopadhyay, Oliver Dalmer, Yi Wang, Aditya Jagannatham…and Sachin Talathi, for being a perfect roommate.

The experiments performed in this work would not have been possible without the help of my undergraduate team – Vanty Do, David Hoffman, Tyler Mayer, Annie Monkowski, Anthony Nguyen, Freddy Plascensia, Rick Sozzi, Nick Statom, Jeff Yin, and Conan Zhang. I also thank Bruce Thomas for help in building my experimental apparatus.

I am grateful to my family for their support in all my endeavors. Their love and encouragement has been instrumental in my success at every level.

The text of Chapter 5, has partially included the following publication: "Upward Flame spread on Vertically-Oriented Fuel Surface: The Effect of Finite Width," *Proc. Combust. Instit.* (Accepted for publication), A. S. Rangwala, S. G. Buckley, and J. L. Torero. The dissertation author is the primary researcher in this publication

VITA

	Born, Mumbai, India
2000	B.S. (Electrical Engineering), College of Engineering, Pune, India
2000-2002	M.S. (Fire Protection Engineering), University of Maryland, College Park
2002-2006	Ph.D., University of California, San Diego

PUBLICATIONS

1. A. S. Rangwala, "Mathematical Modeling of Low Ventilation Small Scale Compartment Fires," ***M.S. Thesis***, University of Maryland, College Park (2002).

2. J. G. Quintiere and A. S. Rangwala, "A Theory of Flame Extinction based on Flame Temperature," ***Fire Mat.*** (2003).

3. Y. Utiskul, J. G. Quintiere, A. S. Rangwala, B. A. Ringwelski, K. Wakatsuki and T. Naruse, "Compartment Fire Phenomena under Limited Ventilation," ***Fire Safety J.,*** Volume 40, Issue 4 (2005).

4. J. L. Consalvi, B. Porterie, M. Coutin, L. Audoin, C. Casselman, A. Rangwala, S. G. Buckley, J. L. Torero, "Upward Propagation over PMMA: Theory, Experiment and Numerical Modeling," ***8th International Symposium on Fire Safety Science***, Beijing, China, Sep 18-23 (2005).

5. A. S. Rangwala, S. G. Buckley and J. L. Torero, "Upward Flame spread on Vertically-Oriented Fuel Surface: The Effect of Finite Width," ***Proc Comb. Inst.*** (Accepted).

FIELDS OF STUDY

Major Field: Engineering

Studies in Fire Protection Engineering
Professor James G. Quintiere, University of Maryland, College Park

Studies in Mechanical Engineering and Combustion Science
Professor Steven G. Buckley, University of California, San Diego

ABSTRACT OF THE DISSERTATION

Flame Spread Analysis using a Variable B-Number

by

Ali S. Rangwala

Doctor of Philosophy in Engineering Sciences (Mechanical Engineering)

University of California, San Diego, 2006

Assoc. Professor Steven G. Buckley, Chair

Flame spread over solid materials is commonly described in the literature by a two-dimensional reactive boundary layer solution first formulated by Emmons (1956). In the recent past, experimental measurements associated with material flammability testing (e.g. NASA-STD-6001) are compared with the Emmons solution, as modified by Pagni and Shih, and found in disagreement. In the classical solution the B-number (Spalding mass transfer number) appears as one of the boundary conditions, and has been traditionally assumed a constant for mathematical simplicity. However, experimental results show that the B-number is not a constant, but varies with time and space. A simple modification to the standard measurement procedure is described, which allows calculation of the B-number from the flame stand-off distance. Measurements of flame spread on solid fuels are performed to determine the flame and pyrolysis front spread rates, as a function of time, and the flame stand-off distance as a function of space and time. The classical combustion problem is revisited to model flame spread over a

combustible surface, including three-dimensional effects. An experimentally-obtained B-number, variable in time and space, is used to model flame propagation, showing good agreement with current and previous experimental data obtained from the literature.

Chapter 1

Introduction

1.1 A Brief Description of the Parameters Involved in the Flame Spread Problem

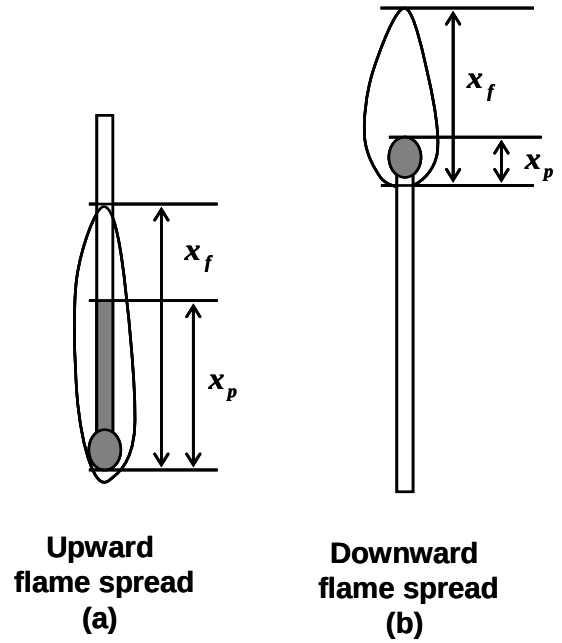

Figure 1.1: Upward and downward flame spread on a matchstick.

The rate of flame spread is determined by the ability of a flame to transfer the heat necessary to pyrolize a solid and to ignite the combustible mixture ahead of it. In concurrent flame spread, the heat transfer and gas-flow is in the direction of the flame propagation and results in a spread process that is generally fast. A simple example is the burning of a matchstick. After ignition the flame on the matchstick burns vigorously when it is held downwards as shown in Figure 1.1 (a). In this position, the flame bathes the unburned wood on its way up, causing more pyrolyzate to evolve with time. When held upwards as shown in Figure 1.1 (b) the matchstick takes a longer time to burn since

the heat from the flame is carried upwards, and only the wood that is very close to the flame tip can ignite.

This simple example is used to explain some of the key parameters involved in the problem that is studied in this work. The flame length, "x_f", is defined as the total length of the visible flame, from its base to the flame tip. "x_p" is the pyrolysis length, which is the length of the solid fuel that is undergoing pyrolysis at a given instant of time, and the flame spread velocity is $\frac{dx_p}{dt}$. The burning rate, $\dot{m}_f''$, is defined as the mass of fuel released per unit area per unit time from the surface. The flame standoff distance $y_f(x)$ is the distance that the flame is located from the surface of the fuel. As explained later, the flame sits at a distance from the fuel surface that depends on the thermodynamic properties of the fuel, the flow field, and ambient conditions. The flame length and standoff distance are measured using video cameras while the pyrolysis length x_p is inferred from the temperature profile at the fuel surface.

A fundamental approach to the flame spread problem is used in this work; a nondimensional number called the B-number (also called the mass transfer number) is used as a measure of the thermodynamic efficiency of the burning process. A methodology is proposed to estimate the B-number using the standoff distance measured in an upward-spreading flame. It is shown that the B-number facilitates a linkage between flammability and material properties that allows measurements at earth-gravity to predict microgravity flame spread.

1.2 General Problem Statement

1.2.1 NASA microgravity tests

The prediction of microgravity flame spread, based on a combination of theory and earth-gravity measurements, is crucial to the design of long-term space vehicles and extra-planetary habitats, and for the prediction of the fire risk in these environments. The necessary flammability requirements for all materials to be used in space vehicles (NASA specifications) are given by a document titled: "Flammability, Odor, Off-gassing, Compatibility Requirements, and Test Procedures for Materials in Environments that Support Combustion" [1]. This document specifies two tests that need to be performed before a material is qualified to be used in a space vehicle: the "Upward Flame Propagation Test" (Test 1) and the "Heat and Visible Smoke Release Rates Test" (Test 2).

The Upward Flame Propagation test is designed with the objective of determining whether, when exposed to a standard ignition source, a material would self-extinguish and not transfer burning debris which could ignite adjacent materials (NASA-NHB 8060.1, 1981). The test is conducted at a worst-case thickness and under a worst-case environment. Under this assumption upward flame spread is considered the worst-case scenario, and material thickness (dependent on the combustible studied) and mounting conditions are chosen to mimic these criteria. The environment oxygen concentration is chosen to meet concentrations found in a spacecraft. No forced-flow is considered and the oxygen entrainment towards the flame is driven by buoyancy alone (NASA-NHB 8060.1 (1981)).

The material to be tested is mounted vertically on a sample holder as shown in Figure 1.2. The material is ignited at the base (the igniter design is discussed in NASA-NHB 8060.1 (1981), and Friedman [2]), and the flame propagation is recorded on a video camera. The passing criteria for this test is *for the flame to self extinguish before the propagation has reached 6 inches (~15 cm), with self-extinction defined as "burned less than 6 inches (~15 cm) when exposed to an ignition source."* Figure 1.2 shows a photograph of a material that has failed this test.

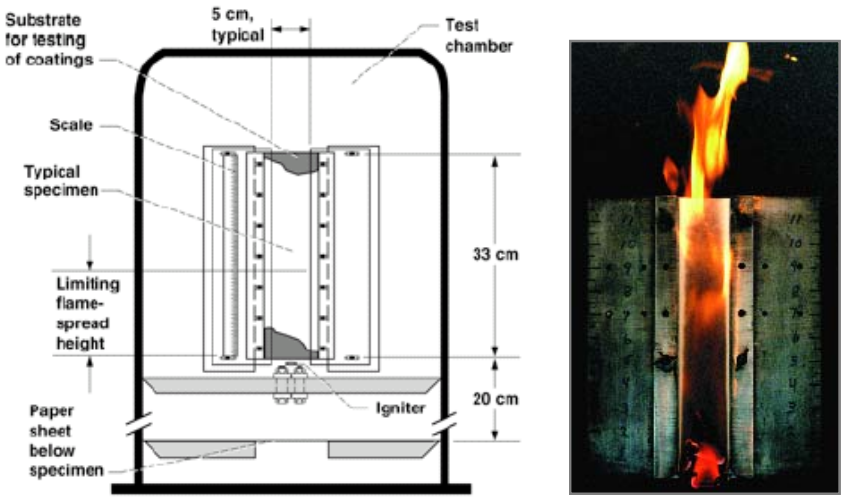

Figure 1.2: Upward flammability test [2]. Picture on the right shows a sample failing the test [77].

The Heat and Visible Smoke Release Rates test [2] is designed to provide supplemental information on the flammability of materials that failed to meet the criteria of Test 1. In addition, this test is required for non-metals for which an area greater than 4 ft^2 (0.37 m^2) is exposed to habitable environments (NASA-NHB 8060.1, 1981, Babrouskas and Grayson [3]). An extensive list of the materials that are tested is provided in "Materials Selection List for Space Hardware Systems [4]."

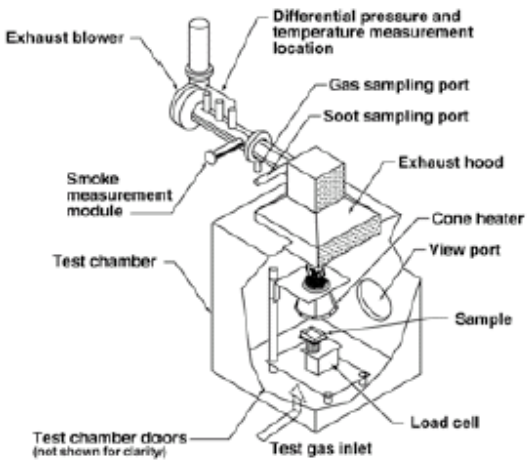

Figure 1.3: Heat and visible smoke release rate test [2].

1.2.2 Deficiences of current tests

The relevance of Test 1 to material flammability for microgravity applications is explored by Ohlemiller and Villa (1991) [5]. Ohlemiller and Villa conducted a series of tests following the protocol of Test 1 with modifications including pre-heating by external radiation and compare the results with tests conducted with the cone calorimeter and the L.I.F.T. (ASTM-E-1321). They find that Test 1 does not address key issues of material flammability, because the video recordings do not provide any quantifiable data that can be obtained from the test.

Additional criticism towards the use of the current methodology is found in microgravity combustion literature (Torero *et al.*, 1997 [6], Rangwala *et al.* [7], [8], [9], [10]). Studies have questioned whether the concept of co-current spread is indeed the worst case scenario (Grayson *et al.*, 1994 [11], Ferkul *et al.* [12] 1993, and Kashiwagi *et al.* 1997 [13]) and reverse flammability rankings (a material flammability ranking based on downward/opposed flow flame spread) are presented [14]. However, the literature also supports the importance of these studies; three factors enhance the hazard and frequency of fire initiation events in both the International Space Station and the projected human

mission to Mars: the length of the missions, the high voltage of on-board power supplies and the greater volume of high temperature scientific instrumentation (Ivanov *et al.*, 1999) [15].

The importane of understanding flammability returns attention to Test 1 and its applicability as a flammability test. Test 1 uses an on/off screening criterion and there is no quantifiable data that connects material flammability to this test. This study develops a methodology of extracting a material flammability-related nondimensional number (B-number) from a test apparatus similar to Test 1, allowing a more meaningful data-recovery from the test apparatus in comparison to the current video recordings. The B-number extracted from this test can then be used in a flame spread model (discussed in Chapter 2) to estimate flame propagation even in complex configurations as well. The B-number can also be used to rank materials based on their propensity to sustain a co-current flame spread. The theoretical background for microgravity flames is based on the work of Emmons (1956) [16] and on the studies by Kosdon *et al.* (1968) [17], Pagni and Shih (1978) [18], and Anamalai and Sibulkin (1979) [19], for vertical natural convection flames.

1.3 Specific Problem Statement

1. Present conservation equations for steady laminar momentum, mass and energy transport. Apply the classical boundary layer assumptions to solve for the flow field, given pyrolysis and combustion of a vertically oriented solid fuel. (Chapter 2)
2. Create a methodology to obtain the B-number from the standoff distance of an upward propagating flame. (Chapter 2)

3. Apply the methodology to study the upward burning of vertically oriented solid fuel. Compare the experimental results with the developed theory. (Chapter 3 and 4)
4. Because experimental results show that the width of the solid fuel plays an important role in flame propagation, study fuel leakage via lateral diffusion. (Chapter 5)
5. Calulate the B-number using the standoff distance measurement in an earth-gravity test, similar to NASA's test 1.Extrapolate the test results to a microgravity environment. (Chapter 6).

Uniqueness:

The following aspects of the current study make it different from the work done previously (a detailed literature review is included in Section 1.4):

1. This work uses the B-number as a function of time to model the rate of propagation of the flame spread ($\frac{dx_p}{dt}$).
2. The B-number is determined using an experimentally-measured standoff distance. Using the standoff distance to measure the B-number circumvents the need to measure the conduction, radiation and re-radiation losses that are difficult to estimate and may change based on the geometry of the sample and the flow configuration.

The present problem is different from the forced-convection flat plate boundary layer problem, since the fluid flow is induced solely by buoyancy forces. The partial differential equations describing the two problems are almost identical; the two specific differences that appear in the present problem are: (a) a buoyancy term must be added to the momentum conservation equation and, (b) the velocity at an infinite distance from the

plate must be set equal to zero. The boundary layer thickness grows as the $1/4^{th}$ power of the distance from the leading edge.

1.4 Previous Related Studies

When a heat source is in contact with a combustible material (liquid or solid), ignition can occur. Once the fuel is ignited, a flame propagates across its surface establishing a diffusion flame over the fuel. The burning of the fuel is due to the transfer of heat from the flame, which provides the necessary heat needed to vaporize the fuel, further feeding the flame. Thus, the study of flame spread on a combustible surface requires an in-depth understanding of *diffusion flames, ignition* and *burning rate theory.* These three areas taken together can provide a fundamental description of the behavior of flame spread on any surface (liquid, solid, liquid soaked solid, and gas). A literature review of flame spread should investigate these three areas as a foundation. The theory of microgravity flame spread is also based on these three fundamental areas. An absence of strong buoyancy-driven convective flow in microgravity causes interesting differences between normal and microgravity flame spread. Therefore, care needs to be taken when extrapolating results from earth gravity tests to environments in space. A fundamental understanding of the key concepts involved in the three mentioned fields is necessary when conducting any earth gravity test meant for testing materials for usage in space.

1.4.1 Diffusion flame, ignition, and burning rate:

An ideal diffusion flame (Burke and Schumann [20]) consists of an infinitesimally thin exothermic reaction-zone which separates the fuel and oxidizer. The flame is called a diffusion flame because oxygen and fuel diffuse towards an infinitesimally thin surface to form a flame. Ideally, a flame exists where fuel and oxygen

meet in stoichiometric proportions. Thus a flame is defined as an infinitesimally thin sheet that is established over the surface of the fuel, where fuel and oxygen are reacting stoichiometrically producing intense heat (flame temperature = 1500 °C – 2000 °C).

Species diffusion, flow, mixing and heat transfer all play an important role in the description of diffusion flames; traditionally laminar or turbulent boundary layer type heat and mass-transfer analysis are used to study such nonpremixed flames [21]. Diffusion flames are homogeneous or heterogeneous. A homogeneous flame has both fuel and oxygen in a gaseous state or both fuel and oxidizer in a solid state, such as a mono or bipropellant rocket. A typical example is the combustion of a jet of natural gas issuing in air. Flames most commonly observed in everyday experience are primarily heterogeneous, where a solid or liquid fuel burns in an oxidizing gaseous atmosphere. Diffusion flames can exist as liquid fuel flames, solid fuel flames or gaseous fuel flames. Liquid fuel flames were first studied by Kinabara (1930-42) [22] where experiments were conducted on eight organic liquids. Further details about flame spread on liquid surfaces are found in the literature in the work in Burgoyne *et al.* [23-25].

The current study involves the study of heterogeneous diffusion flames established on a solid surface. Under the action of a heat flux, the solid melts to a liquid state, which then vaporizes and diffuses upwards. Closer to the surface of the solid, there is a high concentration of fuel vapor, and as one moves away, the concentration decreases. The fuel and air mixture reaches the upper flammable limit, at a certain height above the fuel surface and under the action of a pilot a flame can establish itself over the surface of the fuel. The sustenance of this flame is dependent on the ability of the solid fuel to continue providing fuel vapor.

Depending on the flow established over the solid fuel (forced / natural convection), the flame stabilizes over the fuel surface at a specific distance. This distance is called the "*standoff*" distance, which literally means how far the flame is located above the fuel surface. The current work is based on the measurement of the standoff distance of an upward-spreading flame, and on using this measurement to predict a material related property called the "B-number" or the mass-transfer number. More detail about this concept is presented in upcoming chapters.

Ignition refers to the marked transition of a system from a non-reactive equilibrium state to a self-sustaining reactive state. It plays a critical role in fire growth, where flame spread over a combustible surface is considered as a continuous ignition process, in which the flame serves both as a source of heat that helps heat up the fuel to its pyrolysis temperature and as a ignition pilot. A substantial amount of research has been done on the study of ignition, with reviews by Welker (1970) [26], Kanury (1972-77) [27, 28], Drysdale (1985) [29], and recently by Atreya (1998) [30].

1.4.2 Flame Spread

As mentioned earlier, a combination of the concepts of diffusion flame analysis, ignition, and burning rate theory, comprise the description of the flame spread problem. An abundance of classical papers look into the problem of flame spread in various geometries. Excellent reviews are published by Friedman (1968) [2], Magee and McClavey (1971) [31], Sirignano (1972) [32], Williams (1976) [33], Pello (1983) [34], Drysdale (1985) [29], Wichman (1992) [35], Joulian [36] and most recently by Quintiere [37]. Pioneering work on modeling flame spread includes the work of Emmons [16] and Lees [38] in 1956. Emmons [16] work provides a solution for the burning rate of a

diffusion flame established over a liquid fuel and subject to a forced flow parallel to the surface. He obtains an analytical expression that shows that the local burning rate or mass loss rate varies inversely with the square root of the distance from the leading edge and varies directly with the square root of the air velocity. Due to the simplicity of the closed-form equation, Emmons' classical solution is used widely and provides a starting point for flame propagation studies done later.

A mass-transfer number, or "B-number," which is a property of the pyrolyzing material determines the boundary condition at the fuel surface. The concept of a mass-transfer number is introduced by Spalding [21] in 1950 to develop an expression for the droplet burning-rate as a function of a mass-transfer or "B-number", physically relating the heat release related to combustion (the numerator) to the losses associated with combustion (the denominator) [39].

Emmons utilizes the Shvab-Zeldovich [40] formulation to eliminate the highly non-linear reaction-rate term from the energy and species equations. If the Prandtl number (Pr) equals one, Emmons shows that the momentum equation may be decoupled from the species and energy equation and the solution to the wall-burning rate is simply related to the velocity gradient at the surface, thus requiring only a solution of the momentum equation.

A similar solution for buoyancy-driven flow is obtained by Kosdon, Williams and Buman [17]. They develop a similarity theory for the laminar natural convection boundary-layer along a vertical wall, which considers property variations, mass addition in the boundary layer at the wall, and boundary-layer combustion. Using cellulose cylinders to obtain experimental data it is determined that theory over-predicts the

experimental results by a factor of approximately two. Kosdon *et al.,* neglect radiative heat exchange and justify the discrepancies due to this omission.

Viscosity, specific heat, and conductivity are assumed to be equal to a constant in the analyses discussed so far. Hegde *et al.* [41], question this assumption, where the set of equations developed by Emmons are solved numerically using variable thermodynamic properties (temperature-dependent). An increase of 8% in accuracy is obtained with the use of variable properties, when compared with experimental burning rate values of PMMA in air [42].

Kim, deRis, and Kroesser [43] completed an analysis of the laminar pyrolysis zone of a freely burning fuel surface, similar to that of Kosdon, *et al.* [17]. They solve the conservation equations numerically for a wide variety of fuels. Theoretical predictions of burning-rate agree reasonably well for fuels with low molecular weights, where fuel properties most nearly correspond to the assumption of the variable property model.

The two main disadvantages of the models developed by Emmons [16], Kosdon *et al.* [17] and Kim *et al.* [43], are: (1) they do not include radiation effects, and (2) are limited to the pyrolysis length of the fuel. Thus, they are not effective in solving for the flame height, which usually extends beyond the pyrolysis length. This problem is solved by Pagni and Shih [18] by introducing the concept of "*excess-pyrolyzate*" or the fuel that is not burned within the pyrolysis region; this fuel escapes upstream, forming a combusting plume rather than a boundary layer flame such as that existing within the pyrolysis length. Pagni and Shih [18] solve the problem of laminar free/forced convection burning by basing initial conditions on the pyrolysis zone results and using an integral scheme proposed by Yang *et al.* [44], to solve for the over-fire region (region above the

pyrolysis length). Pagni and Shih's results are confirmed by Annamalai *et al.* [19], [45], who replaced the surface boundary condition by a simplified polynomial fit, similar to the form suggested by Pohlhausen [46]. However, when Annamalai *et al.* [45] plot the experimentally-determined pyrolysis lengths versus the theory there is an overprediction of the data by a factor of almost two. Though Pagni and Shih's solution brings a closure to the problem by formulating a theory predicting flame height with a classical theoretical approach based on the Emmons model, there is still a mismatch between experiment and theory [47], [6].

Most of the flame spread research in the 1980s and 1990s is concentrated on developing *empirical correlations* to model flame spread results. These correlations are based on test data like the Radiant Panel Rate of Flame Spread Test [48]. Other experimental correlations are developed from test data by Saito [49], [50], Delichatsios [51], Quintiere and Harkleroad [52], Kulkarni [53], and many other researchers; additional reviews are given by Joulain [36] and Kulkarni [54].

Given the extensive amount of available data, these correlations work well for most materials that are tested. However, as any engineering fit to experimental data, these correlations rely heavily on test-specific constants, which change with geometry and are dependent on the experimental apparatus used to determine them. Numerical models to predict flame spread rate are developed using the Fire Dynamic Simulator (FDS) code developed by NIST [10, 55] and other codes. However, these 3-dimensional codes rely heavily on empirical constants to model the solid phase. The need to study fire safety in space justifies a return to classical theory, because every material to be used in space in a microgravity environment cannot be tested on earth.

No work has been found in recent literature to substantiate the validity of using empirical correlations, developed using earth-based tests, in a microgravity environment. The absence of gravity creates complications that reduce the validity of empirical constants. Therefore, there is a need to revisit the classical theory with the purpose of examining some of its previously-accepted assumptions.

Numerical evaluation of the assumptions used in the classical boundary layer theory has been carried out by Rouvreau *et al.* [56, 57]. Based on their study, the boundary layer approximation breaks down and separation of the flow occurs at an injection velocity greater than 0.01 m/s. The current study does not apply to this regime. The current research proves that in the range that the classical theory is valid (injection velocity < 0.01 m/s), the reason for overprediction by the theory is due to the improper characterization of the B-number. The previous constant B-number used in calculating flame height is in fact a variable that changes with time and space. This research effort develops an experimental method of calculating a B-number, which in turn is used to model flame spread. The B-number calculated using this approach can then be used to develop a 3-dimensional numerical code that includes a solution of the Navier-Stokes equations and energy equation, with gas-phase combustion and solid-phase pyrolysis. This can give an accurate flame spread model irrespective of geometry, and gravity conditions.

1.4.3 Turbulent wall fires

Although the current study deals with laminar flame propagation alone, this section provides some a view into some of the research done to study turbulent wall fires that may be applicable. For upward flame spread, the boundary layer and the flame are generally laminar for less than 0.2 - 0.4 meter wall heights, and become increasingly turbulent as height is increased [58]. Experimentally, Orloff *et al.* [58] show that the heat transfer from the flame to the solid surface also changes from primarily convective to primarily radiative as flame height increases. Flame radiation is primarily due to soot emission [59], and it is necessary to know the soot volume fraction throughout the flow field in order to predict radiation correctly. This problem becomes more complicated when the flow gets turbulent. Further studies on turbulent flame spread are found in references [51-52], [60-66].

1.4.4 Microgravity-flame spread

Microgravity flames are interesting from the point of view of spacecraft fire safety. Early experiments conducted by Altenkirch *et al.* [67-69], study the effect of varying pressures and gravity levels on downward flame spread. Microgravity, which is the condition of apparent (near) weightlessness, can only be achieved on or near Earth by putting an object in a state of free fall. In this way, NASA conducts microgravity experiments on Earth using drop-facilities, which achieve about 2 - 5 seconds of microgravity. Olson [70] conducted experiments in a drop tower using thin paper sheets and very low opposed-flow velocities. Olson's measurements show that the spread rate first increases and then decreases as opposed flow velocity is increased [70]. Similar experiments carried out by Vedha Nayagam and Altenkirch [67] also show the increase

in flame spread with increasing opposed flow velocities. As explained in greater detail in Chapter 6, gas velocities in microgravity are of the same order of magnitude as diffusion velocities. Flames are always laminar with Reynolds number in the range of 1000-2000. Tarifa *et al.* [71] conducted experiments with PMMA rods and sheets to show that the flame spread rate in microgravity is between the rate of normal-gravity downward and upward spread.

A series of experiments on thin filter paper sheets in microgravity carried out by Bhatacharjee *et al.* [69], [72], [68], [73], and [74], show that the flame structure, together with the gas-phase surface radiation, are key parameters that control flame spread rate. Performed in an opposed-flow configuration, their experiments provide a flammability map for the material studied. A critical fuel thickness [73], above which sustained flame spread is not possible, is established as a result of these experiments. The influence of g-jitter on a boundary-layer diffusion flame has been studied by Torero *et al.* [75].

Recently, a 3-dimensional numerical model is applied to predict flame spread in microgravity by Xi *et al.* [76]; however, there are still no experimental data to validate their model.

1.5 Summary

Flame spread over condensed fuels is an important topic in fire research. There has been a significant amount of research done in this area over the last fifty years. The process of flame spread is dependent on energy, momentum, and species transfer in the region surrounding the flame reaction zone. The next chapter discusses these equations and develops a theory, to be evaluated using an experimental setup similar to NASA's Test 1. The primary goal is to develop a meaningful test methodology, which can ve

more readily applied to evaluation of microgravity flame spread than NASA's current Test 1.

1.6 References

1. NASA, "Flammability, Odor, off gassing, and Compatibility Requirements and Test Procedures for Materials in Environments that Support Combustion," *NASA-NHB 8060.1*, vol. (1981).

2. R. Friedman, "Fire safety in the low gravity spacecraft environment," *Second International Microgravity Combustion Workshop*, NASA Lewis Research Center (1993).

3. V. Babrauskas and S. J. Grayson, *Heat Release in Fires*, Elsevier Applied Science, (1992).

4. MSFC-HDBK-527-REV F, *Materials Selection List for Space Hardware Systems*, (1988).

5. T.J. and Villa Ohlemiller, K.M, "Material Flammability Test Assessment for Space Station Freedom," *National Institute of Standards and Technology, NISTIR-4591*. 1991.

6. J. L. Torero, N. J. Bahr and E. J. Carman, "Assessment of material flammability for microgravity environments," *48th International Astronautical Federation congress*, Turin, Italy (1997).

7. J-L Consalvi, B. Portierie, M. Coutin, L. Audouin, A. S. Rangwala, S. G. Buckley, and J. L. Torero, "Diffusion Flames Upwardly Propagating over PMMA: Theory, Experiment and Numerical Modelling," *Int. Symp. Fire Safety Science*, Beijing, China, IAFSS (2005).

8. A. S. Rangwala, S. G. Buckley, and J. L. Torero, "Modeling and Analysis of the Upward Burning of PMMA," *43 rd AIAA Aerospace Sciences Meeting and Exhibit,* AIAA, Reno, NV (2005).

9. J. L. Torero, A. S. Rangwala, and S. G. Buckley, "Towards Determination of the B number for Co-Current Flame Spread using the Fire Dynamic Simulator (FDS) code: Comparison between Model and Experiment," *Fall Technical Meeting of the Western States Section of the Combustion Institute*, University of California, Los Angeles (2003).

10. A. S. Rangwala, S. G. Buckley, and J. L. Torero, "Modeling Upward Flame Spread Using a Time Varying B-Number," *WSS/CI*, Boise, Idaho (2006).

11. G. Grayson, K. R. Sacksteder, P. V. Ferkul, and J. S. T'ien, “Flame Spreading over a Thin Solid in Low-speed Concurrent Flow-Drop Tower Experimental Results and Comparison with Theory," *Microgravity Science and Technology*, vol. 7, p. 187-195 (1994).

12. P. V. Ferkul and J. S. T'ien, “A Model of Low-Speed Concurrent Flow Flame Spread Over a Thin Fuel," *Combust. Sci. Tech.*, vol. 99, p. 345-370 (1994).

13. T. Kashiwagi, W. E. Mell, K. McGrattan, H. R. Baum, S. L. Olson, O. Fujita, M. Kikuchi, and K. Ito, "Ignition, Transition, Flame Spread in Multidimensional Configurations in Microgravity," *Fourth International Microgravity Combustion Workshop*, NASA Lewis Research Center (1997).

14. J. S. T'ien, "The Possibility of a Reversal of Material Flammability Ranking from Normal Gravity to Microgravity," *Combust. Flame*, vol. 80, p. 353-357 (1990).

15. A. V. Ivanov, V. Ye. Balashov, T. V. Andreeva, and A. S. Melikhov, *Experimental Verification of Material Flammability in Space,* NASA/CR-1999-209405 (1999).

16. H. Emmons, "The Film Combustion of Liquid Fuel," *Z. angew. Math. Mech*, vol. 36, p. 60 -7 (1956).

17. F. J. Kosdon, F. A. Williams, and C. Buman, "Combustion of Vertical Cellulosic Cylinders in Air," *Proc. Combust. Instit.*, vol. 12, p. 252-264 (1969).

18. P. J. Pagni and T. M. Shih, "Excess Pyrolyzate," *Proc. Combust. Instit.*, vol. 16, p. 1329-1343 (1978).

19. K. Annamalai and M. Sibulkin, "Flame Spread Over Combustible Surfaces for Laminar Flow Systems. Part 1: Excess Fuel and Heat Flux," *Combust. Sci. Tech.*, vol. 19, p. 167-183 (1979).

20. S. P. Burke and T. E. Schumann, "Diffusion flames," *Proc. Combust. Instit.*, vol. 1, p. 2 - 11 (1928).

21. D. B. Spalding, "Combustion of Liquid Fuel in Gas Stream," *Fuel*, vol.29, p. 2-7 (1950).

22. T. Kinbara, *Scientific Papers, Inst. Phys. Chem. Res. Japan*, vol.16, p. 91 (1931).

23. J. H. Burgoyne, A. F. Roberts, and P. G. Quinton, "The Spread of Flame across a Liquid Surface 1 - the Induction Period," *Proc Roy. Soc. A.*, vol. 308, p. 39-53 (1968).

24. J. H. Burgoyne and A. F. Roberts, "The Spread of Flame across Liquid Surface – Steady 2 -State Conditions," *Proc Roy. Soc. A.*, vol. 308, p. 55 - 68 (1968).

25. J. H. Burgoyne and A. F. Roberts, "The Spread of Flame across a Liquid Surface 3 - A Theoretical Model," *Proc Roy. Soc. A.*, vol.308, p. 69-79 (1968).

26. J. R. Hallman, J. R. Welker, and C. M. Sliepcevich, "Polymer Surface Reflectance-Absorptance Characteristics," *Polymer Engineering & Science*, vol. 14, p. 717-723 (1974).

27. A. Murty Kanury, "Ignition of Cellulosic Solids - A Review," *Fire Research Abstracts and Reviews*, vol. 14, p. 24-52 (1972).

28. A. Murty Kanury, "Ignition of Cellulosic Solids: Minimum Pyrolyzate Mass Flux Criterion," *Combust. Sci. Tech.*, vol. 16, p. 89 (1977).

29. D. Drysdale, *An Introduction to Fire Dynamics,* John Wiley & Sons (1999).

30. A. Atreya, "Ignition of Fires," *Phil. Trans. R. Soc. Lond. A*, vol. 356, p. 2873-2813 (1998).

31. F. A. Lastrina, R. S Magee, and R. F. Mc Alevy, "Flame Spread Over Fuel Beds: Solid Phase Energy Considerations," *Proc. Combust. Instit.*, vol. 13, p. 935 (1971).

32. W. A. Sirignano, "A Critical Discussion of Theories of Flame Spread Across Solid Fuel and Liquid Fuels," *Combust. Sci. Tech.*, vol. 6, p. 95 - 105 (1972).

33. F. A. Williams, "Mechanisms of Fire Spread," *Proc. Combust. Instit.*, vol. 16, p. 1281-1293 (1976).

34. A. C. Fernandez-Pello and Hirano, "Controlling Mechanisms of Flame Spread," *Combust. Sci. Tech.*, vol. 32, p. 1-31 (1983).

35. I. S. Wichman, *Prog. Energy Combust. Sci.*, vol.18, p. 553 (1992).

36. Pierre Joulian, "Convective and Radiative Transport in Pool and Wall Fires: 20 Years of Research in Poitiers," *Fire Safety J.*, vol.26, p. 99-149 (1996).

37. J. G. Quintiere, *Fundamentals of Fire Phenomena (in press)*, John Wiley and Sons (2006).

38. L. Lees, "Laminar Heat Transfer over Blunt Nosed Bodies at Hypersonic Flight Speeds," *Jet Propulsion.*, vol. 26, p. 259-269 (1956).

39. A. Murty Kanury, *An Introduction to Combustion Phenomena*, Gordon & Breach Science Publishers, Inc (1977).

40. F. A. Williams, *Combustion Theory*, Addison-Wesley (1965).

41. P. J. Paul, M. Hegde, and H. S. Mukunda, "Free Convective Combustion with Variable Properties," *Proc. Combust. Instit.*, vol. 21, p. 33-43 (1986).

42. K. A. Murthy, J. De Ris, and M. C. Yuen, *Proc. Combust. Instit.*, vol. 14 (1973).

43. J.S. Kim, J. De Ris, and F. William Kroesser, "Laminar Free-Convective Burning of Fuel Surfaces," *Proc. Combust. Instit.*, vol. 13, p. 949-960 (1971).

44. K. T. Yang, "Laminar Free Convective Wake Above a Heated Vertical Plate," *ASME Trans. Series E. J. of App. Mech.*, vol. 86, p. 131-138 (1964).

45. K. Annamalai and M. Sibulkin, "Flame Spread Over Combustible Surfaces for Laminar Flow Systems. Part 2: Flame Heights and Fire Spread Rates.," *Combust. Sci. Tech.*, vol. 19, p. 185-193 (1979).

46. K. Pohlhausen, *Z. angew. Math. Mech*, vol. 1, p. 252 (1921).

47. A. C. Fernandez Pello, "A Theoretical Model for the Upward Laminar Spread of Flames over Vertical Fuel Surfaces," *Combust. Flame*, vol. 31, p. 135-148 (1978).

48. J. G. Quintiere, "A Simplified Theory for Generalizing Results from a Radiant Panel Rate of Flame Spread Apparattus," *Fire and Materials*, vol. 5, (1981).

49. J. G. Quintiere, K. Saito, and F. A. Williams, "Upward Turbulent Flame Spread," *Fire Safety Science- Proceedings of the First International Symposium*, vol. 1, p. 75 (1986).

50. F. A Williams, I. S. Wichman, K. Saito, and J. G. Quintiere, "Upward Turbulent Flame Spread on Wood under External Radiation," *J. Heat Transfer*, vol. 111 (1989).

51. M. M. Delichatsios and M. A. Delichatsios, "Effects of Transient Pyrolysis on Wind-Assisted and Upward Flame Spread," *Combust. Flame*, vol. 89, p. 5-16 (1992).

52. J. Quintiere, M. Harkleroad, and Y. Hasemi, "Wall Fires and Implications for Upward Flame Spread," *AIAA*, vol. 85, p. 0456 (1985).

53. A. K. Kulkarni and M. Sibulkin, "Burning Rate Measurements on Vertical Fuel Surfaces," *Combust. Flame*, vol. 44, p. 185-186 (1982).

54. E. G. Brehob, C. I. Kim, and A. K. Kulkarni, “Numerical Model of Upward Flame Spread on Practical Wall Materials,” *Fire Safety J.*, vol. 36, p. 225-240 (2001).

55. K. B. McGrattan, *Fire Dynamics Simulator (Version 4): Users Guide*, NIST SP 1019, NIST Special Publication (2004).

56. S. Rouvreau, P. Cordeiro P., P. Joulain, H. Y. Wang, and J. L. Torero, “Numerical Evaluation of the Influence of Fuel Generation on the Geometry of a Diffusion Flame: Implications to Microgravity Fire Safety,” *International Symposium on Fire Safety Science*, vol. (2002).

57. S. Rouvreau, P. Joulain, H. Y. Wang, P. Cordeiro, and J. L. Torero, "Numerical Evaluation of Boundary Layer Assumptions Used for the Prediction of the Standoff Distance of a Laminar Diffusion Flame," *Proc. Combust. Instit.*, vol. 29, p. 2257 -2534 (2002).

58. L. Orloff, J. De Ris, and G. H. Markstein, "Upward Turbulent Fire Spread and Burning of Fuel Surface," *Proc. Combust. Instit.*, vol. 15, p. 183-192 (1974).

59. J. de Ris, "Fire Radiation- A Review," *Proc. Combust. Instit.*, vol. 17 (1979).

60. O. A. Plumb and L. A. Kennedy, "Prediction of Buoyancy Controlled Turbulent Wall Diffusion Flames," *Proc. Combust. Instit.*, vol. 16, p. 1699 - 1707 (1976).

61. F. Tamanini, "A Numerical Model for the Prediction of Radiation Contolled Turbulent Wall Fires," *Proc. Combust. Instit.*, vol. 17, p. 1075 - 1085 (1979).

62. J. West, L. Tang, R. A. Altenkirch, S. Bhattacharjee, K. Sacksteder, and M. A, Delichatsios, "Quiescent Flame Spread over Thick Fuels in Microgravity," *Proc. Combust. Instit.*, vol. 26, p. 1335-1343 (1996).

63. M. O. Annarumma, J. M. Most, and P. Joulain, "On the Numerical Modeling of Buoyancy-Dominated Turbulent Vertical Diffusion Flames," *Combust. Flame*, vol. 85, p. 403-415 (1991).

64. T. Ahmad, and G. M. Faeth, “Turbulent Wall Fires,” *Proc. Combust. Instit.*, vol. 17, p. 1149 -1160 (1979).

65. Y. Hasemi and M. Yoshida, *Third Fire Safety Conference*, Edinborough, Scotland (1991).

66. M. A. Delichatsios, *Comb. Sci. and Tech*, vol.39, p. 195-214 (1984).

67. M. Vedha-Nayagam and Robert A. Altenkirch, “Gravitational Effects on Flames Spreading over Thick Solid Surfaces,” *Acta Astronautica*, vol.12, p. 565-572 (1985).

68. D. B. Bullard, L. Tang, R. A. Altenkirch, and S. Bhattacharjee, "Unsteady flame spread over solid fuels in microgravity," *Advances in Space Research*, vol.13, p. 171-184 (1993).

69. S. Bhattacharjee and R. A. Altenkirch, “The effect of surface radiation on flame spread in a quiescent, microgravity environment,” *Combust. Flame*, vol.84, p. 160-169 (1991).

70. S. L. Olson, Fujita, O., Kikuchi, M. and Ito, K. "Ignition,Transition, Flame Spread in Multidimensional Configurations in Microgravity." *Fourth International Microgravity Combustion Workshop*. 1997. NASA Lewis Research Center.

71. C. Sanchez-Tarifa, G. Corchero, and G. L. Juste, "An Experimental Programme on Flame Spreading at Reduced Gravity Conditions," *Microgravity Science and Tech.*, vol. 1, p. 1 (1988).

72. A. R. Alternkirch, S. Bhattacharjee, N. Srikantaiah, and M. Vedhanayagam, "A Theoretical Description of Flame Spreading over Solid Combustibles in Quiescent Environment at Zero Gravity," *Combustion Sci and Tech.*, vol. 69, p. 1-15 (1990).

73. S. Bhattacharjee, K. Wakai, and S. Takahashi, "Predictions of a Critical Fuel Thickness for Flame Extinction in a Quiescent Microgravity Environment," *Combust. Flame*, vol.132, p. 523-532 (2003).

74. S. Bhattacharjee, R. Ayala, K. Wakai, and S. Takahashi, "Opposed-Flow Flame Spread in Microgravity-Theoretical Prediction of Spread Rate and Flammability Map," *Proc. Comb. Instit.*, vol. 30, p. 2279-2286 (2005).

75. S. Rouvreau, P. Cordeiro, J. L. Torero, and P. Joulain, "Influence of g-jitter on a Laminar Boundary Layer Type Diffusion Flame," *Proc. Comb. Instit.*, vol.30, p. 519-526 (2005).

76. J. Xi and F. Weicheng, "Numerical Prediction of Flame Spread over Solid Combustibles in a Microgravity Environment," *Fire Safety J.*, vol. 24, p. 279-298 (1995).

77. C. D. Engel, *Private Communication*, Qualis Corp, (2005).

Chapter 2

Relationship between the Standoff Distance and the B-number (Theory)

2.1 Introduction

The standoff distance of an upward-spreading flame measured as a function of time is used to calculate the B-number. The method is similar to that outlined by Torero *et al.* [1], where results in a microgravity environment with a forced-flow are discussed. The current work, however, is based on a freely-flowing buoyant convective field in normal earth-gravity. Previous work by, Kanury [2], Orloff *et al.* [3], and Annamalai *et al.* [4], attempts to characterize material flammability with the B-number, first introduced by Spalding [5] in 1950 to characterize liquid fuel droplet burning. However, this work differs from the previous work reported in the literature, in the way the B-number is estimated. The B-number is traditionally calculated from material properties, ΔH_C (heat of combustion, kJ/g), L (latent heat of vaporization, kJ/g), and T_p (pyrolysis temperature K), which are measured using a cone-calorimeter. The current methodology measures the B-number experimentally, using the standoff distance y_f (cm) of the flame.

The linkage between the standoff distance and the B-number is obtained from an analysis of a vertical wall burning under natural-convection. Figure 2.1 shows a schematic of a model experiment representing a developing wall fire. The solid fuel is pyrolyzing in the region x_p, and flame height is given by x_f. Fuel vapors are released from the surface to feed the flame, which is confined to the buoyancy-induced boundary layer. The region $x_f - x_p$, where the flame extends beyond the pyrolysis length, is called the combusting plume region [6], and heat transfer from this region to the fresh fuel

above x_p is responsible for the upward spread of the flame. The purpose of the flame spread model is to model flame height as a function of time based on material properties that are known *a priori*. The mathematical formulation starting from the conservation equations is discussed in the next section.

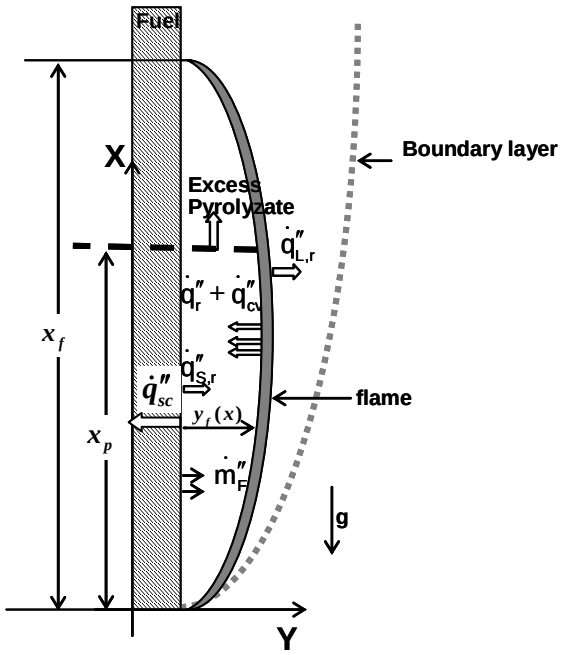

Figure 2.1: Upward-spreading flame model x_f = length of flame, x_p = pyrolysis length, $y_f(x)$ = standoff distance.

2.2 Mathematical Formulation

Figure 2.1 shows a schematic of a model experiment to represent a developing wall fire. The solid fuel is pyrolyzing in the region x_p, and flame height is given by x_f. Fuel vapors are released from the surface and participate in the flame, which is confined to the buoyancy-induced boundary layer. The region $x_f - x_p$, where the flame extends beyond the pyrolysis length, is called the combusting plume region [6], and heat transfer from this region to the virgin fuel above x_p is responsible for the upward spread of the flame.

2.2.1 Conservation equations

The steady-state laminar diffusion flame equations for a variable density boundary layer are [7]:

Continuity:

$$\frac{\partial(\rho u)}{\partial x} + \frac{\partial(\rho v)}{\partial y} = 0\,. \tag{2-1}$$

Momentum along a surface that is vertically oriented:

$$\rho\left(u\frac{\partial u}{\partial x} + v\frac{\partial u}{\partial y}\right) = \frac{\partial}{\partial y}\left(\mu\frac{\partial u}{\partial y}\right) + g(\rho_\infty - \rho)\,. \tag{2-2}$$

Energy:

$$\rho\left(u\frac{\partial h}{\partial x} + v\frac{\partial h}{\partial y}\right) = \frac{\partial}{\partial y}\left(\frac{k}{C_p}\frac{\partial h}{\partial y}\right) + \dot{q}'''\,, \tag{2-3}$$

where the specific enthalpy,

$$h = \int_{T_\infty}^{T} C_p dT\ .$$

Species:

$$\rho\left(u\frac{\partial Y_i}{\partial x} + v\frac{\partial Y_i}{\partial y}\right) = \frac{\partial}{\partial y}\left(\rho D_i\frac{\partial Y_i}{\partial y}\right) + \dot{m}_i'''\,, \tag{2-4}$$

where species 'i' has mass concentration Y_i and volumetric mass generation $\dot{m}_i'''$.

State:

$$\rho T = \rho_\infty T_\infty\,, \tag{2-5}$$

Chemistry:

$$\nu_F\,\mathrm{Fuel} + \nu_o\mathrm{O}_2 \rightarrow \nu_p\,\mathrm{Products} + \Delta\mathrm{H_C}\,. \tag{2-6}$$

The above equations involve the following physical approximations [8]: ideal gas, velocities less than the speed of sound, transport properties $k/\rho C_p$ and ρD independent of composition, Le = 1, no species diffusion driven by pressure and temperature, uniform molecular weights in the equation of state, and a single global chemical reaction. Radiation and viscous dissipation are not included. Gebhart [9] shows that viscous dissipation is negligible under natural convection. The radiation effects are incorporated indirectly, when determining the B-number (discussed in section 2.2.3). The overall stoichiometry relates $\dot{q}'''$ and $\dot{m}_i'''$ as follows:

$$\frac{\dot{q}'''}{\Delta H_C} = \frac{-\dot{m}_F'''}{M_F \nu_F} = \frac{-\dot{m}_O'''}{M_O \nu_O}, \tag{2-7}$$

where M_F and M_O are fuel and oxidizer molecular weights respectively. The combustion reaction releases heat ΔH_C while it consumes fuel mass of $M_F \upsilon_F$ and oxidant mass of $M_O \upsilon_O$. The source terms, $\dot{q}'''$ and $\dot{m}_i'''$ are eliminated from the energy and species equations by defining Shvab-Zeldovich [10] variables:

$$\beta_1 = \frac{h}{L} - \frac{(Y_O - Y_{O_\infty})\Delta H_C}{M_O \nu_O L}, \tag{2-8}$$

and

$$\beta_2 = \frac{h}{L} - \frac{Y_F \Delta H_C}{M_F \nu_F L}, \tag{2-9}$$

where, L is the fuel's effective heat of vaporization. In terms of β_1 and β_2 the energy and species equations become:

$$\rho u\left(\frac{\partial \beta_i}{\partial x}\right) + \rho v\left(\frac{\partial \beta_i}{\partial y}\right) = \frac{\partial}{\partial y}\left(\frac{k}{C_p}\frac{\partial \beta_i}{\partial y}\right) \text{ for i = 1, 2.} \tag{2-10}$$

The boundary conditions for this problem are:

$$u = 0 \text{ at } y = 0\,,\ u \to 0 \text{ as } y \to \infty \text{ and } \beta_1,\ \beta_2 \to 0 \text{ as } y \to \infty\,. \tag{2-11}$$

Since β_1 and β_2 have the same differential equation, and also have the same boundary condition, an elegant solution to this problem is obtained by defining a normalized function $\mathrm{F(x,y)}$ [8], where:

$$\beta_i(x,y) = \beta_i(x,0)F(x,y)\,,\quad \begin{matrix} F(x,0) = 1 \\ F(x,y) \to 0 \; as \; y \to \infty \end{matrix} \tag{2-12}$$

The definition of β_1 provides:

$$\beta_1(x,0) = -\frac{Y_{O_\infty}\Delta H_C}{M_O \nu_O L} - \frac{h_{vap}}{L} \equiv -B \tag{2-13}$$

The dimensionless term 'B' is called the Spalding B-number after Spalding [11]. This group expresses the ratio of chemical-energy released to energy required to vaporize the fuel (per unit mass of the fuel). With the heat flux specifications in Figure 2.1, the energy boundary condition at $y = 0$ for steady burning becomes:

$$\dot{m}''_f L = k\left(\frac{dT}{dy}\right)_{y=0} + \left[\dot{q}''_{f,r} - \dot{q}''_{s,r} - \dot{q}''_{s,c}\right]. \tag{2-14}$$

The terms in the square bracket, which represent the flame radiation, surface re-radiation heat loss, and an in-depth conduction loss are accumulated together by defining an effective L_M given by:

$$\dot{m}''_f L_M = k\left(\frac{dT}{dy}\right)_{y=0}. \tag{2-15}$$

$$L_M = L - \frac{\left[\dot{q}''_{f,r} - \dot{q}''_{s,r} - \dot{q}''_{s,c}\right]}{\dot{m}''_f}, \tag{2-16}$$

$$= L + Q \text{, where, } Q = \frac{\left[\dot{q}''_{s,r} + \dot{q}''_{s,c} - \dot{q}''_{f,r}\right]}{\dot{m}''_f}. \qquad (2\text{-}17)$$

The introduction of Equation (2-16), makes this problem identical to the pure diffusive/convective model of Emmons. Based on the above methodology, two different B-numbers are defined based on the presence or absence of *Q*. The two B-numbers (Table 2.1), are called the adiabatic B-number (B_A), and the realistic B-number (B_T).

Table 2.1: Definition of an adiabatic and a realistic B-number; B_T incorporates conductive and radiative losses through Q defined by Equation (2-17). The fraction of heat radiated by the flame to the environment and not reaching the fuel surface is represented by "χ".

B-number	
Adiabatic mass-transfer number	$B_A = \dfrac{(\Delta H_C Y_{O_2,\infty}) - C_{P,\infty}(T_{ig} - T_\infty)}{L}$
Modified B-number (incorporating all the loss terms)	$B_T = \dfrac{(1-\chi)(\Delta H_C Y_{O_2,\infty}) - C_{P,\infty}(T_{ig} - T_\infty)}{\Delta H_P + Q}$

2.2.2 The adiabatic (B_A) and realistic B-number (B_T)

The adiabatic B-number is similar to the one used in Emmons' [12] classical solution, where radiative and conductive losses were neglected. It is the maximum B-number that a fuel can attain, and depends only on material properties ΔH_C, L, and T_p. It is shown in later sections that incorporating the adiabatic B-number in a flame spread model leads to overprediction of flame height and flame spread rate. B_T incorporates all forms of heat losses from the surface through the variable *Q*. Heat release rate from the flame enters the B-number through ΔH_C, which is generally referred to as the heat of combustion, and which does not incorporate any radiative losses from the flame to the

environment. Figure 2.1 shows a schematic of the heat loss mechanisms. An evaluation of the heat loss terms that could be incorporated into the B-number is conducted.

Radiative Heat transfer

Radiation is identified as an important heat transfer mechanism for low Reynolds number flames. Altenkirch *et al.* [13], and Ferkul and Ti'en [14], identify the importance of radiation in a configuration very similar to the present study. The experimental study of Altenkirch *et al.* [13], conducted on board of the Space-Shuttle dealt with opposed-flame spread over a thick PMMA slab. The work of Ferkul and Ti'en [14] is a numerical study where radiation is incorporated in the gas and solid phases. The flame is represented as a homogeneous, gray-gas flame with a mean beam length L_e. Assuming the boundary-layer as a thin layer, the flame radiative-heat flux is represented by:

$$\dot{q}''_{f,r} = \varepsilon_f \sigma (T_f^{\,4} - T_s^{\,4}), \tag{2-18}$$

where ε_f is the flame emissivity, given by Orloff *et al.* [15]: $\varepsilon_f = 1 - e^{(0.875 ln[\tau_f])}$ and $\tau_f = e^{-0.061 - 0.117 L_p}$. L_p is the wall height in (meters).

$\dot{q}''_{s,r}$, which represents surface re-radiation, can estimated as:

$$\dot{q}''_{s,r} = \varepsilon_s \sigma (T_s^{\,4} - T_\infty^{\,4}), \tag{2-19}$$

where, for PMMA, $\varepsilon_S \approx 1$ [16, 17].

In both cases the view-factor is assumed to be unity [3], and the surface-area of the flame is equal to that of the pyrolyzing fuel. Quantitative values obtained from Equations (2-18) and (2-19) require knowledge of the flame temperature and the emissivity of the flame. Values for these parameters are difficult to find in the literature, where most work has concentrated on larger flames representative of fires [7]. For high

flame temperatures, radiative-feedback dominates over surface-radiation losses; for low flame temperatures losses are dominant. The assumption that net radiative exchange is neglected is further explored in the literature [3, 7, 17, 26, 27], and is considered questionable, depending on the specific experimental conditions.

Conductive Heat transfer

Heat conduction through the fuel in the +/- x-direction is neglected, away from the leading and trailing edges. Evaluation of temperature histories show that the temperature gradients within the pyrolyzing fuel remain very small, therefore conductive heat losses in this direction should also be small. The theoretical development of Pagni and Shih [6], assumes a thermally thin fuel; conduction within the fuel is not considered. For the present study, the material is thick and therefore temperature gradients within the surface affect the energy balance at the surface. In-depth conduction losses, $\dot{q}''_{s,c}$, are approximated by:

$$\dot{q}''_{s,c} = -\left(k_s \frac{\partial T}{\partial y}\right)_{y=0} \approx \frac{k_s (T_p - T_\infty)}{\delta_T}, \tag{2-20}$$

where δ_T is the thermal penetration depth (Figure 6.1, Chapter 6), given by $\delta_T = \sqrt{\alpha_s t}$. Detailed analysis of the time-dependent evolution of the conductive heat flux at the surface is found in the literature for similar conditions but will not be used here [18]. The estimate is preferred since the uncertainties on the time of ignition, the effect of the ignition system, and the variable flow conditions preclude exact experimental determination of the solid temperature distribution.

2.2.3 The realistic B-number, B_T

Introducing all the above heat losses into the energy balance given by Equation (2-17), the following expression for Q is obtained:

$$Q = \frac{\left(\frac{k_s}{\delta_T} \left(T_w - T_\infty \right) + \sigma \quad \varepsilon_s \quad \left(T_w^4 - T_\infty^4 \right) - \sigma \varepsilon_{fl} \left(T_{fl}^4 - T_w^4 \right) \right)}{\dot{m}_f''} . \qquad (2\text{-}21)$$

Equation (2-21) shows that Q is a function of the flame temperature (radiative losses from the flame) and the streamwise coordinate ("x", through $\dot{m}_f''$). From the previous discussion on radiative and conductive losses, an uncertainty is observed associated with the determination of the flame temperature and the individual heat losses. Radiative and conductive losses change based on the position, soot content of the flame, thickness etc.

Treatment of radiative exchange has been accomplished in different ways. Although the B-number, as formulated by Emmons [12], fully describes the heat exchange at the surface, it does not allow for an evaluation of this parameter independent of the heat losses. The decrease in flame-temperature and the net radiative exchange at the surface are very difficult to quantify. An alternative is found by Pagni and Shih [6], who propose an alternate definition to the B-number given by:

$$B = RB_A , \qquad (2\text{-}22)$$

where "R" is a coefficient that encompasses all radiative exchange. If R > 1, radiative exchange results in a net contribution to the surface, if R < 1, radiative exchange is considered a net heat loss from the surface. This concept is used to describe the differences in measured B-numbers, for identical fuels in independent studies under different configurations [29, 30]. The advantage of this formulation is the possibility of

defining a B_A which is an outcome of the adiabatic problem, therefore invariant with the heat losses and a significant property of the particular fire scenario. Although the definition of "R" is of great practical use, it is important to notice that "R" is defined as a constant with no dependency on "x," therefore is not a sufficient correction for a thermally thick fuel.

The "χ" corresponds to the fraction of the total energy released by the flame that is radiated to the environment and is a function only of the emissivity of the flame. Such accounting for the heat radiated by the flame, implicitly, as a corrective term in the total heat release rate is used by Kanury [2], where he experimentally measures the radiation flux, and finds that χ is a constant for a given polymer. Surface re-radiation and radiative feedback (Figure 2.1) to the surface are incorporated through Q:

$$Q = \frac{\left[\dot{q}''_{f,r} + \dot{q}''_{e} - \dot{q}''_{s,r} - \dot{q}''_{s,c}\right]}{\dot{m}''_{F}}. \tag{2-23}$$

The adiabatic mass-transfer number (B_A) assumes that all the heat generated through the combustion process is used to heat the oxidizer, and to evaporate the fuel at the surface. This ideal value provides the potential for propagation of the material under conditions corresponding to infinite chemistry. Since there is no loss term (Q), associated with B_A, it is estimated simply from the heat of combustion, ignition temperature, and latent heat of vaporization of the fuel. A more realistic mass-transfer number, will have χ and Q, in its formulation. The value of χ and Q depend on the nature of the flow field, and a realistic B-number that incorporates these loss terms is determined using the current experimental procedure. Since the standoff distance is defined by transport in the vicinity of the reaction, it is mostly affected by the external supply of oxidizer and fuel-

transport from the surface. It can therefore be linked to the fuel in a direct manner, to estimate a realistic B-number that varies with the streamwise direction due to the variable loss term Q. This value could be used in a fire model to model a worst-case scenario to estimate the risk associated with a particular material in an environment prone to fire hazards. A fuel safety ranking system using the B-number is ideal for characterizing material flammability in space, where high oxygen concentrations (typically 30% by volume) and confined spaces could increase fire hazard; a clear benefit is the ability to measure the B-number under earth-gravity conditions, avoiding the need for expensive microgravity experiments.

2.2.4 Mathematical Solution

The equations 2-1, 2-2, and 2-10 are reduced to a set of simultaneous ordinary differential equations by first satisfying the continuity equation (2-1) by the stream function ψ, such that $\rho u / \rho_w = \partial\psi / \partial y$ and $\rho v / \rho_w = -\partial\psi / \partial x$. The momentum and energy-species equation can then be expressed in terms of a single similarity variable η to give,

$$\begin{aligned} f''' + 3ff'' - 2f'^2 &= -[B + \tau - BF(\eta)] && \eta \le \eta_f \\ &= -[\frac{(B+\tau)}{F_f}F(\eta) - BF(\eta)] && \eta \ge \eta_f \quad . \qquad (2\text{-}24) \\ F'' + 3\,\mathrm{Pr}\, fF' &= 0 \end{aligned}$$

where the stream function,

$$\varphi = 4C\ \nu_w x^{3/4} f(\eta),$$

$$\text{with } \eta = x^{-1/4} C \int_0^y \frac{\rho}{\rho_w} dy \text{ and } C = \left(\frac{Lg}{4C_P T_\infty \nu_w{}^2}\right)^{1/4} (cm^{-3/4}), \qquad (2\text{-}25)$$

for free comvection. The value of the similarity variable, $\eta = \eta_f$, represents the flame location. $F_f = (B+1)r / B(r+1)$ and $\tau = h_w / L$, are constants that depend on the value of B and r chosen. It is assumed that the diffusion time of the fuel and oxygen is much larger than the chemical reaction time and thus the flame sheet approximation is valid. Equations (2-24) have boundary conditions:

$$\begin{aligned} &f'(0) = 0,\ f(0) = BF'(0) / 3\,\mathrm{Pr} \quad and \quad f'(\infty) = 0 \\ &F(0) = 1,\ F(\infty) = 0 \end{aligned} \tag{2-26}$$

The boundary conditions are converted to initial-value conditions by using the methodology outlined by Klamkin [19]. Once this is achieved, the set of two coupled ordinary differential equations can solved numerically using a shooting-method [20]. Mathematica 4.1 is used to formulate the mathematical solution (Appendix 1). A solution of the nondimensional flow field (f'), plotted with respect to the similarity variable (η) is shown in Figure 2.2. The velocity increases as the B-number increases.Figure 2.2 shows the nondimensional flowfield plotted for three different B-numbers

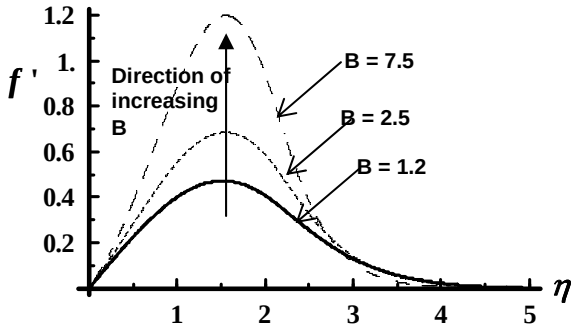

Figure 2.2: The solution of the set of ordinary differential equations (2-18). Increasing the B-number causes an increase in the magnitude of the velocity-field which is directly related to f'. The burning-rate, proportional to the velocity, increases with an increase in the B-number. r = 0.12.

The transformation from (x,η) back to the physical (x,y) is achieved by using the inverse of the Howarth-Dorodnitsyn [21] transformation, by which Equation (2-25) is rewritten as:

$$y = (x^{1/4}/C)\int_0^{\eta}(\rho/\rho_w)d\eta\,. \tag{2-27}$$

The standoff distance is obtained by expressing (ρ/ρ_w) in terms of the B-number and integrating from zero to η_f [8]:

$$y_f = (x^{1/4}/C)\int_0^{\eta_f}\left[\left(\frac{h}{h_w}-1\right)\left(\frac{T_p-T_\infty}{T_p}\right)+1\right]d\eta\,, \tag{2-28}$$

where $\dfrac{h}{h_w}=\dfrac{B+\tau-BF}{\tau}$. It is observed from Equation (2-28), that the standoff distance and the B-number are related by a relationship of the form:

$$y_f = A_{free}x^{1/4}\,. \tag{2-29}$$

A_{free}, is a constant that represents *1/C* times the integral in Equation (2-28). The integral takes different values based on the B-number. The subscript "free," denotes that the flowfield is driven by natural-convection. A similar relationship is also obtained for a

forced convective flow-field and is discussed in Section 2.3. The relationship between A_{free} and the B-number is plotted in Figure 2.3. Six different fuel properties (Table 2.2) are used and a linear relationship is observed in pracice. If the standoff distance y_f and corresponding x are known (from experiment), the value of A_{free} is obtainable using Equation 2-23. The corresponding B-number is then obtained from the plot shown in Figure 2.3.

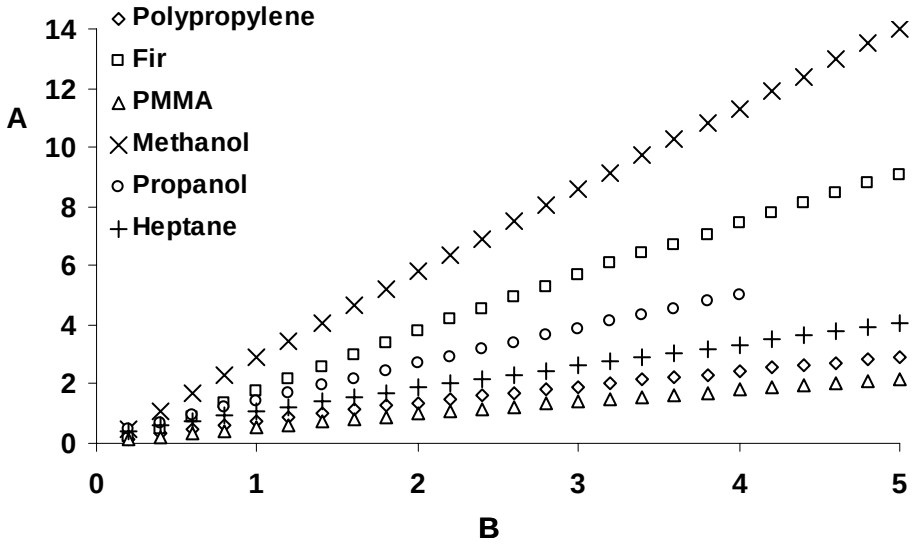

Figure 2.3: A_{free} as a function of the B-number for six different fuels. A_{free} is obtained by solving the ODEs represented by Equation (2-24) and subsequently the integral in Equation (2-28) using different values of the B-number.

Burning-Rate $\dot{m}_f''(x)$:

The free-convective local pyrolysis rate is given as [8]:

$$\dot{m}_f''(x) = -3f(0)\cdot\left[\frac{g\rho_w{}^2\mu_w{}^2 L}{4\overline{C}_p T_\infty x}\right]^{1/4}, \tag{2-30}$$

where, $\dot{m}_f''(x)$, is the mass flux released per unit area of fuel.

Table 2.2: Material properties used in plotting Figure 2.3.

Material	**L (J/g)**	**R**	**Tv (K)**
Polypropylene	2030[4]	0.0672[4]	703[4]
Fir (wood)	2430[22]	0.194[4]	683[23],[24]
PMMA	1590[25]	0.12[4]	660 [4]
Rigid Polyurethane foam	1190[22]	0.12	663[24]
Flexible Polyurethane foam	1340[22]	0.12	708[24]
Methanol	1260[26]	0.154[26]	338[26]
Propanol	890[26]	0.0960[26]	371[26]
Heptane	480[26]	0.0655[26]	371[26]

Flame length x_f

The upward progression of the flame is determined by measuring the flame length x_f with respect to the pyrolysis length x_p. Pagni and Shih [6] and Annamalai and Sibulkin [27], extend the similarity solution beyond the pyrolysis length to theoretically determine the flame height. x_f depends on the excess fuel fraction F_e, which is a ratio of excess-pyrolyzate to the total pyrolyzate. Using results from Annamalai and Sibulkin [27], the flame height is given as:

$$x_f = x_p(1-F_e)^{\frac{-1}{n+1}}, \tag{2-31}$$

where $n = -1/4$, and $F_e = \dfrac{\dot{M}'_{f,e}}{\dot{M}'_f}$ is the excess-fuel-fraction that is present beyond the pyrolysis length x_p. $\dot{M}'_f$ is the total mass released from the fuel surface and is obtained by integrating Equation (2-30) over the pyrolysis length:

$$\dot{M}_f' = \int_0^{x_p} -3f(0)\cdot\left[\frac{\rho_w{}^2\mu_w{}^2 Lg}{4\bar{C}_p T_\infty x}\right]^{1/4} dx = -3f(0)\left[\frac{\rho_w{}^2\mu_w{}^2 Lg}{4\bar{C}_p T_\infty}\right]^{1/4}\int_0^{x_p} x^{-1/4}dx$$
$$= -4f(0)\left[\frac{\rho_w{}^2\mu_w{}^2 Lg}{4\bar{C}_p T_\infty}\right]^{1/4} x_p{}^{3/4} \tag{2-32}$$

$\dot{M}_{f,e}'$ is given by $\left(\int_0^{y_f}(\rho u Y_F)_x dy\right)$ and is the excess pyrolyzate defined by Pagni and Shih[6].

2.3 Forced Convection

A similar analysis is developed for forced convection as well. The buoyancy term $(\frac{g(\rho_\infty - \rho)}{\rho})$, is not present and this simplifies the mathematical solution. Based on Emmons [12] solution, the two ordinary differential equations to be solved are:

$$\begin{aligned} f''' + f.f'' &= 0 \\ F'' + f.F' &= 0 \end{aligned}, \tag{2-33}$$

with boundary conditions given by

$$\begin{aligned} &f'(0) = 0,\ f(0) = BF'(0)/\,\mathrm{Pr}\ \ and\ \ f'(\infty) = 2 \\ &F(0) = 1,\ F(\infty) = 0 \end{aligned}, \tag{2-34}$$

where the stream function, $\varphi = (x/\,\mathrm{Re})^{1/2} f(\eta)$ with $\eta = \frac{1}{2}x^{-1/2}\,\mathrm{Re}\int_0^y \frac{\rho}{\rho_\infty}dy$. The stand off distance is once again expressed as a function of the B-number and is given by:

$$y_f = \frac{2x}{\sqrt{\mathrm{Re}_x}}\int_0^{\eta_f}\left[\frac{h}{h_w}\left(\frac{T_w - T_\infty}{T_\infty}\right) + 1\right]d\eta\,. \tag{2-35}$$

It is observed in Equation (2-35) that the standoff distance and the B-number are once again related by a relationship that looks like $y_f = A_{forced}x^{1/2}$. The difference

between A_{forced} and A_{free}, is shown in Figure 2.4, for PMMA. Since A_{forced} will depend on the Reynolds number Re_X, the relationship is plotted for difference flow velocities.

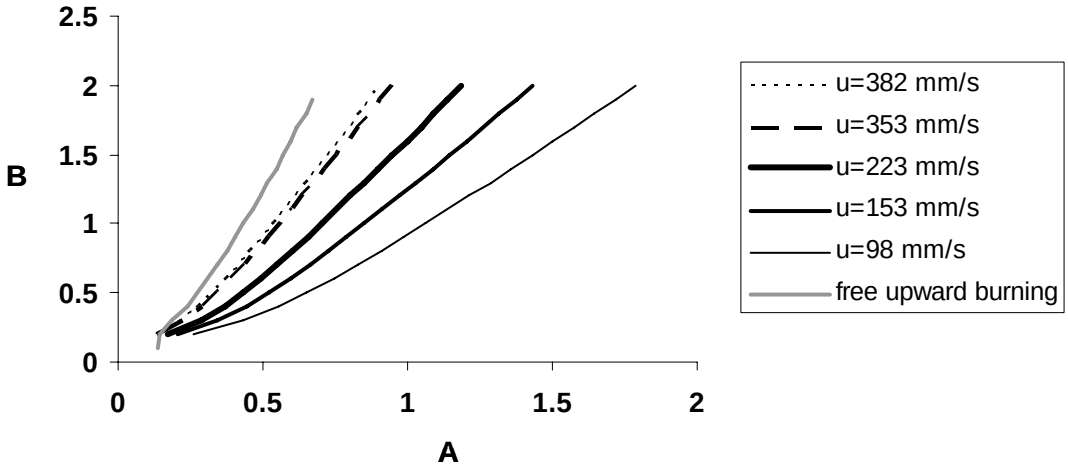

Figure 2.4: Relationship between the B-number and A for natural and forced-convection.

2.4 Summary

1. Theoretical results show that a relationship of the form $y_f = A(B)x^{1/4}$, exists between the B-number and the standoff distance. It is also shown that the relationship between the B-number and A is linear.
2. If one can successfully measure the standoff distance of a flame from the surface of the fuel, a B-number can be estimated, using Equation (2-23) and Figure 2.3
3. The loss term Q is accounted for automatically in the B-number, when the B-number is obtained using a standoff distance. This is explained in greater detail in Chapter 4
4. The flame length is required to obtain cocurrent flame spread rates. The mathematical analysis proposed by Emmons [12], predicts burning rate and flow characteristics only from the origin $x = 0$ until the pyrolysis length (x_p). The

flame length usually extends beyond x_p, because the fuel burned per unit area at the flame location is less than the gaseous fuel liberated per unit area at the surface [28]. Thus, there is an excess fuel (excess pyrolyzate) that is available in the combusting plume region. Numerical results for this excess pyrolyzate are previously derived by Pagni and Shih (1978) [29] and later by Annamalai and Sibulkin (1979) [27]. This analysis uses the theory developed by Annamalai and Sibulkin to obtain a flame length relationship as shown in Equation (2-25).

2.5 References

1. J. L. Torero, T. Vietoris, G. Legros, and P. Joulain, "Estimation of a Total Mass Transfer Number from Stand-Off Distance of a Spreading Flame," *Combust. Sci. Tech.*, vol. 174, p. 187-203 (2002).

2. A. Murty Kanury, "Modeling of Pool Fires with a Variety of Polymers," *Proc. Combust. Instit.*, vol. 15, p. 193-201 (1974).

3. L. Orloff, J. De Ris, and G. H. Markstein, "Upward Turbulent Fire Spread and Burning of Fuel Surface," *Proc. Combust. Instit.*, vol. 15, p. 183-192 (1974).

4. K. Annamalai and M. Sibulkin, "Spread Over Combustible Surfaces for Laminar Flow Systems Part I: Excess Fuel and Heat Flux," *Combust. Sci. Tech.*, vol. 19, p. 167-183 (1979).

5. D. B. Spalding, "Combustion of Liquid Fuel in Gas Stream," *Fuel*, vol. 29, p. 2-7 (1950).

6. P. J. Pagni and T. M. Shih, "Excess Pyrolyzate," *Proc. Combust. Instit.*, vol. 16, p. 1329-1343 (1978).

7. E. G. Brehob, C. I. Kim, and A. K. Kulkarni, "Numerical Model of Upward Flame Spread on Practical Wall Materials," *Fire Safety J.*, vol. 36, p. 225-240 (2001).

8. J. S. Kim, J. De Ris, and F. W. Kroesser, "Laminar Free-Convective Burning of Fuel Surfaces," *Proc. Combust. Instit.*, vol. 13, p. 949-960 (1971).

9. B. Gebhart, "Effect of Viscous Dissipation in Natural Convection," *JFM*, vol. 14, p. 225-232 (1962).

10. F. A. Williams, "Mechanisms of Fire Spread," *Proc. Combust. Instit.*, vol. 16, p. 1281-1293 (1976).

11. D. B. Spalding, "The Combustion of Liquid Fuels," *Proc. Combust. Instit.*, vol. 4, p. 847 - 864 (1953).

12. H. Emmons, "The Film Combustion of Liquid Fuel," *Z. angew. Math. Mech*, vol. 36, p. 60 -7 (1956).

13. R. A. Altenkirch, L. Tang, K. Sacksteder, S. Bhattacharjee, and M. A. Delichatsios, "Inherently Unsteady Flame Spread to Extinction over Thick Fuels in Microgravity," *Proc. Combust. Instit.*, vol. 27, p. 2215 (1998).

14. P. V. Ferkul and J. S. T'ien, "A Model of Low-Speed Concurrent Flow Flame Spread Over a Thin Fuel," *Combust. Sci. Tech.*, vol. 99, p. 345 -370 (1994).

15. L. Orloff, A. Modak, and R. L. Alpert, "Burning of Large Scale Vertical Surfaces," *Proc. Combust. Instit.*, vol. 16, p. 1345 (1978).

16. T. Steinhaus, *Thermal Properties of PMMA: A Calibration Material for the Development of a Material Flammability Test for Microgravity Environments*, in *Master's Thesis*, University of Maryland: College Park (1999).

17. J. R. Hallman, J. R. Welker, and C. M. Sliepcevich, "Polymer Surface Reflectance-Absorptance Characteristics," *Polymer Eng. & Sci.*, vol. 14, p. 717-723 (1974).

18. R. T. Long, J. L. Torero, J. G. Quintiere, and A. C. Fernandez-Pello, "Scale and Transport Considerations on Piloted Ignition of PMMA," *Proc. Fire Safety Sci.*, vol. 6 (1999).

19. Klamkin S. Murray, "On the Transformation of a Class of Boundary Value Problems into Initial Value Problems for Ordinary Differential Equations," *SIAM Review*, vol. 4, p. 43-47 (1962).

20. J. Stoer and R. Bulirsch, *Introduction to Numerical Analysis*, New York: Springer-Verlag (1980).

21. L. Howarth, "Concerning the Effect of Compressibility on Laminar Boundary Layers and their Seperation," *Proc. Roy. Soc. A*, vol. 1948, p. 16-42 (1947).

22. A. Tewarson and R. F. Pion, "Flammabilty of Plastics-1, Burning Intensity," *Combust. Flame*, vol. 26, p. 85-103 (1976).

23. A. M. Kanury, "Ignition of Cellulosic Solids - A Review," *Fire Research Abs. Rev.*, vol. 14, p. 24-52 (1972).

24. J. G. Quintiere and M. F. Harkleroad "New Concepts for Measuring Flame Spread Properties." *Fire Safety Sci. Eng.*, Philadelphia (1985).

25. K. Annamalai and M. Sibulkin, "Flame Spread Over Combustible Surfaces for Laminar Flow Systems. Part 1: Excess Fuel and Heat Flux," *Combust. Sci. Tech.*, vol. 19, p. 167-183 (1979).

26. E. F. Obert, *Internal Combusiton Engines*, International Textbook Co., Scranton, Penn. p. 234-235 (1968).

27. K. Annamalai and M. Sibulkin, "Flame Spread Over Combustible Surfaces for Laminar Flow Systems. Part 2: Flame Heights and Fire Spread Rates.," *Combust. Sci. Tech.*, vol. 19, p. 185-193 (1979).

28. D. B. Spalding, *Some Fundamentals of Combustion*, Butterworths, London (1955).

29. P.J. Pagni and T.M. Shih, "Excess Pyrolyzate," *Proc. Combust. Instit.,* vol. 16, p. 1329-1343 (1978).

Chapter 3

Experimental Setup

3.1 Introduction

The flame spread model developed in Chapter 2, is tested using an experimental apparatus described in this chapter. Five samples of solid fuels (PMMA, Polypropylene, Pine Wood, Rigid Polyurethane Foam and Flexible Polyurethane Foam), are mounted on a sample-holder similar to NASA's Test 1 Upward Flammability Test Apparatus. A digital camera is used to take a side-view image of the flame propagating upwards. The details of the experimental design and ignition method are described in the following sections. In addition, tests are also conducted using Fiberfrax (high temperature ceramic porous blocks) soaked in methanol, to study the effect of size and lateral-entrainment effects. These experiments are similar to those conducted by Ahmad and Faeth [1], with the difference that different-sized blocks are used in this study.

3.2 Experimental Setup for Testing Solid Fuels

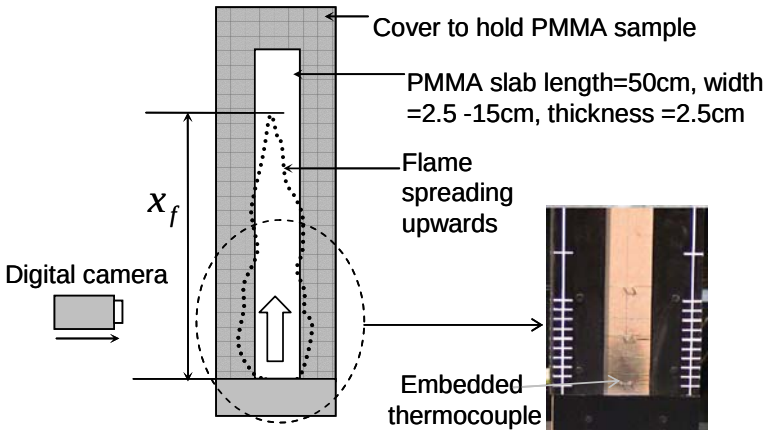

Figure 3.1: Experimental setup

The experimental combustion appararus consists of a vertical sample of the solid fuel (PMMA, Polypropylene, Foam, Wood) 50 cm in height, 1.5 cm in thickness, and 5

cm in width, mounted on an insulation-board and covered with a metal-plate, as illustrated in Figure 3.1. The metallic cover, extending 5 cm on each side of the sample, allows only the front surface of the fuel to ignite and burn.

Three different techniques are used to ignite the sample at the base. The first consists of soaking a wick with methanol and attaching it to the base of the fuel. The wick is ignited, using a match, and the burning wick ignites the solid fuel. Another method uses a nichrome wire coil, heated by applying a variable voltage to heat the base of the solid until ignition. However, this method is not used on polypropylene, because the polypropylene drips when heated, causing damage to the nichrome wire. The methanol wick proves to be the most effective ignition method in this case. The sample is also ignited at the bottom using a gas burner. When a flame of approximately 4 cm height is observed on the surface of the fuel, the burner is turned off. This method of ignition is used on wider samples, which are harder to ignite. It is very important to achieve an even ignition, to ensure repeatability of the tests.

A ruled reference on the plate provides a visual indication of the extent of flame spread at a given time. Five thermocouples (Chromel-Alumel 0.25 mm diameter) are fed through holes drilled from the back of the sample and melted onto the surface, to ensure that the thermocouples do not dislodge during the setting-up phase. Five additional thermocouples are placed on the back of the sample, between the fuel and the insulation. The thermocouples are all connected to a data-acquisition system (National Instruments: PCI-6031 E, coupled with SCB-100), and Labview is used to record temperatures at a sampling rate of 1 Hz. The time of arrival of the pyrolysis at each thermocouple location is defined by the time at which the temperature recorded by the thermocouple reaches the

nearly constant vaporization temperature of the fuel (PMMA T_p = 660 K [2]). Figure 3.2 shows the temperature profile of the 5 thermocouples with respect to time for an experimental run. The thermocouples at the back read the temperature between the insulation and the back surface of the sample. It is observed that the thermal wave never penetrates entirely to the back surface.

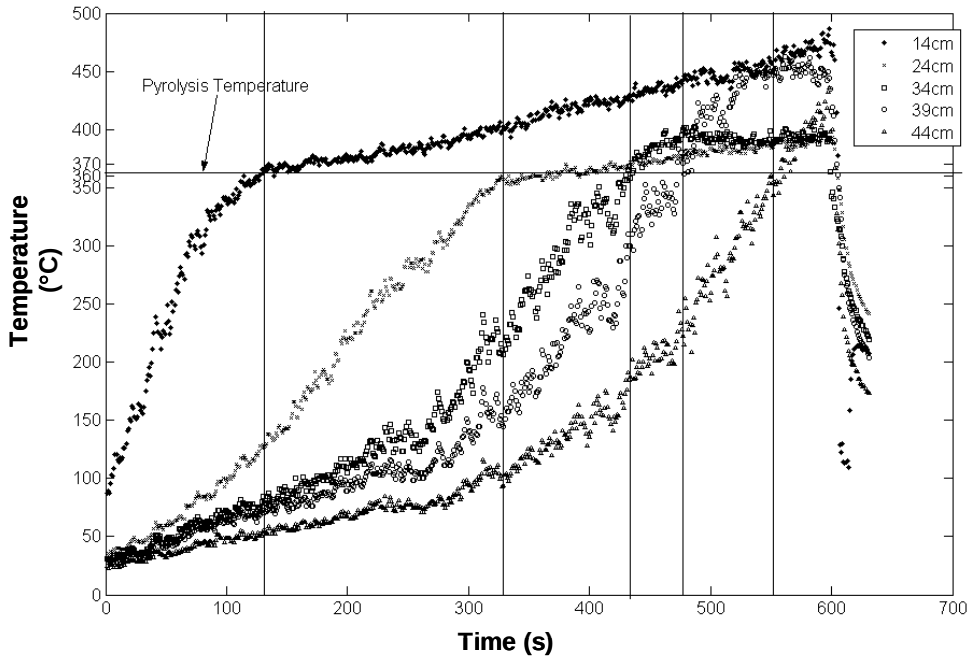

Figure 3.2: Pyrolysis temperature measured by surface thermocouples.

The primary source of error in the time measurement lies in the embedding of the thermocouples in the solid surface. If the thermocouple junction is embedded too deeply into the solid, the vaporization temperature is recorded after the pyrolysis front passes. On the other hand, if the thermocouple probe protrudes outwards, there is a possibility of it not reading the pyrolysis temperature accurately, being strongly influenced by the flame temperature instead. Another source of inaccuracy is the precision in measuring the arrival time of the pyrolysis front. Unlike downward flame spread, the temperature profiles in upward spread are shallower, and the surface temperature approaches the

vaporization temperature in an asymptotic fashion, making it difficult to recognize the exact time of the pyrolysis arrival at the thermocouple junction. To circumvent these problems, a set of five repetitive experiments were performed for each fuel sample, and an average value is used. It is observed that the deviation between individual experimental runs is not more than 10%.

A digital camera (Canon G5) is used to obtain a side-view of the flame. Before igniting a sample, the camera is calibrated by taking a picture of a graph paper that is aligned along the vertical axis of the fuel, as shown in Figure 3.3. Four calibration images are taken by placing the graph paper at four different locations, as shown in Figure 3.3. An average pixel/cm count is obtained from the four images taken. This value of pixels/cm is later used during the post-processing of the images, while calculating the standoff distance. The field of view is chosen to obtain an error in the standoff distance of less than 5%.

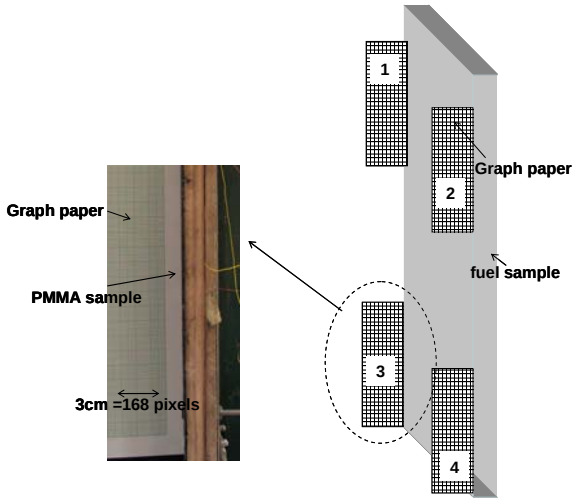

Figure 3.3: Calibration using a graph paper, aligned vertically against the solid fuel at four different locations.

Based on the characteristic time scales for propagation, an average of all images in a 10-second period is used to obtain an average standoff distance and flame-shape. An

experimental run usually lasts for between 200 and 250 s. The flame shows signs of turbulence when the flame reaches a height of 25 cm. The progression of the flame (taken from the side-view camera) is shown in Figure 3.4. Each image is interspaced by 20 s. The flame height, x_f, is recorded as the distance from the base of the fuel, to the tip of the flame. Figure 3.4 also shows the pyrolysis length, x_p, which is obtained from the surface thermocouple measurements.

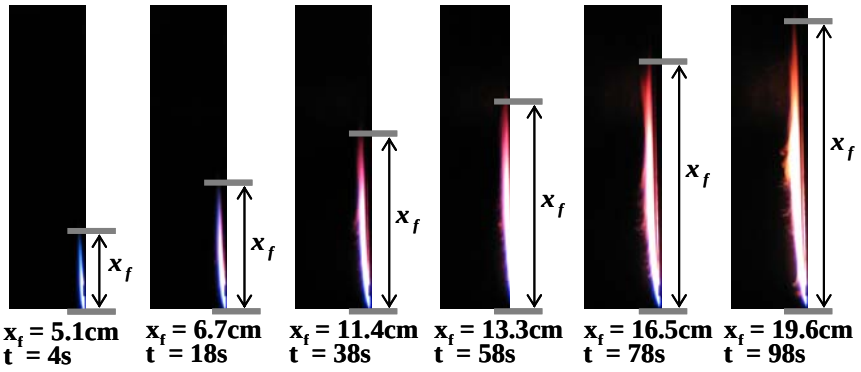

Figure 3.4: Progress of flame after ignition

Once an image is obtained, it is converted into a grayscale image, and passed through an edge-detection algorithm as shown in Figure 3.5, using ImageJ [3] software. The measured standoff distance is corrected for fuel regression through measurements of the burned samples after the test (Figure 3.5). Linear functions of time and location are established for the regression rates and added to the standoff distance; this correction never exceedes 10% of the total value.

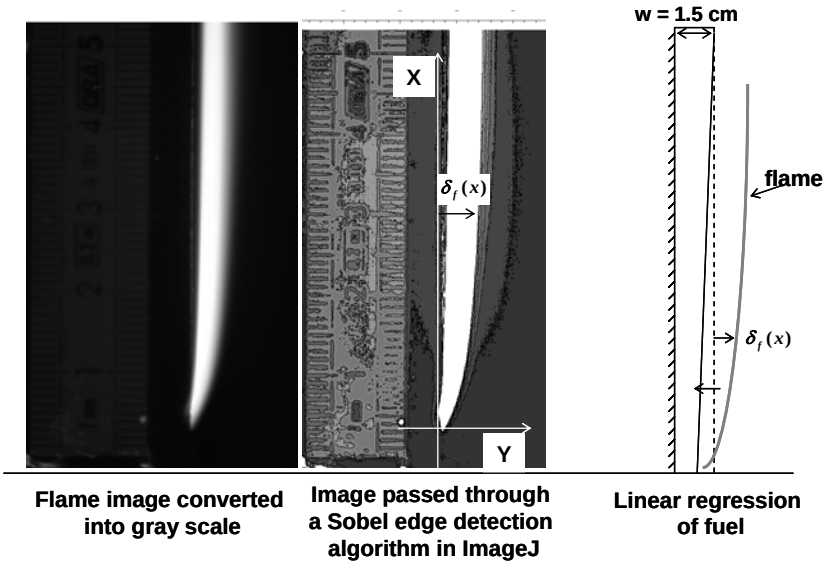

Figure 3.5: Edge-detection, and surface regression measurements.

The width of the fuel is found to influence the flame height during upward flame spread. To analyze this effect in greater detail, three more sample holders are constructed, to allow testing of samples with widths of 2.5 cm, 10 cm, and 15 cm, in addition to the 5 cm width initially tested. These samples of different widths are ignited in a similar way as mentioned previously. A detailed description of the results and analysis based on the widths of the fuel is given in Chapter 5.

3.3 Liquid Fuels

Flame height and flame standoff distance measurements are also conducted on liquid fuel samples, following an experimental layout similar to that of Ahmad and Faeth [4], (Figure 6). A porous-wick made from Fiberfrax high temperature ceramic foam is soaked with a liquid fuel (methanol) and ignited at the bottom. The standoff distance and flame heights are recorded for different sizes of fuel soaked wicks. Figure 3.6 and 3.7 show the experimental setup used. An image calibration process, as explained earlier, is carried out before the start of each experimental run.

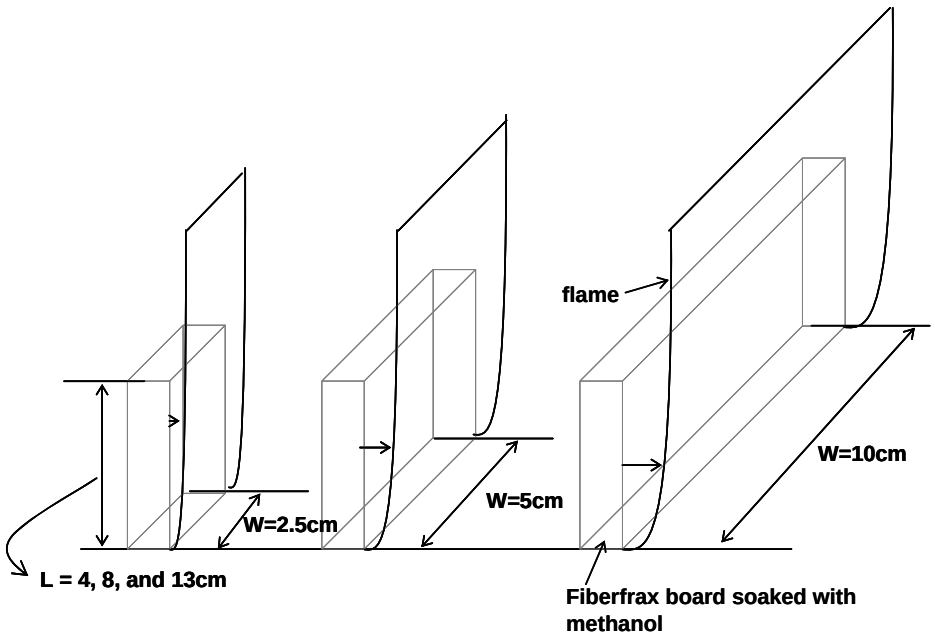

Figure 3.6: Experimental setup for liquid fuels.

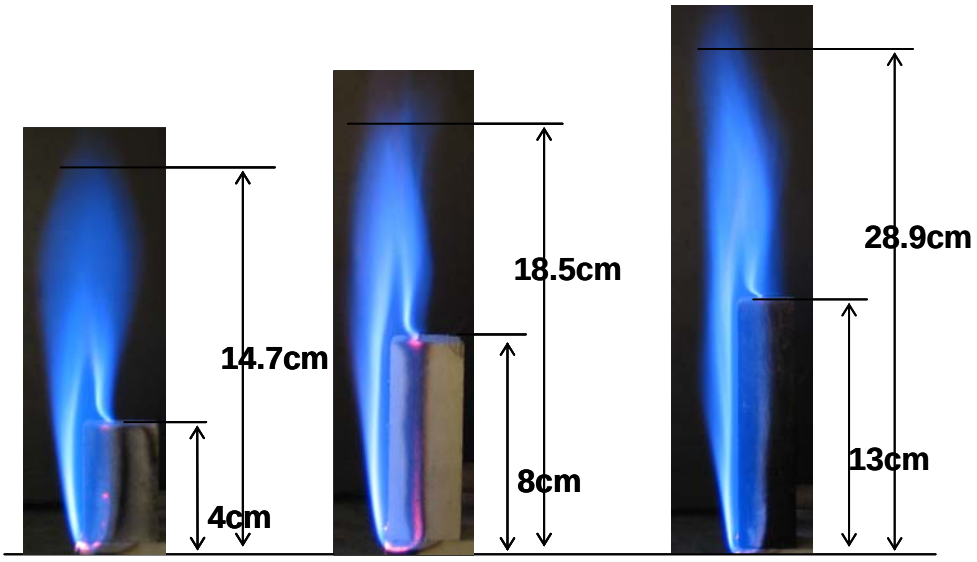

Figure 3.7: Methanol flames for different sized wicks.

High resolution flame side-view images are also used to measure flame standoff distances from the liquid fuel flames. The primary advantages of using a liquid fuel are: (a) the pyrolysis length is well defined (the length of the wick) and (b) there is no fuel regression. Assuming that the time required to vaporize the fuel is very high compared to the time required for burning, a quasi-steady approximation is made. Using the measured

standoff distance, the B-number for the liquid fuel is calculated for different widths of the fuel sample. The experimental results and analysis for liquid fuels are discussed in Chapter 4.

3.4 Summary

1. The experimental apparatus used in this work is similar to the Test 1 [3] apparatus used by NASA. The only addition is the use of a high resolution side-view camera that is used to capture the standoff distance as a function of time
2. Using the side-view camera and the embedded thermocouples, x_p, x_f, and δ_f are recorded as a function of time.
3. Profiles of x_f vs. t and x_f vs. x_p for other fuel samples tested are shown in Appendix 2.

3.5 References

1. T. Ahmad, *Investigation of the Combustion Region of Fire-Induced Plumes along Upright Surfaces*, Ph.D dissertation, Mechanical Engineering, Pennsylvania State University (1978).
2. A. C. Fernandez Pello, *Laminar Flame Spread over Flat Solid Surfaces*, Ph.D dissertation, Mechanical and Aerospace Engineering, University of California, San Diego (1975).
3. W. Rasband (NIH), *ImageJ*, http://rsb.info.nih.gov/ij/ (2006).
4. T. Ahmad and G. M. Faeth, "Turbulent Wall Fires," *Proc. Combust. Instit.,* vol. 17**,** p. 1149 -1160 (1979).

Chapter 4

Experimental Results and Discussion

4.1 Introduction

Five different solids, PMMA, wood, polypropylene, rigid foam, and flexible polyurethane foam, are tested in the experimental apparatus described in Chapter 3. In addition Fiberfrax is soaked with a known quantity of methanol, and used to test the effect of width on upward flame spread. The theory introduced in Chapter 2 is applied to estimate the B-number using the experimentally determined standoff distance. The evolution of the B-number calculated from the standoff distance is used to predict flame spread rate. Experiments show that the B-number is not a constant, but changes with time and space. Previous studies [1 - 4], have used the B-number as a constant, independent of space and time. This is because the loss term, Q, in the definition of the B-number, is either assumed to be equal to zero [1], or a constant, depending on the radiative-emission of the flame [5]. Using the standoff distance to estimate the B-number circumvents the need to calculate the loss-term independently. Results from experiments with PMMA are discussed in this section and general trends for the other samples tested are explained. Standoff distance and B-number profiles for the remaining solid fuels tested are included in Appendix 2.

4.2 Flame length, Pyrolysis Length and Flame-Standoff Distance

The flame length is defined as the distance from the leading edge to the tip of the flame. The images taken from the side-view camera are used to obtain the flame length as a function of time, and shown in Figure 4.1. Thermocouples embedded in the solid are used to give the progression of the pyrolysis front, as explained in Chapter 3. As

mentioned earlier, the time taken for a thermocouple to reach a temperature of 660 K is recorded as the time at which the pyrolysis front has reached thermocouple location. Figure 4.1 shows pyrolysis and flame lengths plotted as a function of time (PMMA). The data is compared with previous experimental results by Pello [6] and good agreement is observed with the current experimental work. An error of 10% is incorporated in the experimental data as a result of averaging results from five different experimental runs.

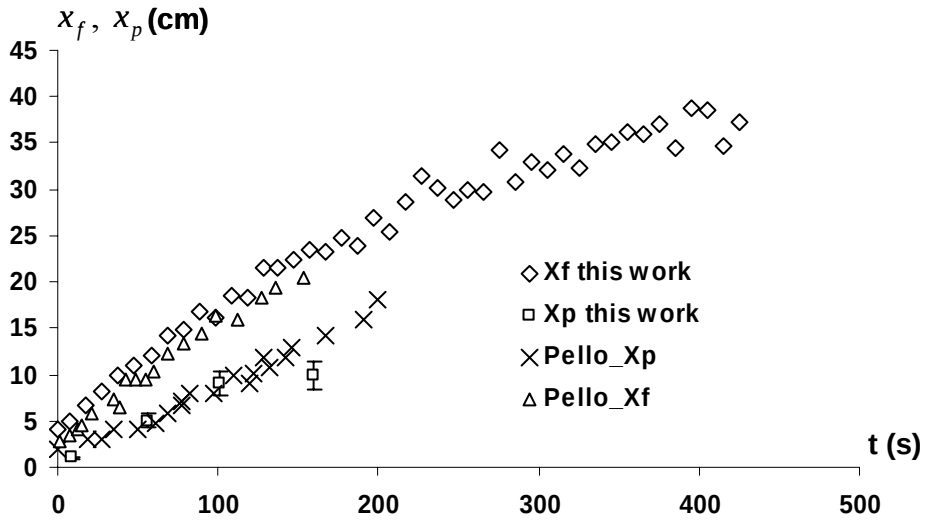

Figure 4.1: Progression of the pyrolysis-front and the flame tip with time. The current experimental data has close agreement with earlier work done by Pello [6].

The standoff distance of the upward-spreading flame is obtained from the side-view images taken by the digital camera. Figure 4.2 shows a plot of the standoff distance y_f (cm), plotted with respect to the streamwise direction x (cm), at 10-second time intervals for a 5 cm wide sample of PMMA. Appendix 2 has similar plots for the other solid samples that were tested. Figure 4.2 shows that with the progress of time, the standoff distance increases. As x_p increases, the mass-burning-rate increases, causing more fuel to be vaporized per unit time. This increase causes the flame to lift further up from the surface of the fuel, causing an increase in standoff distance.

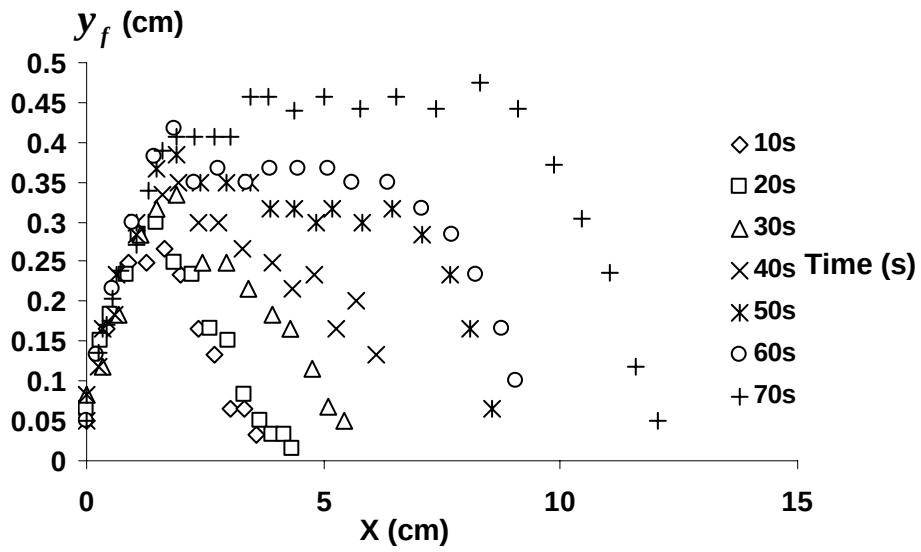

Figure 4.2: Standoff distance as a function of the streamwise direction. As time increases the flame length increases and the standoff distance also increases.

Using Equation (2-29), an experimental value of "A_{free}" is obtained from Figure 4.2, which allows calculation of the B-number from the standoff distance. A plot of the B-number as a function of *x* and time is discussed in the next section (Section 4.3).

Figure 4.3 shows the experimental evolution of a nondimensional flame standoff distance plotted against the normalized streamwise-direction x. The normalization is carried out using a pyrolysis length analogous to that incorporated by Pagni and Shih [3]. The standoff distance is nondimensionalized by a characteristic boundary-layer thickness, $y_f^* = L_{plate} \Big/ \sqrt{\frac{U_B L_{plate}}{\nu_\infty}}$, with $U_B = \sqrt{g \frac{\left(T_{ig} - T_\infty\right)}{T_\infty} L_{plate}}$. Normalizing the standoff distance and the streamwise direction brings about two important regions of interest, (a) the leading edge and (b) the trailing edge, as shown in Figure 4.3. The leading edge represents the region between $x / x_p = 0$ and $x / x_p = 0.2$ (20% of x_p), and the trailing edge represents the region between $x / x_p = 0.8$ and $x / x_p = 1$ (100% of x_p).

Beyond $x / x_p = 1$, the surface temperature of the fuel is below the pyrolysis temperature T_p and the burning rate $\dot{m}_f'' = 0$. Thus, the boundary-layer ceases to exist. As discussed earlier this region is called the combusting plume region [3]. The heat flux from the combusting-plume region impinging on the fuel surface ahead of x_p, is the "work-horse" of the flame, responsible for flame propagation. A critical condition is reached when the combusting-plume region ceases to exist. When this happens, there is no flame extending beyond $x / x_p = 1$, and the flame stops propagating. The B-number defined at this point is called the critical B-number (B_C). The critical condition is important during extrapolation of earth-gravity test results to microgravity conditions, and is discussed in Chapter 6 (Implications for Microgravity).

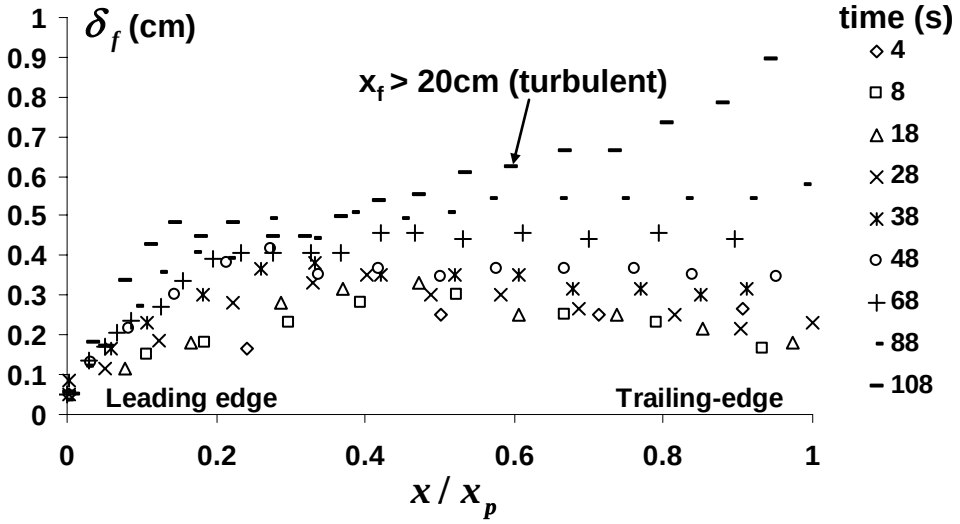

Figure 4.3: Nondimensional standoff distance y_f * as a function of normalized streamwise direction x / x_p.

It is observed in Figure 4.3 that at the leading edge ($x / x_p < 0.2$), the standoff distance increases almost linearly. At the trailing edge ($x / x_p > 0.8$) the standoff

distance decreases gradually. During the early stages the decrease in y_f * is sharp. As the flame gets longer, the trailing edge flame standoff distance increases.

The standoff distance is defined by the transport in the vicinity of the reaction, and is affected by two variables:

1. External supply of the oxidizer, which depends on the geometry/alignment of the fuel-sample. The size of the sample also plays an important role, and is explained in the next chapter (Chapter 5).
2. Fuel-transport from the surface, which depends on material-related properties such as the pyrolysis temperature, heat-of-gasification, and various heat fluxes described by Equation (2.17).

Modeling of solid fuel flame spread is complicated, because of the intricate coupling between gas-phase-ignition, combustion, and solid-phase pyrolysis. The heat required to pyrolyze more fuel is obtained from the gas-phase combustion reaction, and the location of the reaction front depends on the fuel burning-rate $\dot{m}_f''$, which depends on the solid phase, as well as the diffusion, and convection of fuel and oxygen, which occur in the gas phase. The standoff distance incorporates all these effects implicitly and therefore is linked to the fuel in a more direct manner than traditionally used quantities such as flame length and heat-release rate.

It is observed generally in Figure 4.3 that the standoff distance increases as the flame length increases. Therefore, the B-number, which is a function of the standoff distance, will also vary with time and space. This variation and the associated implications are discussed in the next section.

4.2 Evolution of the B-number with Time and Space

As a briedf summary of the earlier discussion, the B-number is defined by Emmons [1] as: $B = \dfrac{(1-\chi)(\Delta H_C Y_{O_2,\infty}) / \upsilon_s - C_{p,\infty}(T_p - T_\infty)}{\Delta H_P + Q}$, where χ corresponds to the fraction of the total energy released by the flame that is radiated to the environment, and the term *Q* represents the normalized non-convective heat transfer at the surface. To simplify the mathematical formulation, Emmons neglects *Q* and χ, and assumes that the fuel heating is due to convective heat flux from the flame alone, thereby defining an adiabatic B-number, $B_A = \dfrac{(\Delta H_C Y_{O_2,\infty}) - C_{p,\infty}(T_p - T_\infty)}{\Delta H_p}$, without any heat losses, and a constant based only on the material properties, ΔH_C, ΔH_p, and, T_p. Attempts to correct for these limitations are found in the literature [3], [4], [5], [7]. For example Pagni and Shih (1978) define a mass-transfer number, *B*, by incorporating a corrective factor, *R*, that includes radiative-exchange from the flame to the environment and the mass-transfer number is re-defined as $B = R\, B_A$. Although the definition of "*R*" is of great practical use, it is important to notice that "*R*" is defined as a constant, with no dependency on "*x*;" therefore, is not a sufficient correction. Previous experimental calculations of the B-number in the literature [3 -5], [8], [9], assume that the loss term *Q* in the denominator is a constant, resulting in a B-number that does not change with time (Table 4.1).

Table 4.1: B-number values listed in literature.

Reference	*B-number*
Pagni[3]	1.5
Annamalai[4]	1.78
Pello[6]	1.71
Kanury[5]	1.32
Holve[10]	1.5

Kanury [5] measures the radiation losses and accounts for them in the B-number, when burning solid pool fires under various oxygen concentrations. But since the flame heights do not change with time, the loss terms remain constant, and the B-number calculated is a constant. Holve *et al.* [10] measure the B-number by burning solid fuels in a counterflow burner configuration. Orloff *et al.* [11], measure the radiative losses, and include this effect in their calculation of the B-number. It is seen from Table 4.1 that depending on Q and χ measurements of different researchers, the B-number varies between 1.3 and 1.8 for PMMA. However, using a B-number in this range leads to an overprediction by the theory when comparison is made with experimental data [6, 12].

In this work, the B-number is determined using the standoff distance, which is measured experimentally. Experimental results show that, for upward laminar flame spread the losses change with respect to time, resulting in a B-number that is small during flame inception, and increases as the flame height increases. It is shown that the time-varying B-number thus obtained yields a much better theoretical agreement with experimental data.

4.2.1 Variation of the B-number with space

Figure 4.4 shows the B-number profile along the streamwise direction for a methanol flame. The loss term *Q* is given by: $Q = \frac{\left[\dot{q}''_{s,r} + \dot{q}''_{s,c} - \dot{q}''_{f,r}\right]}{\dot{m}''_f}$, from Equation (2-17). The burning rate $\dot{m}''_f$ varies inversely with *x,* as shown in Equation (2-30). This makes *Q* increase with the streamwise direction, *x*. The trailing edge B-number is therefore smaller than the leading edge B-number (as seen in Figure 4.4), when the flame lengths are small and the convective heat flux from the flame dominates. However, as the flame gets larger, the radiative transfer from the flame dominates and the B-number increases.

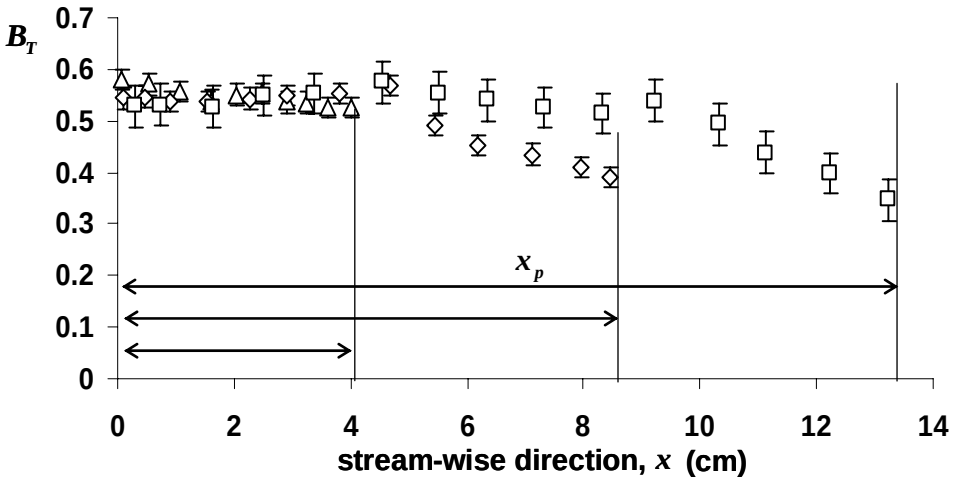

Figure 4.4: Variation of the B-number with x (methanol-soaked Fiberfrax blocks, 2.5 cm wide, and 4, 8, and 13 cm long).

As mentioned earlier, the x-axis is normalized using a pyrolysis length analogous to that incorporated by Pagni and Shih [3], useful for iterpreting the results. Figure 4.5 shows a plot of the B-number for methanol flames, using a normalized *x*-axis for different pyrolysis lengths x_p. Nine Fiberfrax blocks, of width 2.5 cm, 5 cm, and 10 cm,

with lengths 4 cm, 8 cm, and 13 cm, are used. As the flame gets longer, the radiation from the flame increases, causing *Q* to decrease and B to increase.

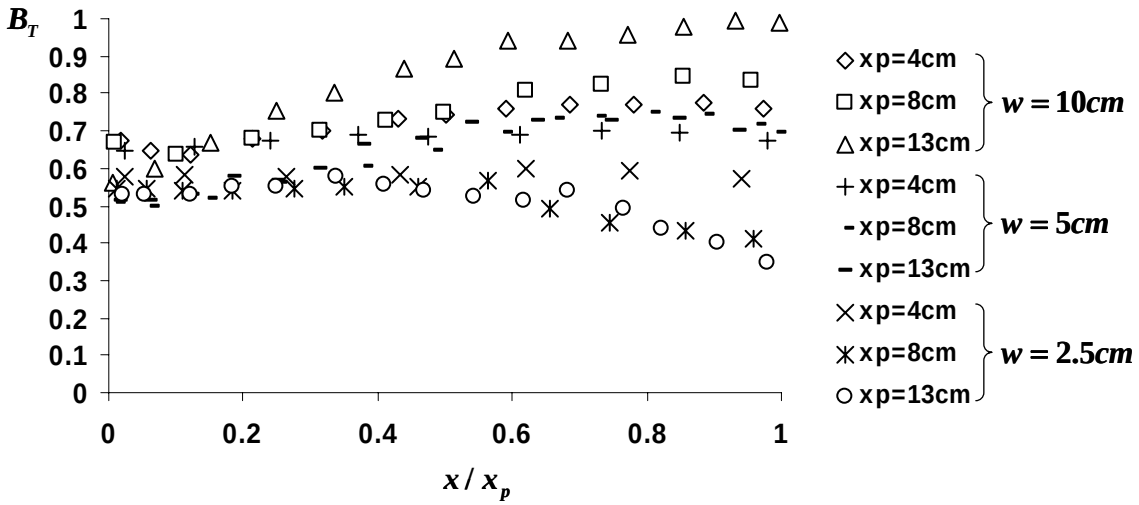

Figure 4.5: The B-number plotted as a function of the normalized streamwise direction (Methanol soaked Fiberfrax). The B-number at the trailing edge, increases as the length of the sample increases, showing that radiation is the dominant mode of heat transfer for larger flame lengths.

In addition the data show that as the width of the sample increases, the B-number increases. The influence of width on the B-number and its implications on flame spread in general, are discussed in Chapter 5.

Figure 4.6, shows the evaluation of the B-number plotted with respect to the normalized *x*-axis for PMMA. It is generally observed that the B-number increases as the flame grows (parameterized by xf) and the importance of radiative transfer increases. The region of flame attachment is hard to quantify due to the proximity of the flame to the surface. This region, which is within about 2 cm from the bottom edge, is where the sample is ignited, and is marked in Figure 4.6 by the label: “leading edge effects.”

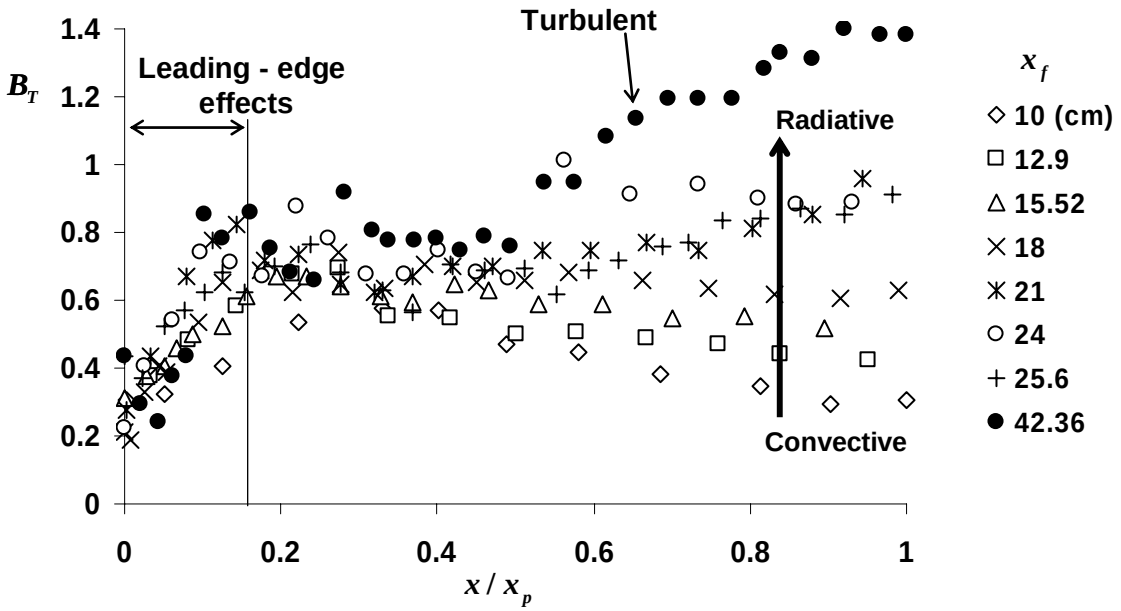

Figure 4.6: Variation of the B-number with space (PMMA, 5 cm wide).

Ideally, the B-number at the leading edge should be maximum, because losses in this region are minimum, and the burning rate $\dot{m}_f''$, varies inversely with $x^{1/4}$ (natural convection Equation (2-20)). However, this is not observed experimentally. A possible reason for this could be due substantial conduction losses to the metal at the bottom of the sample which could cause a reduction in the standoff distance measurement. Another plausible explanation could be the formation of a triple flame (Figure 4.7) at the leading edge.

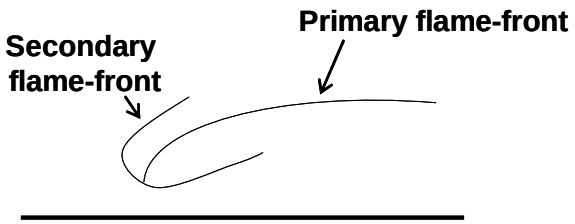

Figure 4.7: Triple flame formation at the leading edge [28]

Near the cold wall, there is a possibility that there could be three flame-fronts as shown in Figure 4.7. As a fuel vapor diffuses towards the flame, it is mixed with a smaller amount of the opposite reactant (oxygen), which diffuses between the flame and the fuel surface at the bottom edge. When these reactants reach the ignition temperature, they react, forming a secondary flame front. A triple flame structure causes the leading edge of the spreading flame to be ill-defined and hazy-looking, when observed by a digital camera. It is, therefore, difficult to quantify the exact flame location close to the leading edge. The experimental flame standoff distance measurement is therefore not accurate close to the location of the flame attachment. Due to this reason, the point where $x / x_p = 0.2$ used as the leading edge of the flame. The actual leading edge is at $x / x_p = 0$, but this point cannot be accurately resolved in these measurements.

Figure 4.6 illustrates the manner by which variations in radiation and conduction losses cause the B-number to change with the streamwise direction. A simple onedimensional energy equation is used to give an order-of-magnitude analysis of these losses, and is discussed in the next section.

4.2.3 A discussion of the loss terms

An examination of the definition of the B-number reveals that Q and χ are the only varying terms. The B-number can be written as:

$$B_T(x,t) = \frac{(1-\chi(x,t))(\Delta H_C Y_{O_2,\infty}) - C_{P,\infty}(T_{ig} - T_\infty)}{\Delta H_P + Q(x,t)}, \qquad (4\text{-}1)$$

where Equation (4-1) explicitly identifies the variation in heat transfer and flame radiation loss as as $\chi(x,t)$ and $Q(x,t)$. An understanding of the variation of change with respect to time and space is therefore warranted.

"χ", corresponds to the fraction of total energy released by the flame that is radiated to the environment, and is a function of the emissivity of the flame. As shown in Figure 3.4 (Chapter 3), during the early stages, the flame is bright blue in color. As time progresses the flame gets brighter as the visible flame-radiation increases. It is shown [7] that χ increases with free-stream velocity and oxygen concentration, using microgravity data by Vietoris *et al.* [13]. The flame temperature, T_f, is a function of oxygen concentration [14] and χ is proportional to T_f. Values of χ for PMMA are reported in the literature to range from 0.17 to 0.35, depending on flow geometry. For a given polymer burning in air, χ is assumed to be a constant. This is a reasonable for pool fire experiments, where the flame size remains constant; however, this simplification applied to an upward flame spread model is questionable.

The loss term $Q = \dfrac{\left[\dot{q}''_{s,r} + \dot{q}''_{s,c} - \dot{q}''_{f,r}\right]}{\dot{m}''_f}$ appearing in the denominator of the B-number changes with the streamwise coordinate through $\dot{m}''_f$. This is observed in Equation (2-30), where $\dot{m}''_f$ is a function of the streamwise direction *x*. The fuel pyrolysis temperature is a constant [16], which makes $\dot{q}''_{s,r}$ a constant. Thus the loss term Q, changes along the streamwise direction due to variations in $\dot{q}''_{f,r}$ and $\dot{q}''_{s,c}$. Calculating these losses is difficult unless a detailed numerical model, such as recently developed by Consalvi *et al.* [17].is used. An alternative to this complication is the calculation of these losses from the measurements of the standoff distance. Individual loss terms are not obtained, however a lumped *Q* is obtained, as shown in Figure 4.8. Knowledge of the B-number as a function of time and space, allows the calculation of the loss term Q, where:

$$Q(x,t) = \frac{(1-\chi(x,t))(r.\Delta H_C Y_{O_2,\infty}) - C_{p,\infty}(T_{ig} - T_\infty) - B(x,t)\Delta H_P}{B(x,t)}, \qquad (4\text{-}2)$$

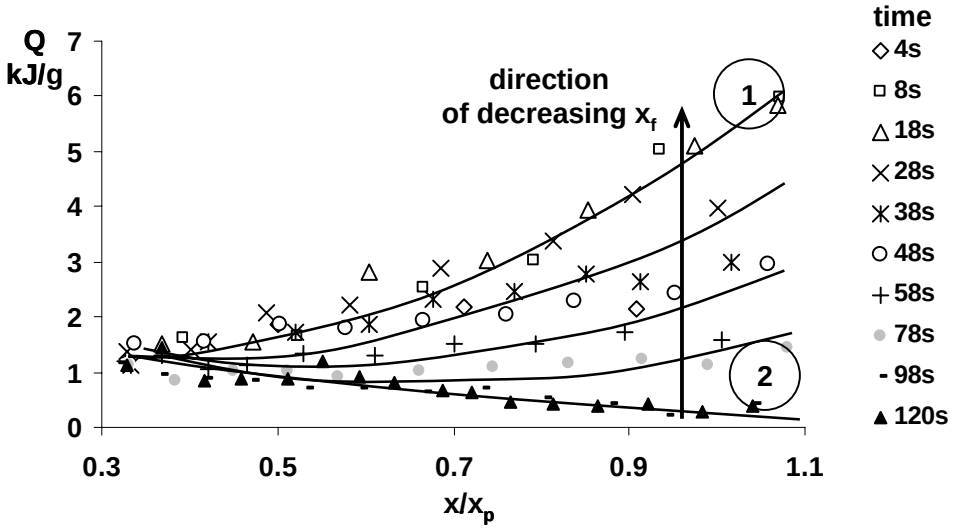

Figure 4.8: The loss term *Q* plotted as a function of the normalized length (PMMA)

Figure 4.8 shows that when the flame lengths are small, *Q* increases exponentially with the normalized streamwise direction (curve 1).The flame height is 5.1 cm at t = 4 s, (Figure 3.4) denoted by curve 1.When flame lengths are small, $\dot{q}''_{f,r}$ is low and decreases as one moves along *x*. As flame length increases, $\dot{q}''_{f,r}$ increases in prominence, effectively reducing *Q*. *Q* follows a linearly-decaying trend as shown by curve 2, at $x_f \gg 20$ cm.

As mentioned earlier, in addition to PMMA, rigid and flexible polyurethane foam, polypropylene, and wood (fir), were tested using the same experimental apparatus described in Chapter 2. Rigid and flexible polyurethane foam show similar B-number profiles as PMMA (Appendix 2). However, polypropylene behaves in a slightly different fashion. Figure 4.9 shows a plot of the B-number as a function of the normalized streamwise direction for polypropylene, illustrating that the trailing edge B-number is

always lower than the leading edge B-number. This is because of the melting and dripping of polypropylene, which increases as the flames get larger. Secondly, polypropylene flames are blue in color and the flame radiation term $\dot{q}''_{f,r}$, does not increase much with flame length as it does with PMMA. For larger flames, it is a;so difficult to quantify surface regression due to excessesisive dripping.Repeated experimental runs showed an error of about 10 % in standoff distance measurements.

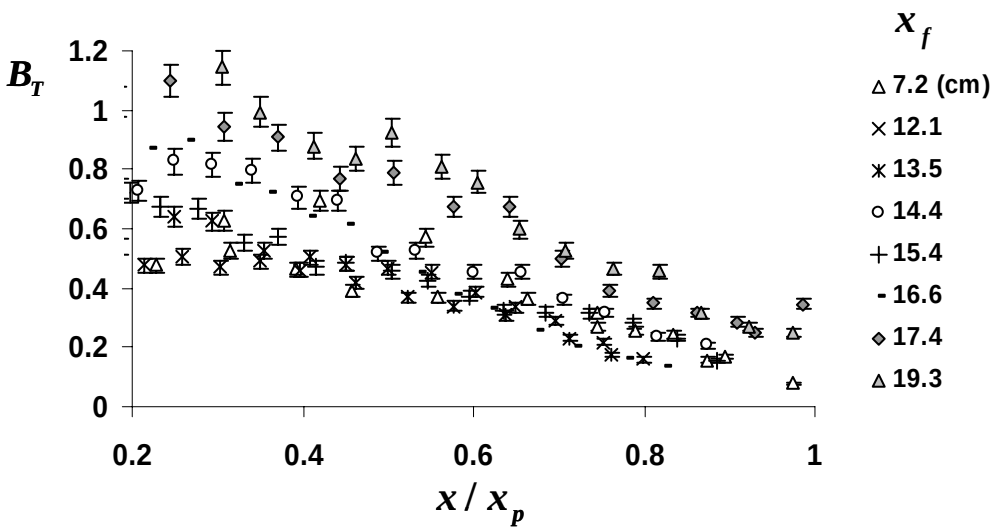

Figure 4.9: Variation of the B-number with space (Polypropylene, 5 cm wide)

The preceeding figures have illustrated how the flame radiation terms, $\dot{q}''_{f,r}$ and χ, change as the flame length increases. The primary mechanism for this is due to soot concentration changes as the flame length changes, which causes the two terms to vary. The next section shows how the leading and trailing edge B-numbers change as a function of time.

4.2.4 Variation of the B-number with time

Using the methodology explained in Chapter 2, a plot of the B-number in specific flame regions as a function of time is obtained from the experimental data, shown in

Figure 4.10. Overall, Figure 4.10 illustrates that the B-number increases with time during the flame spread process. B-number data taken from the leading edge (taken at x / x_p = 0.2) and the trailing edge (x / x_p = 1) are shown, taken from the average of five experiments. The leading edge of the flame follows a power-law relationship with time given by $B = 0.37\ t^{0.15}$. Similarly, the B-number obtained at the trailing edge of the flame x / x_p = 1, represents the trailing edge of the flame follows a power law relationship given by $B = 0.076\ t^{0.5}$.

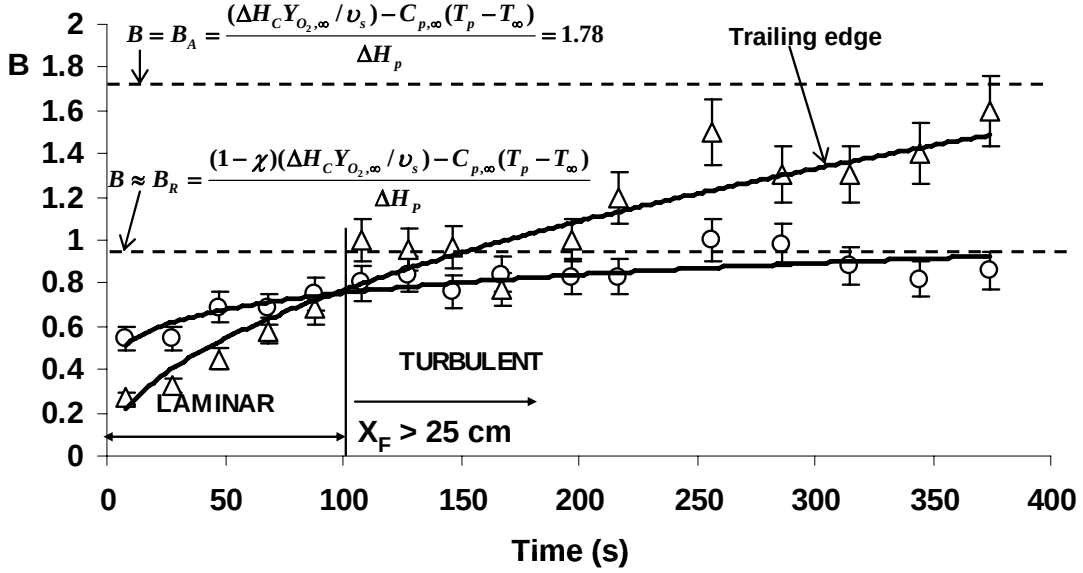

Figure 4.10: Evolution of the B-number with time

For experiments with PMMA the flame is laminar early in the propagation phase, and becomes turbulent after about 100 s, when the flame height equals 22 cm. An interesting observation is that at this point the leading edge and trailing edge curves intersect, and the trailing edge mass transfer number equals the leading edge mass transfer number. It is observed that during the early stages of the fire, when the flame lengths are small, the B-number is higher at the leading edge than at the trailing edge. As

the flame length increases, and the flame becomes turbulent, this trend reverses, and the B-number at the trailing edge increases. This behavior is attributed to the convective and radiative-loss terms in the definition of the B-number as discussed in the previous section. For small flame lengths, the convective heat flux from the flame plays a dominating role. Orloff *et al.* [11] have found that convection is important for flames less than approximately 20 cm in length, and flame radiation becomes dominant for larger flames. Ahmad and Faeth [18] show that convection is approximately 80 to 90% of heat transfer to the fuel for wall fires generated by fuel soaked wicks.

Two straight dotted lines are drawn in Figure 4.10. The lower dotted line represents the maximum B-number for laminar flame propagation (B_R). The leading edge B-number reaches B_R as an asymptotic limit. The trailing edge B-number, increasing with time eventually exceeds B_R. At this point $\left[-\dot{q}''_{f,r} + \dot{q}''_{s,r} + \dot{q}''_{s,c}\right] < 0$, because the flame radiation $\dot{q}''_{f,r}$ exceeds conduction and surface radiation losses. This is possible when the flame gets large and turbulent or when increasing soot concentration causes flame emission to increase.

The upper dotted line represents the adiabatic B-number (B_A). We observe that the experimentally measured B_R, is approximately half the value of the adiabatic B-number B_A. This explains, why previous works, e.g. [19], overestimates the flame height by approximately a factor of two

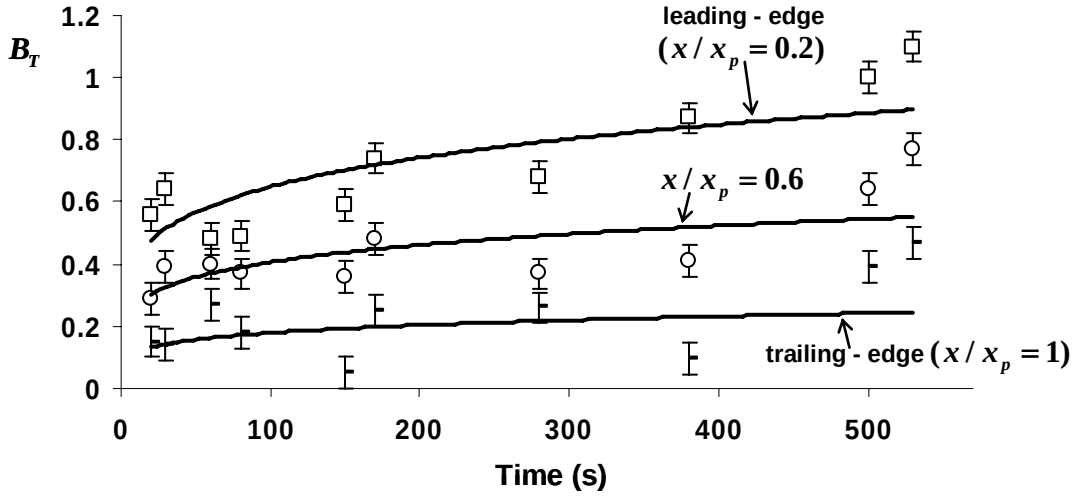

Figure 4.11: Variation of the B-number with time for polypropylene.

The trailing edge B-number does not exceed the leading edge B-number for all fuels. For example, for polypropylene (Figure 4.11) the trailing edge B-number reaches an asymptotic limit which is lower than that achieved by the leading edge B-number.Each data point is the average of three experiments, and the error bars represent one standard deviation of the scatter in the measurements at each point. Polypropylene flames are predominantly blue in color, and hence the radiative emission does not increase. In addition, due to dripping of polypropylene, the flames do not exceed 15 cm, causing it to burn in a laminar regime in the upward configuration.

The results presented in this section have illustrated that for upward laminar flame spread the B-number changes along the streamwise direction, because the loss term Q is not a constant. This results in a B-number that follows a power law relationship with time. This power law relationship is used to predict the flame length with respect to time. Earlier results that used a constant B-number for prediction overpredict flame lengths [6, 12]. This issue, which clearly demonstrates the practical use of the current methodology, is further discussed in Section 4.3.

4.3 Using the Measured B-number Profile to Predict Flame Height and Flame Spread Rate

The flame height is required to obtain co-current flame spread rates. The mathematical analysis proposed by Emmons [1], predicts burning rate and flow characteristics only from the origin to the pyrolysis length (x_p). The flame length usually extends beyond x_p, because overall the fuel burned per unit area in the flame is less than the gaseous fuel liberated per unit area at the surface [20]. Thus there is an excess fuel (*excess pyrolyzate*) that is available in the combusting-plume region. Numerical results for the excess pyrolyzate were previously derived by Pagni and Shih (1978) [3] and later by Annamalai and Sibulkin (1979) [19] in terms of measurable fuel parameters, via. the mass transfer-number B, and the stoichiometric-parameter:

$$r = \frac{Y_{O,\infty} M_f \upsilon_f}{Y_{FT} M_O \upsilon_O}, = \frac{Y_{O,\infty}}{\upsilon_s} = \frac{0.233}{1.92} = 0.12, \text{ for PMMA-air.}$$

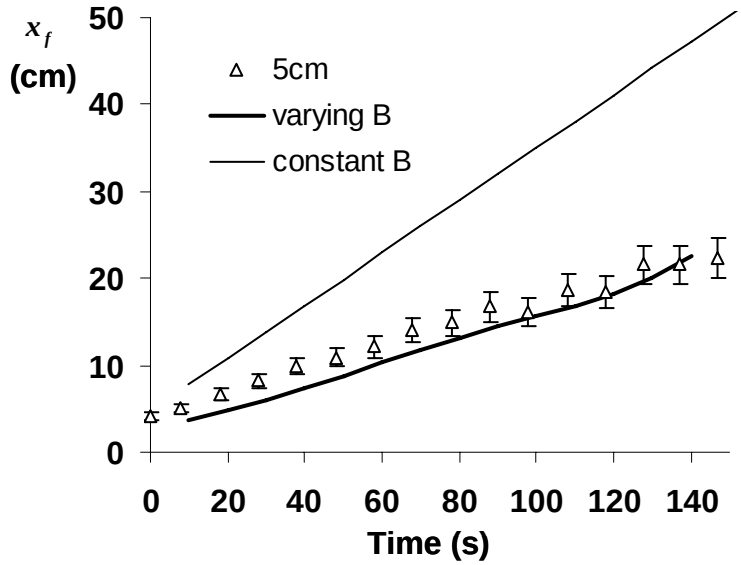

Figure 4.12: Flame height as a function of time

Assuming that all the excess pyrolyzate is burned upstream, a flame height can be obtained with respect to time. Figure 4.12 shows the flame height obtained using a constant B-number value (B =1.32 [5]) for PMMA. It is observed that the theoretical prediction with constant B-number overpredicts the data. This is reported by other researchers in the literature as well [6], [12], [21], [22]. Due to this overprediction flame spread has been modeled using experimental correlations of the form shown in Equation (4-3) over the last 20 years. Delichatsios [23] postulates that flame heights in wall-fires depend only on the total heat-release-rate, and derives a correlation for flame height as:

$$x_f = k\dot{Q}'^{n} \tag{4-3}$$

where k and $n = 2/3$ are constants, and $\dot{Q}'$ is the rate of heat release per unit width. Similar correlations of the form: $x_f = a\, x_p^{\,n}$, n = 2/3 [24], n = 0.71 [6], n = 0.78 [11], are obtained by other researchers as well. These correlations vary depending on materials chosen and need experimental verification. In addition, such correlations do not take into account the layout of the fuel sample; for example recent experiments by Tsai and Drysdale [25] have shown that the progression of the flame front depends on the way the solid fuel is mounted on the wall. In contrast, the laminar flame heights are predicted accurately when a power law relationship of the B-number evolution in time is used. The solid dark line in Figure 4.12 is obtained using $B = 0.37\ t^{0.153}$ relationship obtained from the current experimental results.

The location of the pyrolysis front with respect to time can also be derived using the current approach. Figure 4.13 is reproduced here, from work done by Annamalai and Sibulkin [19], where data from different researchers [6], [26], [27] is plotted.

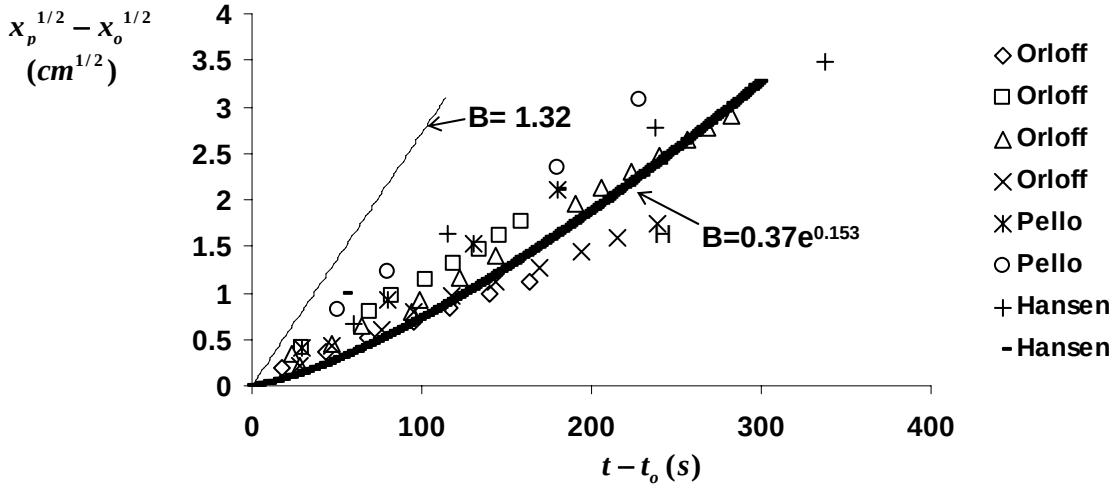

Figure 4.13: Movement of pyrolysis front with time for vertical PMMA slabs burning in air. The dark solid line represents the theoretical prediction, using a power law relationship of the B-number, determined from the current experimental work. The thinner solid line shows the theoretical relationship obtained using a constant B-number.Data taken from work of Annamalai and Sibulkin [19].

The x-axis represents time $t - t_o$ (s), where t_o is the time it takes to ignite an initial region x_o of the solid fuel. t_o and x_o are essentially incorporated to highlight the importance of initial conditions and enable the plotting of data from various researchers [26], [6], [27] on a single figure. Using an integral approach to model the boundary layer equations, Annamalai and Sibulkin [19] develop the following analytical relationship for $x_p^{1/2} - x_o^{1/2}$ as a function of material properties:

$$\frac{x_p^{1/2} - x_o^{1/2}}{t - t_o} = \frac{4\left[1 - 1.25(r/B)^{1/3}\right]}{\pi} \cdot \left[\frac{a_o^2}{\rho_s C_{p,s} K_s (T_g - T_\infty)^2}\right]; \tag{4-4}$$

where,
$$a_o = 0.27 \frac{B^{7/4}}{(B+1)^{1/4}} r^{0.19} \frac{L \rho_w \upsilon_w \left(\frac{g \Delta H_c}{\upsilon_w^2 C_{p,w} T_\infty}\right)^{1/4}}{\mathrm{Pr}^{1/2} \ln(B+1)}. \tag{4-5}$$

Using B = 1.32 for PMMA, the theoretical prediction of the pyrolysis front movement with respect to time is shown by the thin black line in Figure 4.13. The

theoretical result for the pyrolysis length is roughly twice that given by experiments. Since the theoretical slope is sensitive to any error in the heat flux estimations, this points to the fact that the theoretical estimate of the heat flux using a constant B-number is too high. The dark solid line is obtained by substituting the power law relationship for the B-number ($B = 0.37\ t^{0.1543}$) in equations 4-4 and 4-5. It is observed that the theoretical curve using the time-dependant relationship predicts the experimental data much more closely.

A broad goal of this experimental study is to evaluate the current upward flame propagation test [28] that is used by NASA to evaluate material flammability in space. Using the flame standoff distance which is obtained from this test, an evolution of the B-number with time for any fuel sample is obtained. The relationship between the B-number and time follows a power law of the form: $B = k_1 t^{k_2}$, where k_1 and k_2 are constants that are determined using the current test setup. However, one crucial factor in the evaluation of k_1 and k_2 which has not been considered so far is the width of the sample. The test samples that are mounted on the NASA upward flammability test apparatus are typically 5 cm wide. In the real world, however, the given material could have any width. It is shown in the next chapter (Chapter 5) that the constants k_1 and k_2 change with respect to width. A theoretical development explaining why this occurs and an approach to account for the width-effect so that Test 1 is still a viable method of evaluating fire flammability in space is the scope of the next chapter.

4.4 Summary

The theory developed in Chapter 2 is successfully applied to experimental data to determine an evolution of the B-number with respect to time and space. When the heat flux from the flame is predominantly convective in nature, it is observed that the B-

number is high at the leading edge and decreases progressively along the streamwise direction. This is because the loss term Q decreases due to an increase in the burning rate along the streamwise direction. For flames which are highly radiative, the loss term Q decreases and eventually becomes negative, causing the B-number trend to reverse. The experiments conducted in this work show that this may happen when flames exceed a length of 25 cm.

Flame height is needed to obtain flame spread rates. To obtain flame height it is necessary to determine the excess pyrolyzate, which is the mass flux of the fuel that is not burned in the boundary layer, is burned upstream beyond the pyrolysis length. Using the theory developed by Pagni and Shih [3], the excess pyrolyzate is determined.The excess pyrolyzate depends on the B-number; Chapter 5 will show that the excess pyrolyzate is also a function of the width of the fuel. For laminar lames a leakage flux exists, caused by mass diffusion from the sides, which causes a reduction in the excess pyrolyzate. Assuming that all the excess pyrolyzate is burned upstream, a flame length can then be obtained. Earlier estimates of flame length obtained led to an overprediction because the B-number used to calculate the excess pyrolyzate was overestimated. As explained in this chapter, the B-number profile obtained from the standoff distance is more accurate, because it takes into account the loss term Q in the denominator of the B-number.

The experimentally-obtained B-number profile is successfully used to predict flame spread rate for PMMA. In addition, theoretical estimates match experimental data from other researchers as well. The use of the Test 1 apparatus to estimate a B-number for any solid fuel is therefore advocated. A B-number profile thus obtained would be

useful in modeling flame spread in a three-dimensional numerical model (such as FDS) as well.

4.5 References

1. H. Emmons, "The Film Combustion of Liquid Fuel," *Z. angew. Math. Mech*, vol. 36, p. 60 -7 (1956).

2. F. J. Kosdon, F. A. Williams, and C. Buman, "Combustion of Vertical Cellulosic Cylinders in Air," *Proc. Combust. Instit.*, vol. 12, p. 252-264 (1969).

3. P. J. Pagni and T. M. Shih, "Excess Pyrolyzate," *Proc. Combust. Instit.*, vol. 16, p. 1329-1343 (1978).

4. K. Annamalai and M. Sibulkin, "Flame Spread Over Combustible Surfaces for Laminar Flow Systems. Part 1: Excess Fuel and Heat Flux," *Combust. Sci. Tech.* vol. 19, p. 167-183 (1979).

5. A. M. Kanury, "Modeling of Pool Fires with a Variety of Polymers," *Proc. Combust. Instit.*, vol. 15, p. 193-201 (1974).

6. A. C. Fernandez Pello, "A Theoretical Model for the Upward Laminar Spread of Flames Over Vertical Fuel Surfaces," *Combust. Flame*, vol. 31, p. 135-148 (1978).

7. J. L. Torero, "Material Properties that Control Ignition and Spread of a Fire in Microgravity Environments," *34th National Heat Transfer Conference, Pittsburg, Pennsylvania* (2000).

8. D. J Holve, *Diffusion Controlled Combustion of Polymers*, Ph.D. Thesis, University of California, Berkeley (1977)

9. A. Tewarson and S. D. Ogden, "Fire Behavior of Polymethylmethacrylate," *Combust. Flame*, vol. 89, p. 237-259 (1992).

10. D. J. Holve, and R. F. Sawyer, "Diffusion Controlled Combustion of Polymers," *Proc. Combust. Instit.*, vol. 15, p. 351-361 (1974).

11. L. Orloff, J. De Ris, and G. H. Markstein, "Upward Turbulent Fire Spread and Burning of Fuel Surface," *Proc. Combust. Instit.*, vol. 15, p. 183-192 (1974).

12. J. L Torero, T. Vietoris, G. Legros, and P. Joulain, "Estimation of a Total Mass Transfer Number from Stand-off Distance of a Spreading Flame," *Combust. Sci. Tech.*, vol. 174, p. 187-203 (2002).

13. T. Vietoris, P. Joulain, and J. L. Torero, "Experimental Observations on the Geometry and Stability of a Laminar Diffusion Flame in Microgravity." *Sixth International Symposium on Fire Safety Science* (1999).

14. Y. Utiskul, J. G. Quintiere, A. S. Rangwala, B. A. Ringwelski, K. Wakatsuki, and T. Naruse, "Compartment Fire Phenomena under Limited Ventilation," *Fire Safety J.*, vol. 40, p. 367-390 (2005).

15. E. M. Sparrow, *Radiation Heat Transfer*, Taylor & Francis (1978).

16. S. L. Madorsky, *Thermal Degradation of Organic Polymers*, Polymer Reviews, Immergut, Interscience (1964).

17. J-L Consalvi, B. Portierie, M. Coutin, L. Audouin, A. S. Rangwala, S. G. Buckley, and J. L. Torero. "Diffusion Flames Upwardly Propagating over PMMA: Theory, Experiment and Numerical Modelling," *Int. Symp. Fire Safety Science*, Beijing, China, IAFSS (2005).

18. T. Ahmad, and G. M. Faeth, "Turbulent Wall Fires," *Proc. Combust. Instit.*, vol. 17, p. 1149 -1160 (1979).

19. K. Annamalai and M. Sibulkin, "Flame Spread Over Combustible Surfaces for Laminar Flow Systems. Part 2: Flame Heights and Fire Spread Rates.," *Combust. Sci. Tech.*, vol. 19, p. 185-193 (1979).

20. D. B. Spalding, *Some Fundamentals of Combustion*, Butterworths, London (1955).

21. A. C. Fernandez-Pello and Hirano, "Controlling Mechanisms of Flame Spread," *Combust. Sci. Tech.*, vol. 32, p. 1-31 (1983).

22. J. L. Torero, A. S. Rangwala, S. G. Buckley, "Towards Determination of the B number for Co-Current Flame Spread using the Fire Dynamic Simulator (FDS) code: Comparison between Model and Experiment." *Fall Technical Meeting of the Western States Section of the Combustion Institute*, University of California, Los Angeles (2003).

23. M. Delichatsios, B. Paroz, and A. Bhargava, "Flammability Properties for Charring Materials," *Fire Safety J.*, vol. 38, p. 219-228 (2003).

24. J. G. Quintiere, K. Saito, and F. A. Williams, "Upward Turbulent Flame Spread," *Fire Safety Science- Proceedings of the First International Symposium*, p. 75 (1986).

25. Tzung-Hang Tsai, Mao-Jeng Li, I-You Shih, Ralph Jih, and Shwin-Chung Wong, "Experimental and Numerical Study of Autoignition and Pilot Ignition of PMMA Plates in a Cone Calorimeter," *Combust. Flame*, vol. 124, p. 466-480 (2001).

26. L. Orloff, A. Modak, and R. L. Alpert, "Burning of Large Scale Vertical Surfaces," *Proc. Combust. Instit.*, vol. 16, p. 1345 (1978).

27. A. G. Hansen and M. Sibulkin, "Flame Spreading from a Point Source of Ignition on a Vertical Fuel Surface," *Combust. Sci. Tech.*, vol. 9, p. 173-176 (1974).

28. NASA, *Flammability, Odor, Offgassing, and Compatibility Requirements and Test Procedures for Materials in Environments that Support Combustion,* NASA-NHB 8060.1 (1981).

29. J. N. De Ris, *The Spread of a Diffusion Flame over a Combustible Surface*, Ph.D dissertation, Applied Mathematics, Harvard University, Cambridge, MA (1968).

Chapter 5

Influence of Width

5.1 Introduction

In previous work, flame spread has been modeled using a 2-dimensional boundary layer similarity solution. Kosdon *et al.* [1] first implemented the approach for the upward flame spread problem. Enhancements to the model were made by Fernandez-Pello [2], who numerically calculated similarity solutions in the combusting-plume region to predict flame height. Pagni and Shih [3] developed integral solutions and solved them numerically. Ahmad and Faeth [4] made flame height measurements using the wick technique and solved the partial differential equations in the combusting-plume region using a finite-difference scheme. However, all of these models assume an infinite fuel sample width, which is discussed as one of the reasons causing an overprediction of flame height [5].

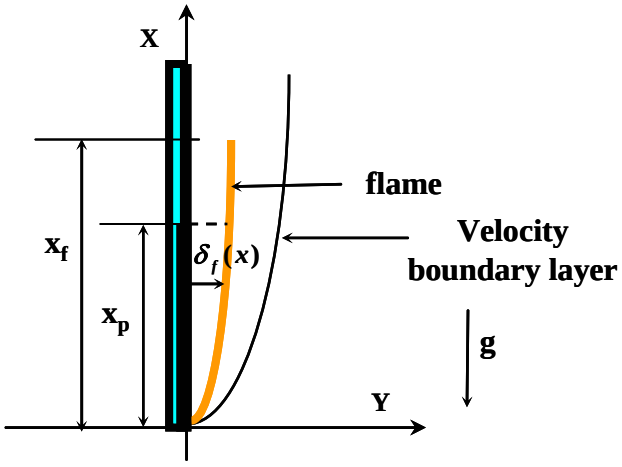

Figure 5.1: Schematic of a developing wall-fire

Figure 5.1 shows a schematic of a model experiment representing a developing wall fire. The solid fuel is pyrolyzing in the region x_p, and flame height is given by x_f.

Fuel vapors are released from the surface and participate in the flame, which is confined to the buoyancy-induced boundary layer. The region $x_f - x_p$, where the flame extends beyond the pyrolysis length, is called the combusting-plume region [3], and heat transfer from this region to the virgin fuel above x_p is responsible for the upward spread of the flame. Delichatsios [6] postulated that flame heights in wall fires depend only on the total heat release rate, and derived a correlation for flame height as:

$$x_f = k\dot{Q}'^n, \tag{5-1}$$

where, k and $n = 2/3$ are constants, and $\dot{Q}'$ is the rate of heat release per unit width. Similar correlations of the form: $x_f = a\, x_p{}^n$, n = 2/3 [7], n = 0.8 [8], n = 0.71 [2], n = 0.78 [9], are obtained by other researchers as well. Previously, the effect of width has been introduced as a geometric factor in flame height correlations [6].

This potion of the thesis revisits the classical problem of flame spread on solid fuels, to incorporate finite-width effects. It is argued that, in addition to the excess pyrolyzate [3], a fraction of the fuel also diffuses to the sides and changes the amount of fuel available to participate in flame spread as excess pyrolyzate. This diffusion ($\dot{M}_Z'$) is significant for narrow fuel-samples (width < 20 cm). The first reported experimental data that included the effect of width for vertical upward-burning were obtained on freely suspended strips of cotton fabric by Thomas and Webster (1960) [10]. They found the rate of upward flame spread, *V*, to be proportional to the square root of the sample width. A simplified mathematical analysis to account for the width of the fuel, in upward and forced flow configurations, was first established by Honda and Ronney [11]. The underlying hypotheses of their work was that for narrow fuel beds, lateral heat and/or

momentum losses limit flame length, and for wide fuel beds, surface radiation losses limit flame length. Based on these two limits, they classified flame spread in two regimes, convectively-stabilized and radiatively-stabilized. This work differs in that it accounts for radiative effects implicitly in the definition of the B-number [12], while reduction in flame height is predicted by a lateral diffusion of the fuel, reducing the amount of fuel that can participate in the combusting-plume region. The current analysis applies to the early stages of flame spread, while the flame is yet laminar ($x_f \leq 15-20cm$). It is argued that during this stage, a diffusion-dominated loss of fuel occurs which makes the flame length a function of the width of the fuel, in addition to the length and thickness. An eventual transition to an entrainment-dominated problem [9] will occur as the flame grows, and becomes turbulent, but this is not the focus of the current study.

5.2 Influence of Width in Flame Propagation (Theory)

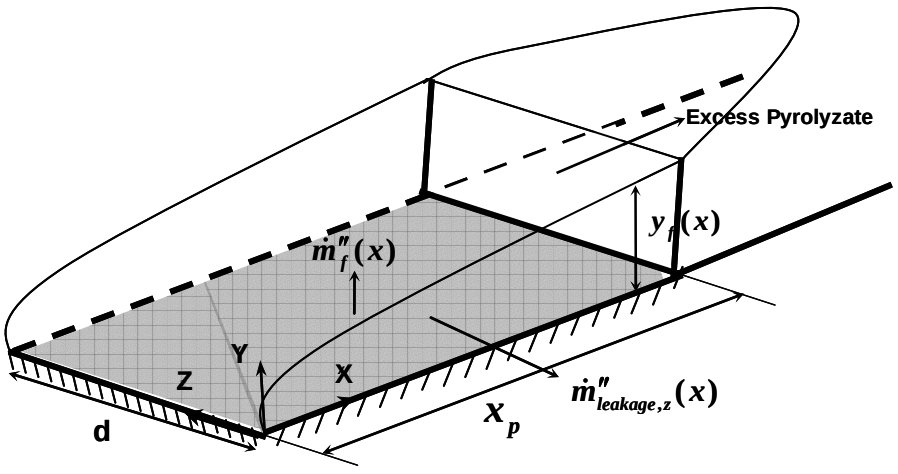

Figure 5.2: Flame geometry

The mathematical analysis carried out here is a modification of that described in Chapter 2. Figure 5.2 shows a schematic of a laminar diffusion flame spreading on the

surface of a solid fuel, which is assumed to be thermally thick. The flame could be spreading under the action of a forced flow or due to upward free convection. In either case, a boundary layer forms and boundary-layer simplifications are applied to solve the mathematical problem [13]. The flame standoff distance $y_f(x)$, is a measure of the distance between the diffusion flame sheet and the surface of the fuel. A derivation for a diffusive loss of fuel through the sides, represented by $\dot{M}_z'$, is presented in this section. The analysis is valid only for laminar flames ($x_f \leq 15-20cm$). A different mechanism controlling turbulent flames is proposed as a part of future work.

As discussed in Chapter 2, the free-convective local pyrolysis rate is given as [14]:

$$\dot{m}_f''(x) = -3f(0)\cdot\left[\frac{\rho_w{}^2\mu_w{}^2 Lg}{4\bar{C}_p T_\infty x}\right]^{1/4}, \tag{5-2}$$

where $\dot{m}_f''(x)$ is the mass-flux released per unit area of fuel. Equation (5-2) suggests that the importance of the losses at the surface, *Q*, increases with distance from the leading edge, since $\dot{m}_f''(x)$ decreases with x.

The relationship for $\dot{m}_f''(x)$ is derived assuming that the fuel has an infinite width. Most practical applications, however, deal with fuels having a finite width. The fuel concentration between the fuel surface and the flame is very high (close to 1) and a significant concentration gradient exists between the flame zone and the ambient at the sides. At the same time, due to high temperatures in the flame zone, Madorsky [15] reports that about 91% of the vapor generated during the pyrolysis of PMMA is the monomer MMA in a vapor-phase. Using the Wilker-Lee model [16], the diffusivity of

MMA-air at ambient temperatures is 0.01 cm^2/s. The diffusivity increases to 0.663 cm^2/s at 360 °C, the pyrolysis temperature of PMMA [17]. At even higher temperatures, much of the fuel is expected to be smaller hydrocarbons, particularly CH_4, which have a higher diffusivity. For the calculations presented here, the conservative, relatively low-temperature value of 0.663 cm^2/s is used. Increases in the diffusion coefficient lead to a higher diffusion velocity of fuel in the region of high fuel concentration gradient at the sides.

Experimentally an observed bulge in the flame profile at the sides of the sample is attributed to the effect of fuel diffusion at the edge of the sample. Simultaneously, a lateral diffusion of fuel would mean a reduction in the amount of fuel that is convected upwards, causing a reduction in $\delta_f(x)$. This is found to be experimentally true, as shown later in Figure 5.4. The fraction of the total mass flux of fuel lost due to lateral diffusion is estimated using an integral approach similar to that of Pagni and Shih [3], using the lateral direction (z-axis, Figure 5.2) instead of the streamwise direction (x-axis, Figure 5.2) that was originally considered by Pagni and Shih [3]. Assuming that the flux is driven by diffusion alone, Fick's law gives:

$$V_Z = D\frac{\partial Y_F}{\partial z} \approx D\frac{Y_{Fi}}{\delta_D}, \tag{5-3}$$

where Y_{Fi} is the initial concentration of fuel at the surface and δ_D is a characteristic fuel diffusion thickness given by:

$$\delta_D = \left(\frac{\phi D}{U_\infty}\frac{Y_{Fi}}{Y_{o_\infty}}x\right)^{1/2}. \tag{5-4}$$

δ_D is determined by assuming that the diffusion length scale is controlled by the outer air-flow conditions (U_∞), the sample dimension (through x) and the oxygen and fuel mass-fractions. $\delta_D \sim \sqrt{Dt}$, where D is the diffusion coefficient and $t \sim (x/g)^{1/2}$ for natural convection [18]. Such a definition of δ_D is used by Atreya [18] to explain the formation of a quasi-steady diffusion length scale thickness that changes with respect to the length scale. For upward propagation, U_∞ is a characteristic velocity defined as:

$$U_\infty = \sqrt{g \frac{(T_V - T_\infty)}{T_\infty} x_p} .$$

To account for the fuel stoichiometry,

$$r = \frac{Y_{O,\infty} M_f \upsilon_f}{Y_{FT} M_O \upsilon_O} = \frac{Y_{O,\infty}}{\upsilon_s} = \frac{0.233}{1.92} = 0.12 ,$$

for PMMA-air is included in the definition of δ_D. The total mass lost by diffusion in the Z-direction can then be obtained by integrating between the surface of the fuel and the location of flame:

$$\dot{M}_z' = \int_0^{y_f} V_z \rho Y_F dy = \frac{D}{\delta_D} \frac{Y_{F,w} \rho_w x^{1/4}}{C} \int_0^{\eta_f} Y_F(\eta) d\eta . \qquad (5\text{-}5)$$

Since a stoichiometric reaction is assumed, $Y_F = Y_F(\eta)$ between the fuel surface and the flame, and $Y_F = 0$, beyond the flame region. The density and fuel-fraction distributions for $0 < \eta \le \eta_f$ are given by [14]:

$$Y_F(\eta) = \frac{\frac{B}{B+1}[B + \tau + r\tau - r]F(\eta) + B \cdot F(\eta) - \tau - B}{B + \tau} . \qquad (5\text{-}6)$$

The term outside the integral,

$$\frac{D}{\delta_D}\frac{Y_{F,w}\rho_w x^{1/4}}{C}$$

arises due to the transformation from x and y to the similarity variables. $\dot{M}_z'$ is integrated from 0 to x_p,

$$(\int_0^{x_p}\left(\frac{D}{\delta_D}\frac{Y_{F,w}\rho_w x^{1/4}}{C}\int_0^{\eta_f} Y_F(\eta)d\eta\right)dx_p) \text{ to give:}$$

$$\dot{M}_z = Ax_p, \tag{5-7}$$

where $A = \frac{4\rho_w}{3C}\left(\int_0^{\eta_f} Y_F(\eta)d\eta\right)\left[\frac{DY_{F,i}}{r}\sqrt{\frac{g(T_V - T_\infty)}{T_\infty}}\right]^{1/2}$

is an integration constant which depends on the B-number. In addition, its value depends on the method by which the diffusion length scale (δ_D) is defined. The value of the integral

$$\int_0^{\eta_f} Y_F(\eta)d\eta = 0.503,$$

and with ρ_w = 1.29 × 10^{-3}, C = 7.8 $m^{-3/4}$, D = 0.663 cm^2/s $Y_{F,i}$ = 1, g = 980 cm/s^2 T_{ig} = 660 K, T_∞ = 293 K, r = 0.12, the value of *A = 0.001*.

Similarly, the total mass released from the fuel-surface is obtained by integrating over the pyrolysis length:

$$\dot{M}_f' = \int_0^{x_p} -3f(0)\cdot\left[\frac{\rho_w{}^2\mu_w{}^2 Lg}{4\bar{C}_p T_\infty x}\right]^{1/4} dx = -3f(0)\left[\frac{\rho_w{}^2\mu_w{}^2 Lg}{4\bar{C}_p T_\infty}\right]^{1/4}\int_0^{x_p} x^{-1/4}dx$$
$$= -4f(0)\left[\frac{\rho_w{}^2\mu_w{}^2 Lg}{4\bar{C}_p T_\infty}\right]^{1/4} x_p{}^{3/4} \tag{5-8}$$

At steady state, the effective burning rate is given by:

$$\dot{M}' = \dot{M}_f' - \frac{x_p}{d/2}\dot{M}_z', \tag{5-9}$$

where $\dot{M}'$ is the effective burning rate following the subtraction of the mass of fuel lost to the sides. This in turn, is used to write an expression for flame spread, taking into account the effect of lateral diffusion of fuel. This also modifies the amount of excess pyrolyzate that is used to preheat the virgin fuel by burning in the combusting-plume region. It is obvious from the above relationship that as the width of the fuel reaches a large value ($d \to \infty$), fuel-diffusion to the sides can be neglected.

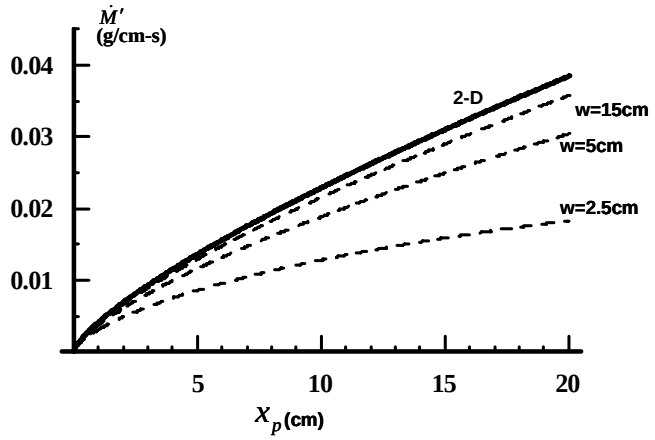

Figure 5.3: Effect of width on burning-rate. Solid line represents 2-D solution

Figure 5.3 shows a plot of $\dot{M}'$ vs. x_p for different widths. The calculated amount of fuel contributing to forward flame spread is observed to decrease by nearly 50% for thin samples (2.5 cm). From the model, for an upward-burning configuration, the burning rate reaches the 2-dimensional solution when the width is about 15 cm. The next section discusses the application of theory to experimental results.

5.3 Experimental Results and Discussion

5.3.1 Flame standoff distance

Figure 5.4, shows the standoff distance plotted as a function of the normalized streamwise direction (x / x_p) for widths of 2.5 cm, 10 cm and 15 cm (PMMA). The pyrolysis length is the same for the three cases ($x_p = 5 \pm 0.5$ cm). It is interesting to note that as the width of the sample increases, the standoff distance increases and the experimental data moves closer to the 2-dimensional solution shown as a solid dark line in Figure 5.4.

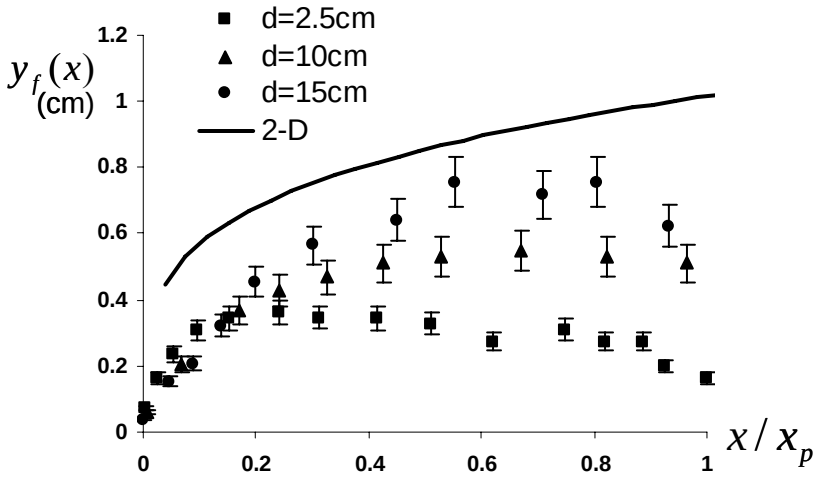

Figure 5.4: Standoff distance plotted as a function of the normalized streamwise direction, for three different widths. Data taken when the pyrolysis length $x_p = 5 \pm 0.5$. The solid line shows the 2-dimensional (infinite-width) solution. Each data point is the average of three experiments, and the error bars represet one standard deviation of the scatter in the measurement at each point.

The B-number for PMMA used to plot the theoretical curve, includes losses due to radiation (B = 1.32) [12]. The decrease in the standoff distance with decreasing width is attributed to lateral fuel-diffusion, because the diffusion of fuel toward the sides would decrease the effective burning rate, thereby causing the flame to move closer to the fuel.

This reduction in flame standoff distance is higher for samples with a smaller width. At the leading edge, where $x / x_p < 0.2$, $y_f(x)$ increases as a function of x but does not change with width significantly. $y_f(x)$ and U_∞ are small at this stage, and most of the pyrolyzate is convected upwards towards the flame, making the effect of lateral diffusion minimal.

5.3.2 Flame length

The upward progression of the flame is determined by measuring the flame length x_f with respect to the pyrolysis length x_p. As mentioned earlier, flame height for upward flame spread has usually been defined as a correlation of the form in Equation (5-1). One of the reasons for this is that, though comparison of theory and experiment show qualitative agreement as noted in Chapter 4, theoretical results for flame height [3], [19] are twice as large as those of the experimental results [17]. In contrast, the current theory is especially useful because it is applied to the classical theory directly to predict a flame height that is very close to experimental measurements.

Pagni and Shih [3] and Annamalai and Sibulkin [20], extend the similarity solution beyond the pyrolysis length to theoretically determine the flame height. Flame height (x_f) depends on the excess fuel-fraction F_e, which is a ratio of excess-pyrolyzate to the total pyrolyzate. The lateral fuel diffusion $\dot{M}_Z'$ reduces F_e, thereby shortening the rising flame and reducing the distance over which it can preheat the virgin-fuel. For this reason, if the width is small enough, the flame spread-rate is significantly diminished and attains a constant value after an initial acceleratory phase. This effect was observed

experimentally by Markstein and de Ris [9]. Using results from Annamalai and Sibulkin [20] the flame height is given as:

$$x_f = x_p(1-F_e)^{\frac{-1}{n+1}}, \tag{5-10}$$

where $n = -1/4$, and $F_e = \dfrac{\dot{M}'_{f,e}}{\dot{M}'_f}$ is the excess-fuel-fraction that is present beyond the pyrolysis length, x_p. With lateral diffusion-flux, $\dot{M}'_{f,e}$ decreases, and we have:

$$F_e = \frac{\left(\int_0^{y_f} (\rho u Y_F)_x dy\right) - \dfrac{x_p}{d/2}\dot{M}'_z}{\dot{M}'_f}, \tag{5-11}$$

where $\left(\int_0^{y_f} (\rho u Y_F)_x dy\right)$ is the excess-pyrolyzate defined by Pagni and Shih [3].

Using properties of PMMA, Equations (5-10) and (5-11) give an expression for x_f as a function of x_p, and the results are plotted in Figure 5.5.

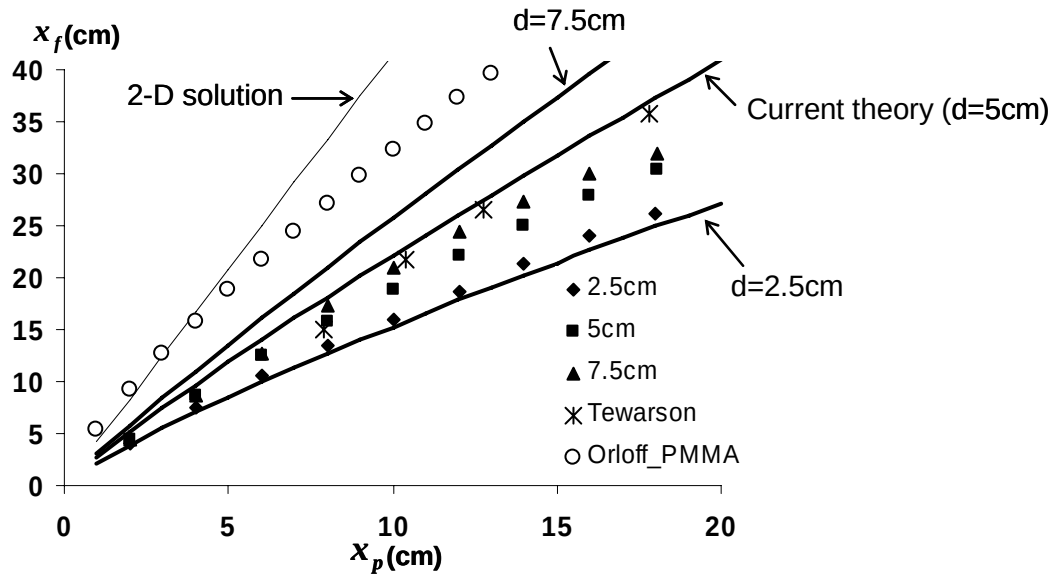

Figure 5.5: Flame height (x_f) vs. pyrolysis length (x_p). Current experiments on 2.5, 5, and 7.5 cm widths are plotted along with experimental data from previous work by Tewarson [21] and Orloff et al. [9]. Solid lines show theoretical curves.

The 2-dimensional solution for infinite width falls within range of data presented by Orloff *et al.* [9]. The experimental results in Orloff *et al*. [9] are obtained using fire-spread measurements on a 41 cm wide PMMA slab, where a 2-dimensional flow field is ensured by using water cooled sidewalls. However, for smaller width samples, the 2-dimensional solution overpredicts flame height. The slope of the experimental data points of the 2.5 cm wide PMMA sample is less than that of the slope of the 7.5 cm wide PMMA sample, clearly showing that as the width of the fuel is increased the flame height increases. This effect is possibly due to the previously unaccounted for diffusion flux ($\dot{M}_Z'$). Lateral diffusion of fuel at the sides would mean a reduction in the excess pyrolyzate, which in turn would make the flame heights shorter for thinner samples and longer for wider samples as shown in Figure 5.5.

Heat loss by conduction could act as a parallel mechanism. However, conduction losses occur predominantly in the solid phase, where a loss of heat due to conduction at

the sides would reduce the pyrolysis rate at the sides compared with the pyrolysis rate at the center of the sample. This study focuses only on the diffusion losses; neglect of solid-phase conduction and other mechanisms in the current treatment likely explain why the results predicted by the current theory do not exactly match the experimental data.

5.4 Summary

1. This chapter proves that the width of the fuel plays an important role in determining the flame height. The study is limited to laminar flames only, as lateral entrainment effects can play a dominating role for larger flames.
2. It is shown that in addition to the excess pyrolyzate [3], a fuel leakage flux issues from the sides, which contributes to a reduction of the flame height. This effect is negligible for wide samples (width >20 cm), but cannot be neglected for smaller widths.
3. The leakage flux $\dot{M}_Z'$ is calculated using the expression developed in Equation (5-7). Although the methodology developed is approximate, a reasonable agreement is found between theory and experimental results. A rigorous analytical model is required to define the diffusion length scale δ_D. This could be a part of future work. In addition, heat loss by conduction could act as a parallel mechanism (besides diffusion), and needs further study.

5.6 Acknowledgement

This chapter has partially included the following publication: "Upward Flame spread on Vertically-Oriented Fuel Surface: The Effect of Finite Width," *Proc. Combust. Instit.* (accepted for publication), A. S. Rangwala, S. G. Buckley, and J. L. Torero. The dissertation author is the primary researcher in this publication

5.7 References

1. F. J. Kosdon, F. A. Williams, and C. Buman, "Combustion of Vertical Cellulosic Cylinders in Air," *Proc. Combust. Instit.*, vol. 12, p. 252-264 (1969).

2. A. C. Fernandez Pello, "A Theoretical Model for the Upward Laminar Spread of Flames Over Vertical Fuel Surfaces," *Combust. Flame*, vol. 31, p. 135-148 (1978).

3. P. J. Pagni and T. M. Shih "Excess Pyrolyzate," *Proc. Combust. Instit.*, vol. 16, p. 1329-1343 (1978).

4. T. Ahmad, and G. M. Faeth, "Turbulent Wall Fires," *Proc. Combust. Instit.*, vol. 17, p. 1149 -1160 (1979).

5. J. L Consalvi, B. Portierie, M. Coutin, L. Audouin, A. S. Rangwala, S. G. Buckley, and J. L. Torero, "Diffusion Flames Upwardly Propagating over PMMA: Theory, Experiment and Numerical Modelling," *Int. Symp. Fire Safety Science (IAFSS)*, Beijing, China, IAFSS (2005).

6. M. Delichatsios, B. Paroz and A. Bhargava, "Flammability Properties for Charring Materials," *Fire Safety J.*, vol. 38, p. 219-228 (2003).

7. J. G. Quintiere, K. Saito, and F. A. Williams, "Upward Turbulent Flame Spread," *Fire Safety Science- Proceedings of the First International Symposium*, p. 75 (1986).

8. M. A. Delichatsios, *Combust. Sci. Tech.*, vol. 39, p. 195-214 (1984).

9. L. Orloff, J. De Ris, and G. H. Markstein, "Upward Turbulent Fire Spread and Burning of Fuel Surface," *Proc. Combust. Instit.*, vol. 15, p. 183-192 (1974).

10. P. H. Thomas, and C. T. Webster, "Some Experiments on the Burning of Fabrics and the Height of Buoyant Diffusion Flames," *Fire Research Note*, vol. 420 (1960).

11. L. K. Honda and P. D. Ronney, "Mechanisms of Concurrent Flow Flame Spread over Solid Fuels," *Proc Comb. Instit.*, vol. 28, p. 2793-2801 (2000).

12. A. M. Kanury, "Modeling of Pool Fires with a Variety of Polymers," *Proc. Combust. Instit.*, vol. 15, p. 193-201 (1974).

13. H. Emmons, "The Film Combustion of Liquid Fuel," *Z. angew. Math. Mech*, vol. 36, p. 60 -7 (1956).

14. J. De Ris, J. S. Kim, and F. William Kroesser, "Laminar Free-Convective Burning of Fuel Surfaces," *Proc. Combust. Instit.*, vol. 13, p. 949-960 (1971).

15. S. L. Madorsky, *Thermal Degradation of Organic Polymers*. Polymer Reviews, Interscience (1964).

16. C. R. Wilke, and C. Y. Lee, "Estimation of Diffusion Coefficients for Gases and Vapors," *Ind. Eng. Chem.*, vol. 47, p. 1253 (1955).

17. A. C. Fernandez Pello, "Flame Spread Modeling," *Combust. Sci. Tech.*, vol. 39, p. 119-134 (1984).

18. A. Atreya, "Ignition of Fires," *Phil. Trans. R. Soc. Lond. A*, vol. 356, p. 2873-2813 (1998).

19. K. Annamalai and M. Sibulkin, "Spread Over Combustible Surfaces for Laminar Flow Systems Part I: Excess Fuel and Heat Flux," *Combust. Sci. Tech.*, vol. 19, p. 167-183 (1979).

20. K. Annamalai and M. Sibulkin, "Flame Spread Over Combustible Surfaces for Laminar Flow Systems. Part 2: Flame Heights and Fire Spread Rates.," *Combust. Sci. Tech.*, vol. 19, p. 185-193 (1979).

21. A. Tewarson and S. D. Ogden, "Fire behavior of polymethylmethacrylate," *Combust. Flame*, vol. 89, p. 237-259 (1992).

Chapter 6

Implications for Microgravity

6.1 Introduction

For a given solid fuel, a B-number may be determined as a function of time from a test apparatus similar to Test 1 by taking a direct measurement of the standoff distance. This chapter explains the usefulness of this concept with regards to material safety tests for spacecraft fire safety.

The buoyant flow generated by density gradients which plays a major role in upward flame spread, loses its significance in a microgravity environment. The problem of interest in spacecraft fire safety is flame spread in low gravity, with a quiescent environment or with low-velocity flows. Discussion of the parameters determining the stability of diffusion flames subject to low-speed flows is of great importance for spacecraft fire safety, since it provides scientific criteria relevant to material flammability. Typical velocities are of the order of 0.1 m/s under 30% oxygen concentration [1]. These gas velocities are of the same order of magnitude as diffusion velocities. The influence of width (Chapter 5) will therefore play a significant role in a microgravity environment.

To begin, this chapter discusses the differences between the controlling mechanism of microgravity and earth-gravity flame spread. A Damkohler number (ratio of the flow residence time to the chemical reaction time) is used to study the two limits that are observed in flame extinguishment experiments in microgravity. Finally, modifications to NASA's Test 1 apparatus are suggested, to estimate a *critical B-number* (B_{crit}) and a *maximum B-number for laminar flame propagation* ($B_{\max}$).

6.2 Analogy between Flame Spread and Ignition Time

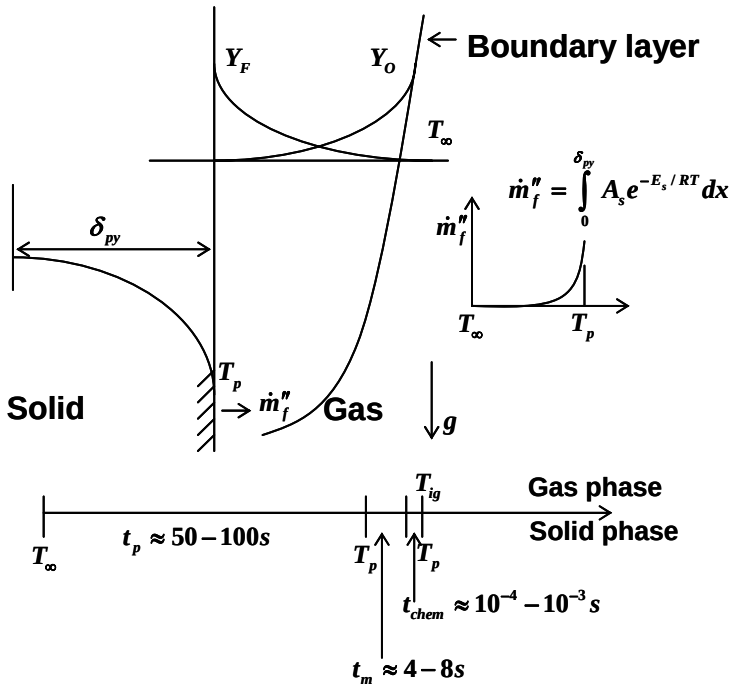

Figure 6.1: Factors involved in ignition of a solid [2] (earth-gravity).

To assess the differences between flame spread in earth gravity and microgravity, a discussion of the factors controlling flame spread is necessary [3]. The similarity between the mechanisms controlling solid ignition and flame spread is advantageous in better understanding the problem at hand. Flame spread is considered as a succession of continuous piloted ignitions, where the flame acts as both a source of solid heating, and as a pilot. The flame speed is considered quasi-steady, and is estimated as the movement of a heated length increasing in temperature from T to T_{ig} in time t_{ig}. If the flame heat flux is assumed to be uniform over the region $(x_f - x_p)$, the surface flame spread is written as:

$$v = \frac{(x_f - x_p)}{t_{ig}} \rightarrow \frac{\text{distance bathed by the flame heat-flux}}{\text{time it takes for the solid fuel to reach } T_{ig}} \qquad (6\text{-}1)$$

To analyze the controlling mechanisms, it is necessary to investigate the factors that influence the numerator and denominator of Equation (6-1).

6.2.1 Ignition time t_{ig}

The ignition time is comprised of three independent time periods that occur before a combustion reaction can take place. Two primary competing mechanisms control T_{ig} :

1. Heating and consequent gasification of the solid
2. Onset of gas-phase chemical reaction

A simple model based on ignition studies, [4 - 9], is presented. When a material initially at temperature, T_∞ is subject to a heat flux (mostly radiant heat flux from the combusting-plume region $(x_f - x_p)$), its surface temperature increases. The temperature distribution inside the material is shown in Figure 6.1. The surface temperature increases, but the surface does not release any flammable gases until a pyrolysis temperature T_p is attained. The time necessary to achieve T_p, is defined as the pyrolysis time t_p. The decomposition to produce gaseous fuel is idealized by an Arhenius-type reaction given by:

$$\dot{m}_f'' = \int_0^{\delta_{py}} A_s e^{-E_s / RT} dx \,, \tag{6-2}$$

where δ_{py} is the critical depth heated. The process is illustrated in Figure 6.1. Once the pyrolysis temperature is attained, the fuel-concentration increases, until reaching the lean flammability limit (Y_{FL}). The time necessary to reach this fuel concentration is called the mixing time t_m .

Once a flammable mixture is attained, and there is a pilot to ignite this mixture, a chemical reaction can take place that causes the "thermal-runaway" or the flaming condition. The time it takes for the chemical reaction to occur is called the chemical time, t_{chem} . This three-step process allows the expression of the time for ignition as:

$$t_{ig} = t_p + t_m + t_{chem} . \tag{6-3}$$

Quintiere [2] conducted an approximate order-of-magnitude analysis to give an estimate of these time periods. As shown in Figure 6.1 (lower portion), t_p is the most significant time under normal (earth-gravity, natural/forced convection) conditions. In fact, in most cases, t_m and t_{chem} are ignored ($t_m + t_{chem} \rightarrow 0$) [10]. This makes the flame spread process controlled by transfer of heat from the flame to the fuel. Ignition time decreases as U_∞ (or U_b for buoyant flow), Y_O, or T increases; decreasing ignition time results in higher v_f .

With no strong buoyancy-generated convective flow, the mixing time t_m is comparable in magnitude to t_p. Experimental results [11, 12], have shown that the flame structure at the leading edge controls the flame spread rate in microgravity. In addition the heat flux from the flame to the fuel surface is lower than the free convection case observed on earth gravity. This increases the dominance of surface and gas radiation losses in microgravity. A material flammability test that is conducted on earth gravity should therefore be able to predict surface and gas radiation losses accurately. The B-number calculated experimentally using the standoff distance incorporates these losses, and can therefore be used to predict flame propagation in microgravity as well.

Heat and mass transfer mechanisms differ in normal and microgravity. Natural convection induces a flow of about 0.5 m/s. However, such a strong convective flow is not possible in microgravity. Microgravity flows are of the order of 0.05 m/s, which are typical scales one would get in diffusive transport. The convective heat transfer coefficient is reduced from approximately 20 kW/m^{2}K to 2 kW/m^{2}K, leading to a significant reduction in t_p. At the same time, the mixing time t_m increases because of the reduction in convective transport resulting in a longer time for the pyrolyzate to mix with oxygen and form a flammable gas mixture. Thus, under microgravity $t_m + t_{chem}$ is not zero and ignition and flame spread is controlled by mixing and gas-phase chemical-kinetics as well.

The influence of t_m and t_{chem} on flame propagation is incorporated in a nondimensional number called the Damkohler number (*Da* number). The theory discussed in Chapter 2, and applied in Chapter 4 and 5, applies only for an infinite *Da* number, in which rate of heat release in the gas-phase is large, so that processes of heat and mass transfer control the spread rate. However, experiments [13] show that finite-rate gas-phase chemistry often exerts a large effect on spread-rates and thereby necessitates development of more complicated analyses. Correlations of spread rate data are obtained on the basis of *Da*-numbers [14], [15], [16], [17], [18]. The next section, discusses the use of the *Da*-number to identify the *quenching* and *blow-off* extinction limits.

6.2.2 Using the Damkohler number to quantify extinction

Gas phase extinction is generally described by means of the *Da*-number. Following the methodology of Yang and T'ien [19], and Chen and T'ien [20], a characteristic residence time for a flame established inside a boundary layer is defined as:

$$\tau_r = \frac{\alpha}{u_\infty{}^2}, \tag{6-4}$$

and a characteristic chemical time,

$$\tau_{ch} = \frac{1}{\rho A T \ \exp(-E / R^o T)}, \tag{6-5}$$

which leads to the following definition for the Da-number:

$$Da = \frac{\tau_r}{\tau_{ch}} = \frac{\rho A T \ \exp(-E / R^o T)}{(u_\infty{}^2 / \alpha)}. \tag{6-6}$$

All the symbols are defined in the nomenclature and the numerical values are extracted from reference [15]. Other definitions of the *Da* number that incorporate surface pyrolysis by means of an Arrhenius expression are found in the literature [16]. τ_r, is the fluid mechanical residence time, which refers to the length of time the fuel vapors remain in the reaction zone dependant on the fluid dynamics of the flame. A diffusion flame is extinguished by the mechanism of blow-off, familiar with the small flames of matches and candles. The mechanism involves the distortion of the reaction zone within the flame such as to reduce its thickness, so that the fuel-vapors have a much shorter period of time in which to react. If the reaction-zone is too thin, the combustion is incomplete and the flame is cooled ultimately to a level where it can no longer be sustained. Blow-off can occur, if sufficient airflow is achieved to reduce τ_r and consequently T_f, thus reducing the *Da*-number below a critical value. τ_{ch} is the chemical reaction time, i.e. the time taken for the chemical reaction of combustion to occur. τ_{ch} can be determined if the reaction rate constants, *A* and *E* (Equation (6-5)), are known. Knowledge of τ_{ch} is important in suppression studies in microgravity.One-step chemical-

kinetic rate constants cannot be determined using the current Test 1 apparatus used by NASA. An inverted cone calorimeter-type apparatus proposed by Olson *et al*. [21] is a useful addition to the current NASA tests to estimate a one-step chemical kinetic mechanism of solid fuels.

Torero *et al.* [13] obtain the *Da*-number as a function of the stream-wise direction for microgravity spread on PMMA for different oxygen concentrations and flow-velocities as shown in Figure 6.2.

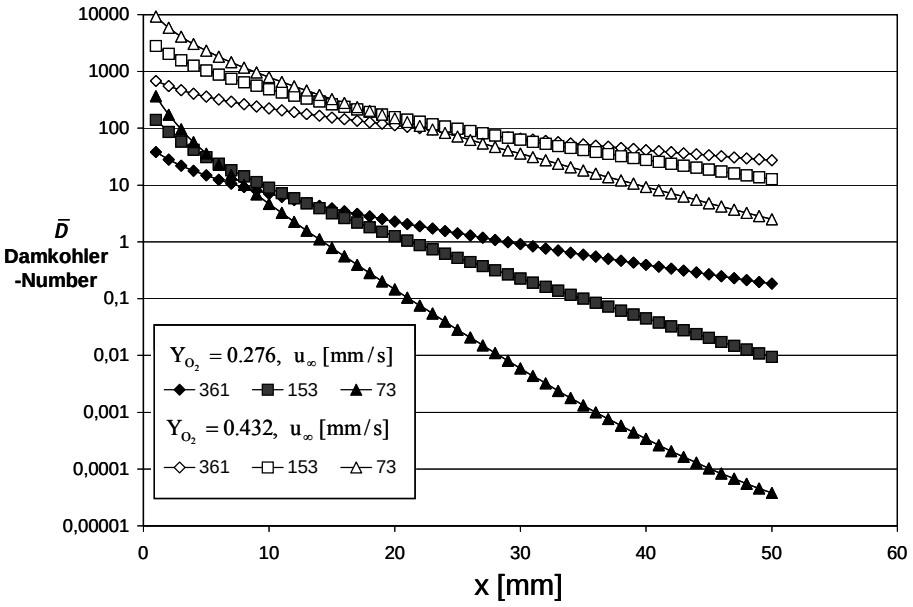

Figure 6.2: Da-number plotted as a function of the streamwise direction. Oxygen concentration and forced flow velocity are varied. At the point of flame attachment (leading edge) the Da-number decreases with an increase in flow velocity. This trend reverses at the trailing edge where the Da-number decreases with an increase in flow velocity. (Figure taken from Torero et al. [22], microgravity data (PMMA)).

Figure 6.2 shows that an increase in oxygen concentration will result in a systematic increase of the *Da*-number. Close to the leading edge, where heat losses to the surface are negligible, and B_T approaches B_A, the *Da*-number is controlled by U_∞ and therefore decreases as the forced-flow velocity increases. This region is susceptible to

blow-off , where the flame becomes unstable at the leading edge. Away from the leading edge, the *Da*-number is controlled by the flame temperature, and thus by B_T. In this region a decrease in U_∞ results in a decrease in B_T, leading to lower flame temperatures and a smaller *Da*-number. This region is susceptible to quenching, where extinction will follow a decrease in U_∞.

A laminar diffusion flame is stable when the flow conditions (velocity and oxygen concentration) are between two limits:

1. The blow-off limit (Figure 6.3)
2. The quenching limit (Figure 6.4)

Figure 6.3: Quenching extinction in low gravity [23]. Flame is attached to a 1.9 cm diameter, 2.54 cm long cylinder. A forced flow velocity ($U_\infty = 5\ cm/s$) is imposed from below. Pressure $P = 1$ atm.

The blow-off limit corresponds to the upper bound of the flow velocity beyond which the energy generated by the flame, becomes insufficient to heat the incoming oxidizer. The quenching limit corresponds to the lower bound for the flow velocity below which heat generation decreases due to the reduction of convective transport and cannot overcome heat losses (radiation from the flame, re-radiation from the fuel, etc.). The two limits are studied by Goldmeer *et al.* [23], where combustion and extinction behavior of a diffusion

flame over PMMA were examined experimentally and numerically during de-pressurization in low gravity.

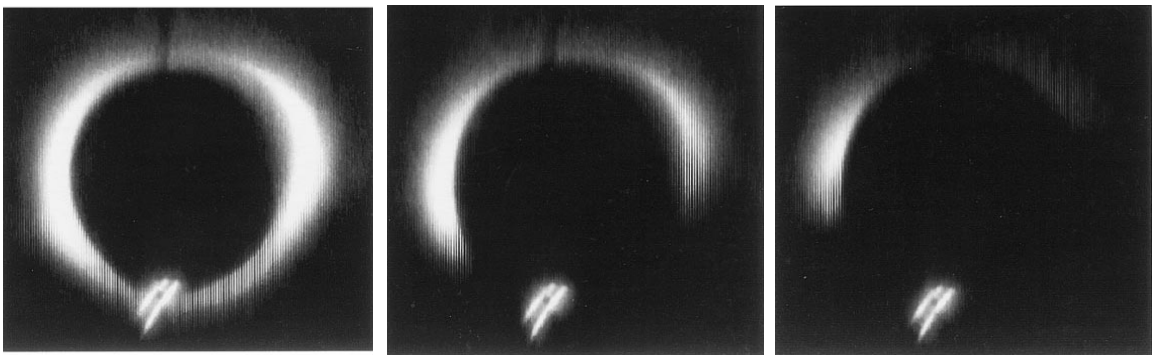

Figure 6.4: Blow-off extinction in low gravity [23]. $U_\infty = 10\ cm/s$**,** $P = 0.242$ atm**.**

An earth-gravity test that addresses material flammability in space should be able to predict these limits for any given material. The standoff distance is important in understanding the quenching mode of flame extinction which is most important in the low velocity conditions expected in microgravity environments. An experimental methodology that could be used to accurately determine the critical B-number associated with the quenching regime is developed in the next section.

6.3 Modifications Proposed for NASA's Test 1 Setup

It has been shown that the standoff distance measurement can be used to calculate the B-number. The B-number thus obtained gives a realistic thermodynamic efficiency of the burning process, since it incorporates the loss term *Q*. To create a flammability ranking scheme for materials to be used in microgravity, it is necessary to obtain a critical B-number, which is the lowest possible B-number that can sustain flame spread. To the knowledge of the author, the work of Roberts and Quince [24] represents the single study that defines a minimum fuel supply stability limit for diffusion flames

established over a condensed fuel. Roberts and Quince [24] use Spalding's droplet burning theory [25] to obtain a theoretical expression for a critical flame temperature based on the "Fire-Point" of a liquid fuel. The Fire-Point is defined as the lowest temperature at which a liquid in an open container will give off enough vapors to continue to burn once ignited. The theory is extended to include solid fuels by Quintiere and Rangwala [26], where the critical burning rate for PMMA is calculated using a critical flame temperature of 1600 K.

Extinction due to quenching has gained increasing attention as the number of combustion studies in microgravity has grown. Relevant to this work is the study of Olson *et al.* [30], who defined quenching limits for opposed flame spread over paper. A quenching branch was defined in an oxidizer mass fraction vs. forced flow velocity plot showing that for velocities lower than 100 mm/s, flames required an increasing oxygen mole fraction to be sustained as the free-stream velocity was reduced. Experiments conducted in short term microgravity facilities and the Space Shuttle have further studied the stability of a diffusion flame over a thin fuel and are reviewed by Joulian [27] and Law and Faeth [28]. Experiments and computations have attempted to demonstrate that radiative heat losses from the flame and surface are responsible for the higher limiting oxygen concentrations.

In an experimental setup similar to NASA's Test 1, criticality is approached when the flame length equals the pyrolysis length. A proposed experimental setup is shown in Figure 6.5, where a solid fuel sample is mounted vertically and ignited at the base, and the resulting upward propagating flame is recorded using a side-view camera. The oxygen concentration Y_{O_2}, is controlled to make $x_f = x_p$, at which point, the flame can

no longer propagate and excess pyrolyzate, or $\dot{M}_e'(x) = 0$. Figure 6.5 shows an upward-spreading flame with $x_f = x_p$. The critical value of oxygen concentration depends on external heat flux [26] and width of the fuel [29].

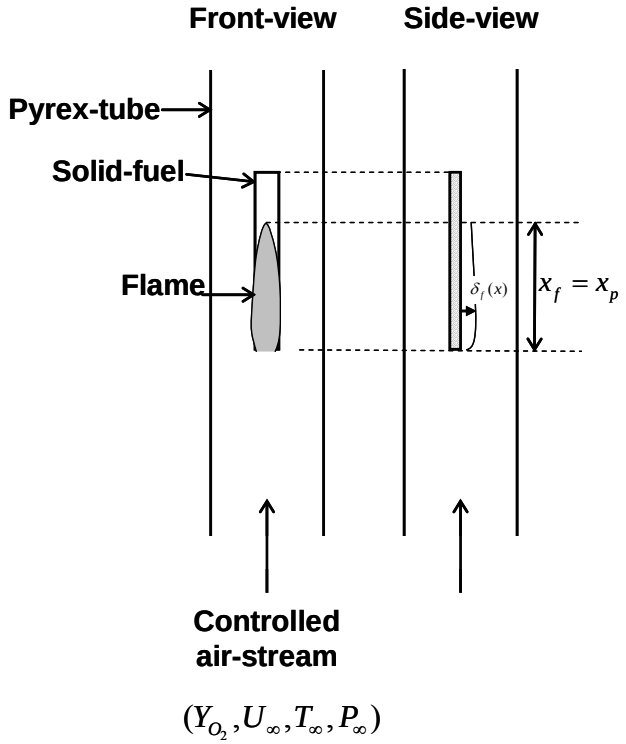

Figure 6.5: The critical condition: excess pyrolyzate = 0. Modifying the current NASA Test 1 set up to include measurement of a critical B-number. A critical B-number is obtained by reducing oxygen concentration in the chamber until $x_f = x_p$. The standoff distance measured at the trailing edge under this condition will give a critical B–number or the minimum possible B-number necessary for flame propagation.

The B-number profile ($B(x)$), would be evaluated using the standoff distance measurement at this critical condition. This could give a quantitative estimate of the critical B-number (B_{crit}) to be used in a risk model for microgravity. The effect of pressure and external heat flux, on B_{crit} are important future aspects of this study.

An estimate of the critical B-number is derived by setting Equation (5-11) equal to zero, giving:

$$F_e = \frac{\left(\int_0^{y_f} (\rho u Y_F)_x dy\right) - \frac{x_p}{d/2}\dot{M}_z'}{\dot{M}_f'} = 0\,. \qquad (6\text{-}7)$$

Using values of the excess pyrolyzate $\left(\int_0^{y_f} (\rho u Y_F)_x dy\right)$, and the lateral diffusion flux ($\dot{M}_z'$) derived in Chapter 5 gives,

$$\left[-r + r\frac{f(\eta_{fl})}{f(0)} - \frac{(1+r)}{f(0)}\int_0^{\eta_{fl}} f' J d\eta\right] - \frac{2x_p}{d}\left[\frac{D}{\delta_D}\frac{Y_{F,w}\rho_w x^{1/4}}{C}\int_0^{\eta_f} Y_F(\eta) d\eta\right] = 0\,. \qquad (6\text{-}8)$$

The value of the B-number, satisfying Equation (6-8) is the critical B-number (B_c). The second term on the left-hand side arises due to finite width effects. For an infinitely wide sample this term is neglected. In this case, the critical B-number depends only on the fuel stoichiometry (through r), and the ambient oxygen concentration $Y_{o_{2,\infty}}$. For PMMA, $B_c = 0.12$, neglecting width effects. Similarly, the maximum B-number (for a given oxygen concentration) is obtained when the B-number vs. time curve reaches an asymptotic value as discussed in Chapter 4. This can be easily obtained using the proposed small modification to the current NASA test set up.

Using the above methodology, a critical B-number (B_C) and a maximum B-number for laminar flame propagation (B_R) is obtained. This could provide an effective ranking scheme for testing material flammability in space, where B_c gives a best case-scenario (ignition, but no spread) and B_R giving a worst-case scenario (maximum flame-propagation rate).

6.3 Using B_R and B_C Values to Predict Flame Propagation in Microgravity

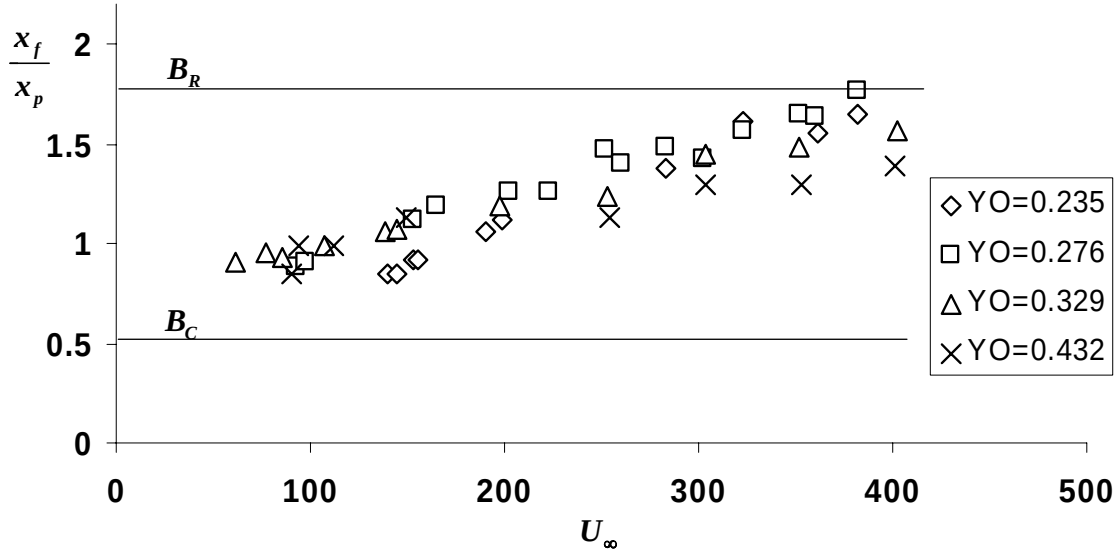

Figure 6.6: Use of B_R and B_C to model flame spread in microgravity

The variation of the flame length normalized by the pyrolysis length as a function of U_∞ for four different values of Y_{O_2} is presented in Figure 6.6. This data is obtained by Torero *et al.* [22] during parabolic flights to benefit from the extended microgravity. Figure 6.6 shows a linear increase of the flame length with U_∞. Below 150 mm/s the ratio x_f / x_p becomes smaller than one. In this region an increase in oxygen concentration results in an increase in the flame length. For U_∞>150 mm/s the flame becomes longer than the pyrolysis length ($x_f / x_p > 1$) implying the presence of excess pyrolyzate. For U_∞>150 mm/s an increase in the oxygen concentration results in a decrease in the flame length. The theoretical predictions for the flame length using B_R and B_c values for PMMA are also shown in Figure 6.6. It is observed that the

microgravity data falls in between the two lines representing ratios of x_f / x_p for $B = B_R$ (upper solid line) and $B = B_C$ (lower solid line).

According to the current theory, x_f / x_p is independent of the free-stream velocity U_∞. This is because the present analysis assumes infinite chemistry and the flame length is defined as the place where total consumption of the excess pyrolyzate occurs. Theory can therefore not predict gas-phase extinction at the trailing edge. The experimental results show that a critical condition is attained at $U_\infty >$ 150 mm/s beyond which the excess pyrolyzate can not burn and $x_f / x_p \approx 1$. The theoretically-determined B_c is below this critical limit. For $U_\infty <$ 150 mm/s an increase in the free-stream oxygen concentration will enhance the gas-phase chemistry and therefore the flame length will increase, for $u_\infty >$150 mm/s the flame length will try to follow the tendencies established by the boundary condition at the edge of the sample, but again, extinction will occur once the flame attains the gas-phase critical condition. This explains the lack of dependency of the on x_f / x_p on x_p, since for fixed flow conditions, x_p will have a weak effect on the critical condition, therefore, the gas-phase will dominate over the excess-pyrolyzate. A detailed study of the trailing edge extinction is required to exactly understand the quenching regime.

6.4 Summary

1. Knowledge of the heated length $(x_f - x_p)$ and ignition time t_{ig} is required to predict flame spread velocity.
2. The profile of the leading edge B-numbr obtained from earth gravity measurements can predict$(x_f - x_p)$. It is important to note that $(x_f - x_p)$ is a function of the width of the fuel as well. Hence it is important to factor in the width of the fuel when extrapolating results to microgravity conditions using earth gravity experiments. The theory developed in Section 5 is useful in achieving this goal.
3. In addition to the leading edge B-number, it is also necessary to know the Damkohler number at the leading edge, since it controls flame extinction.

6.5 References

1. R. Friedman, "Fire safety in the low gravity spacecraft environment," *Second International Microgravity Combustion Workshop*, NASA Lewis Research Center (1993).

2. J. G. Quintiere, *Fundamentals of Fire Phenomena (in press)*, John Wiley and Sons (2006).

3. J. G. Quintiere, "A Theoretical Basis for Flammability Properties," *Fire and Materials*, vol. 30, p. 175-214 (2005).

4. J. G. Quintiere, "A Simplified Theory for Generalizing Results from a Radiant Panel Rate of Flame Spread Apparatus," *Fire and Materials*, vol.5, p. 52-60 (1981).

5. J. G. Quintiere, and M. F. Harkleroad, "New Concepts for Measuring Flame Spread Properties," *National Bureau of Standards*, vol.NBSIR-84-2493 (1984).

6. T. Kashiwagi, "A Study of Flame Spread over a Porous Material under External Radiation Fluxes," *Proc. Combust. Instit.*, vol.15, p. 255-265 (1976).

7. I. S. Wichman, "Theory of Opposed Flame Spread," *Prog. Energy Combust. Sci.*, vol.18, p. 646-651 (1992).

8. M. L. Janssens, "Thermal Model for Piloted Ignition of Wood Including Variable Thermophysical Properties," *Proc. Fire Safety Science*, vol.3, p. 167-176 (1991).

9. A. Atreya, C. Carpenter, and M. Harkleroad, "The Effect of Sample Orientation on Piloted Ignition and Flame Spread," *Proc. Fire Safety Science*, vol.1, p. 97-109 (1985).

10. K. M. Tu and J. G. Quintiere, "Wall Flame Heights with External Radiation," *Fire Technology*, vol. 23, p. 195 (1991).

11. D. B. Bullard, L. Tang, R. A. Altenkirch, and S. Bhattacharjee, "Unsteady Flame Spread over Solid Fuels in Microgravity," *Advances in Space Research*, vol.13, p. 171-184 (1993).

12. M. Vedha-Nayagam and R. A. Altenkirch, "Gravitational Effects on Flames Spreading over Thick Solid Surfaces," *Acta Astronautica*, vol.12, p. 565-572 (1985).

13. J. L. Torero, "Material properties that control ignition and spread of a fire in microgravity environments," *34th National Heat Transfer Conference, Pittsburg, Pennsylvania*, vol. (2000).

14. A. C. Fernandez-Pello, *The Solid Phase*, in *Combustion Fundamentals of Fire*, G. Cox, Editor, Academic Press, New York, p. 32 -100 (1995).

15. I. S. Wichman and F. A. Williams, *Combust. Sci. Tech.*, vol.33, p. 207 (1983).

16. A. C. Fernandez Pello S. R. Ray and I. Glassman, *Proc. Combust. Instit.*, vol.18, p. 579-589 (1982).

17. A. C. Fernandez-Pello and Hirano, "Controlling Mechanisms of Flame Spread," *Combust. Sci. Tech.*, vol.32, p. 1-31 (1983).

18. F. A. Williams, I. S. Wichman, and I. Glassman, "Theoretical Aspects of Flame Spread in an Opposed Flow over Flat Surfaces of Solid Fuels," *Proc. Combust. Instit.*, vol.19, p. 835-845 (1982).

19. K. T. Yang, "Laminar Free Convective Wake Above a Heated Vertical Plate," *ASME Trans. Series E. J. of App. Mech.*, vol.86, p. 131-138 (1964).

20. H. C. Chen and J. S. T'ien, "Diffusion Flame Stabilization at the Leading Edge of a Fuel Plate," *Combust. Sci. Tech.*, vol.50, p. 283-306 (1986).

21. H. D. Beeson, S. L. Olson, J. P. Haas, and J. S. Baas, "An Earth-Based Equivalent Low Stretch Apparatus for Material Flammability Assessment in Microgravity

and Extraterrestrial Environments," *Proc. Combust. Instit.*, vol.30, p. 2335-2343 (2005).

22. J. L. Torero, T. Vietoris, G. Legros, and P. Joulain, "Estimation of a Total Mass Transfer Number from Stand-off Distance of a Spreading Flame," *Combust. Sci. Tech.*, vol.174, p. 187-203 (2002).

23. J. S. Goldmeer, J. S. T'ien, and D. L. Urban, "Combustion and Extinction of PMMA Cylinders during Depressurization in Low gravity," *Fire Safety J.*, vol.32, p. 61-88 (1999).

24. A. F. Roberts and B. W. Quince, "A Limiting Condition for Burning of Flammable Liquids," *Combust. Flame*, vol. 20, p. 245-251 (1973).

25. D. B. Spalding, *Some Fundamentals of Combustion*, Butterworths, London (1955).

26. A. S. Rangwala J. G. Quintiere, "A Theory for Flame Extinction Based on Flame Temperature," *Fire and Materials*, vol.28, p. 387-402 (2004).

27. P. Joulain, "Diffusion Flame Combustion in Oxidizing Flow," *Microgravity Sci. Tech.*, vol. 4, p. 178-191 (1993).

28. C. K. Law and G. M. Faeth, "Opportunities and Challenges of Combustion in Microgravity," *Prog. Energy Combus. Sci.*, vol.20, p. 65-113 (1994).

29. A. S. Rangwala, S. G. Buckley, and J. L. Torero, "Upward Flame Spread on a Vertically-Oriented Fuel Surface: The Effect of Finite Width," *Proc. Combust. Instit.*, vol.30 (accepted) (2005).

30. S. L. Olson, P. V. Ferkul, and J. S. T'ien, "Near Limit Flame Spread over a Thin Solid Fuel in Microgravity," *Proc. Combust. Instit.*, vol. 22, p. 1213-1222 (1986).

Chapter 7

Summary and Future Work

7.1 Summary

The B-number provides a valuable link between flame propagation and material-related properties. An experimentally-measured standoff distance is used to calculate a B-number, with which a testing methodology to evaluate the flammability characteristics of a material is developed. An experimentally-obtained B-number, variable in time and space, can then be used to model flame propagation, and shows good agreement with current and previous experimental data obtained from literature. The B-number calculated using this approach could be used to develop a 3-dimensional numerical code that includes a solution of the Navier-Stokes equations and energy equation, with gas-phase combustion and solid-phase pyrolysis. This can give an accurate flame spread model for any geometric, and gravitational conditions. In short, this research aims to (a) develop a methodology to obtain a B-number from the standoff distance measurement of an upward spreading flame, (b) apply this methodology using an experimental apparatus similar to NASA's Test 1 to obtain B-numbers for a variety of fuels and (c) apply the theory and experimental data to predict flame propagation in microgravity.

As discussed in Chapter 1, a significant amount of research has been completed on flame spread over condensed fuels. However, most of the research in the last 20 years has focused on developing empirical correlations to model flame height and flame propagation, because the classical solution on flame spread overpredicts flame height. The current work shows that the reason for this discrepancy may lie in the incorrect estimation of the B-number. While classical theory assumes that the B-number is a

constant, it is shown in this work that the B-number is dependent on space and time. The B-number was previously evaluated using material properties ΔH_C, L, and T_p, which were measured for fuels of interest using a cone-calorimeter. This work uses the experimentally-measured standoff distance during flame spread to determine the B-number, thereby circumventing the need to measure the conduction, radiation and re-radiation losses that are difficult to estimate and may change based on the geometry of the sample and the flow configuration.

A theoretical relationship of the form $y_f = A(B)x^{1/4}$ exists between the B-number and the standoff distance. It is shown that if one can successfully measure the standoff distance of a flame from the surface of the fuel, a B-number can be determined using Equation (2-23) and Figure 2.3. Experiments conducted with PMMA show that this methodology can be applied to obtain a B-number which is in much better theoretical agreement than previous efforts. As explained in Chapter 4, the loss term Q is accounted for automatically in the B-number, when the B-number is obtained using a standoff distance.

The flame length is required to obtain co-current flame spread rates. The mathematical analysis proposed by Emmons [1], predicts burning rate and flow characteristics only from the origin $x = 0$ until the pyrolysis length (x_p). The flame length usually extends beyond x_p, because the fuel burned per unit area at the flame location is less than the gaseous fuel liberated per unit area at the surface. Thus, there is an excess fuel (excess pyrolyzate) that is available in the combusting plume region. This analysis uses the theory developed by Annamalai and Sibulkin [2] to obtain a flame

length relationship as shown in Equation (2-25). In addition, Annamalai and Sibulkin's theory is extended to include the width of the fuel as well. It is shown that in addition to the excess pyrolyzate, a fuel leakage flux issues from the sides, which contributes to a reduction of the flame height. This effect is negligible for wide samples (width > 20 cm), but cannot be neglected for smaller widths.

Discussion of the parameters determining the stability of diffusion flames is of great importance for spacecraft fire safety since it provides scientific criteria relevant to material flammability. By applying the modifications to NASA's test 1 suggested in this study, a critical B-number and a maximum B-number for laminar flame propagation can be established. A risk-based analysis for microgravity flame spread can then be conducted using numerical codes such as FDS.

7.2 Future work

Applicability of the current methodology to numerical solvers such as FDS

The classical solution developed by Emmons [1] relies on the assumption that the mass burning rate is proportional to the shear stress at the surface. The constant of proportionality is the B-number for a forced-flow flame spread. In other words,

$$\dot{m}''_f = C\frac{\tau_o}{U_\infty}, \text{ where } \tau_o = \mu\left(\frac{\partial u}{\partial y} + \frac{\partial v}{\partial y}\right)^{y=0}, \tag{7-1}$$

and $C = B$, for a two-dimensional geometry. The constant of proportionality C is dependent on material properties and the flow-field. C can be determined using a simplified boundary condition based on images of the stand-off distance of a flame. This simplified boundary condition could help derive a more complex pyrolysis kinetics expression that would help future modeling efforts. Computer codes such as Jasmine or

FDS cannot define the solid phase accurately. For example, currently FDS uses a one-dimensional heat conduction equation for the material temperature in the direction pointing into the solid, given by [3]:

$$\rho_s C_s \frac{\partial T_s}{\partial t} = \frac{\partial}{\partial x}\left(k_s \frac{\partial T_s}{\partial x} \right); \quad k_s \frac{\partial T_s}{\partial x}(0,t) = \dot{q}''_{s,c} + \dot{q}''_r - \dot{m}''_f \Delta H_C \tag{7-2}$$

To correctly estimate the burning rate $\dot{m}''_f$, the grid size needs to be about 1 cm. However, due to computational costs, typical grid sizes are typically 10 to 50 cm when modeling room fires in FDS. These grid sizes are too large to correctly estimate solid phase pyrolysis. For this reason, current numerical codes are efficient with the gas phase but cannot describe the interaction between the hot gases and the solid fuel. Detailed codes use Arhenius-type expressions to model the fuel degradation; however, this makes the code too cumbersome, thereby reducing its practical applications to real world dimensions.

The shear stress at the surface, τ_o is a gas phase quantity and can be determined accurately using FDS. Thus the burning rate $\dot{m}''_f$, can be determined without solving for the solid phase, which allows faster computation in numerical codes. As mentioned earlier, the constant of proportionality *C* can be obtained using the current test methodology. This represents a large advance compared to the current FDS solver, because it reduces the dependence on various material-related properties such as $k\rho C$, T_{ig}, and *FPI* (fire propagation index) to only one variable (the B-number). In addition, probability distribution functions can be used to understand the range of B-numbers (B_{crit}

to B_{max}). Given a fire scenario, this information could then be used to create a risk assessment model applicable to any geometry and environmental condition.

Issue of flow separation

As mentioned in Chapter 1, the boundary layer approximation breaks down and separation of the flow occurs at an injection velocity greater than 0.01 m/s. Flow separation can occur due to (a) chemical kinetics and / or (b) radiation feedback. The burning rate can be expressed by an Arhenius relationship given by: $\dot{m}''_f = A_s e^{-E_s/RT}$. The pre-exponential constant A_s is large, especially for energetic materials such as perchlorates and perchlorites (used in fertilizers). Understanding their burning behavior is an important issue in fire research and more work needs to be done in this area. Studies have shown that if a material is subjected to a large external heat flux, separation of flow can occur. Under these circumstances, the relationship $\dot{m}''_f = C\frac{\tau_o}{U_\infty}$, does not hold. Further experiments and research is required to better understand flammability characteristics of energetic materials and address the issue of flow separation caused due to an increased external heat flux.

7.3 References

1. H. Emmons, "The Film Combustion of Liquid Fuel," *Z. angew. Math. Mech*, vol. 36, p. 60 -7 (1956).

2. K. Annamalai and M. Sibulkin, "Flame Spread Over Combustible Surfaces for Laminar Flow Systems. Part 2: Flame Heights and Fire Spread Rates.," *Combust. Sci. Tech.*, vol. 19, p. 185-193 (1979).

3. K. Mc Grattan, *Fire Dynamics Simulator (Version 4) technical Reference Guide*, NIST, (2005).

Appendix 1

A1.1 Mathematica Command File

```
(*Properties for PMMA*)
B = .2;
jj = 1;
While[B < 2,
 step[a_] := If[a < fconstant, 0, 1];
 pres[b_] := SetPrecision[b, 3];
 (*Set Precision sets the precision of stdoff to 3 digits*)
 bb = -.186; (* initial guess of f(0), Kosdon et al. [1]*)
 Pr = 1;
 L = 1590; (*J/gm*) (* Annamalai and Sibulkin1 [2]*)
 r = .12;
 fconstant = ((B + 1)/B) * (r/(r + 1));
 Cp2 = 1.52;  (*J/g C, calculated at flame temp*)
 Cp1 = 1.0 ;  (*at normal Temp*)
 Tv = 660; (* K *)(*Annamalai and Sibulkin [2]*)
Ti = 300;  (* K *)
hw = Cp1 (Tv - Ti);
tau = hw / L;
 visc = 0.484; (*viscocity of air at 300 C , cm2/s*)
 g = 980; (*cm/s2*)
 Co = (L * g/(4 * Cp2 * 300 * (visc ^ 2)))^.25;

 (* Define a step-function beta*)
 beta[x] = step[y4[x]] (B + tau - B * y4[x]) +
    (1 - step[y4[x]]) * (B + tau) * y4[x]/fconstant - (1 - step[y4[x]]) * B * y4[x];
 finit = {{1.5}, {-.3}};
 youter = 5; (* outer value of η *)
deltv = .0001;

 (* Increment on the initial guesses used to generate the Jacobian*)
 zz = NDSolve[{y1'[x] == y2[x],
    y2'[x] == y3[x],
    y3'[x] == -3 y1[x] y3[x] + 2 y2[x]^2 - beta[x],
    y4'[x] == y5[x] ,
    y5'[x] == 3 * Pr * ( - y1[x] * y5[x]),
    y1[0] == bb, y2[0] == 0, y3[0] == finit[[1, 1]],
    y4[0] == 1, y5[0] == finit[[2, 1]]},
   {y1[x], y2[x], y3[x], y4[x], y5[x]}, {x, 0, youter}];
```

```
eps1 = -(zz /. x → youter)[[1, 2, 2]];
eps2 = -(zz /. x → youter)[[1, 4, 2]];
Print["Uerror=  ", eps1, "   f''[0]=  ", finit[[1, 1]],
  "  Terror= ", eps2, "  Tprime[0] =   ", finit[[2, 1]]];
While[Abs[eps1] + Abs[eps2] > .0001,

 (*Calculate the change due to changing the velocity gradient guess*)
 beta[x_] = step[y4[x]] (B + tau - B * y4[x]) +
    (1 - step[y4[x]]) * (B + tau) * y4[x] / fconstant - (1 - step[y4[x]]) * B * y4[x];
 zz = NDSolve[
   {y1'[x] == y2[x],
    y2'[x] == y3[x],
    y3'[x] == -3 y1[x] y3[x] + 2 y2[x]^2 - beta[x],
    y4'[x] == y5[x],
    y5'[x] == 3 Pr (- y1[x] y5[x]), y1[0] == (B / (3 Pr)) * y5[0],
    y2[0] == 0, y3[0] == finit[[1, 1]] + deltv,
    y4[0] == 1, y5[0] == finit[[2, 1]]},
   {y1[x], y2[x], y3[x], y4[x], y5[x]},
   {x, 0, youter}, MaxSteps → 2000];
 eps12 = -(zz /. x → youter)[[1, 2, 2]];
 eps22 = -(zz /. x → youter)[[1, 4, 2]];

 (*Calculate the change due to changing the temperature gradient guess*)
 zz = NDSolve[
   {y1'[x] == y2[x],
    y2'[x] == y3[x],
    y3'[x] == -3 y1[x] y3[x] + 2 y2[x]^2 - beta[x],
    y4'[x] == y5[x],
    y5'[x] == 3 Pr (- y1[x] y5[x]),
    y1[0] == (B / (3 Pr)) * y5[0], y2[0] == 0, y3[0] == finit[[1, 1]],
    y4[0] == 1, y5[0] == finit[[2, 1]] + deltv},
   {y1[x], y2[x], y3[x], y4[x], y5[x]},
   {x, 0, youter}, MaxSteps → 2000];
 eps13 = -(zz /. x → youter)[[1, 2, 2]];
 eps23 = -(zz /. x → youter)[[1, 4, 2]];

 (*Calculate the Jacobian*)
 alf = {{(eps12 - eps1) / deltv, (eps13 - eps1) / deltv},
        {(eps22 - eps2) / deltv, (eps23 - eps2) / deltv}};

 (*Calculate the new guesses*)
 deltvnew = -Inverse[alf] . {{eps1}, {eps2}};
 finitnew = finit + deltvnew;
```

```
(*Update everything and save the old numbers*)
 finitold = finit;
 eps1old = eps1;
 eps2old = eps2;
 finit = finitnew;

 (*Run the new numbers to see if the solution has converged*)
 zz = NDSolve[
    {y1'[x] == y2[x],
     y2'[x] == y3[x],
     y3'[x] == -3 y1[x] y3[x] + 2 y2[x]^2 - beta[x],
     y4'[x] == y5[x],
     y5'[x] == 3 Pr (- y1[x] y5[x]),
     y1[0] == (B / (3 Pr)) * y5[0], y2[0] == 0, y3[0] == finit[[1, 1]],
     y4[0] == 1, y5[0] == finit[[2, 1]]},
    {y1[x], y2[x], y3[x], y4[x], y5[x]},
    {x, 0, youter}, MaxSteps → 2000];
eps1 = -(zz /. x → youter)[[1, 2, 2]];
 eps2 = -(zz /. x → youter)[[1, 4, 2]];

Print["Uerror=  ", eps1, "   f''[0]=  ", finit[[1, 1]],
   "  Terror= ", eps2, "  Tprime[0] =   ", finit[[2, 1]]];]

(*Standoff distance*)
pp = Flatten[Table[Evaluate[{beta[x] /. zz, x}, {x, 1, 5, .01}]]];
n = 1;
tat = 1;
While[tat > 0,
 tat = pp[[n + 2]] - pp[[n]];
 n = n + 2;]
xf = pp[[n - 1]];
yc = pres[Integrate[((B + tau - B * y4[x] /. zz)), {x, 0, xf}] // N];
stdoff[jj] = pres[yc * L / (Cp1 (Tv - Ti)) / Co];
densityi = 1.29 * 0.001;
(*denisty of ambient air g/cm3*)
fo[jj] = (zz /. x → 0)[[1, 1, 2]];
beta2[x] = B / (B + 1) ((B + tau) / r + tau - 1) * y4[x];
beta1[x] = -B * y4[x];
Yf[x] = (beta2[x] - beta1[x] - B - tau) / ((B + tau) / r);
kk2 = Integrate[(Yf[x] * y2[x] /. zz), {x, 0, xf}] // N;
```

```
(*Excess-pyrolyzate*)
Mexcess[jj] = kk2[[1]] * 2^(3/2) * ( visc^2 * g * L / (Cp2 * Ti) )^(1/4) * densityi;
Mp[jj] = -4 * fo[jj] * densityi * ( L * g * visc^2 / (4 * Cp2 * Ti) )^(1/4);
Feold[jj] = Mexcess[jj] / Mp[jj];
n = -1/4;                          (* Free Convection *)
xflame1[jj] = (1 - Feold[jj])^(-1/(n+1));      (*OLD*)
jj = jj + 1;

Print["B= ", B, ", constant = ",
  stdoff[jj - 1], " fo= ", fo[jj - 1]];
B = B + 0.1;]
```

The numerical solution used, is based on the method discussed by M. J. McCready [3].

A1.2 References

1. F. J. Kosdon, F. A. Williams, and C. Buman, "Combustion of Vertical Cellulosic Cylinders in Air," *Proc. Combust. Instit.*, vol. 12, p. 252-264 (1969).

2. K. Annamalai and M. Sibulkin, "Flame Spread Over Combustible Surfaces for Laminar Flow Systems. Part 1: Excess Fuel and Heat Flux," *Combust. Sci. Tech.*, vol. 19, p. 167-183 (1979).

3. M. J. Mcready, "Solution of the Natural Convection Boundary-layer Flow near a Heated Flat Plate," http://www.nd.edu/~mjm/thermal_boundarylayer.nb, May, 2006.

Appendix 2

Experimental results and observations of some of the other fuels tested

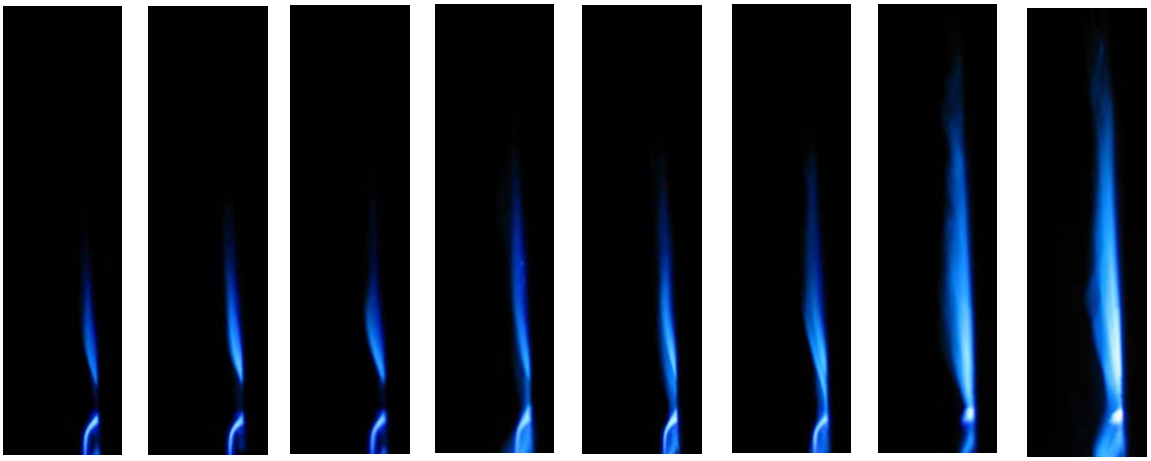

Figure A2.1 Photographs of vertical flame spread along polypropylene. The polypropylene sample is ignited at the base using a methanol wick, and flame pictures are recorded using a digital camera. The dripping of polypropylene is clearly noticeable from the figure.

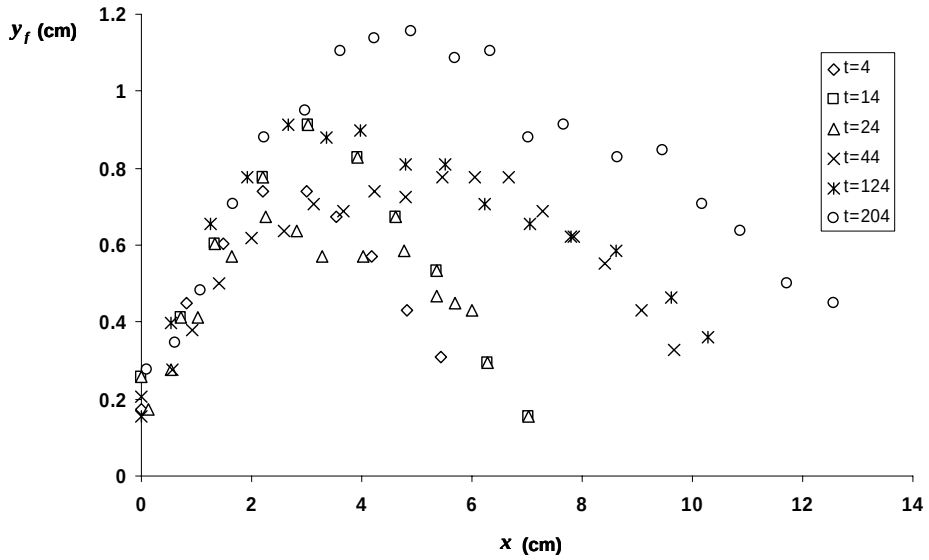

Figure A2.2: Standoff distance as a function of the streamwise direction for polypropylene.

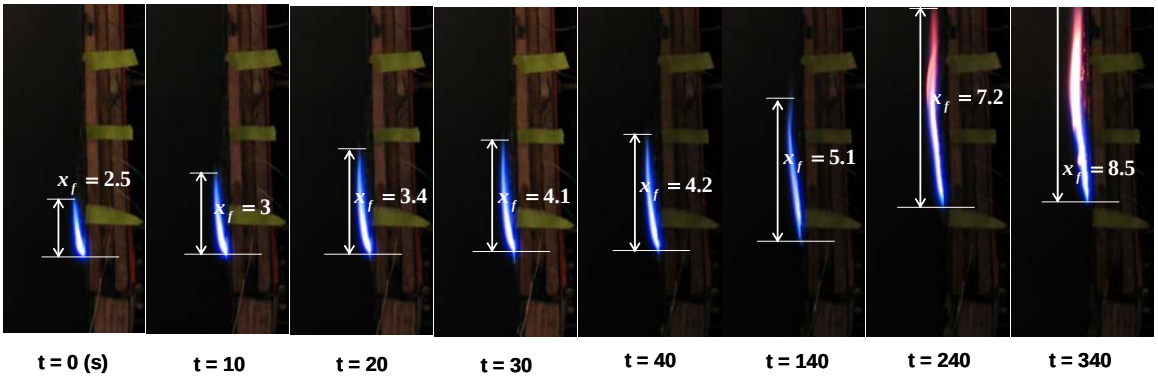

Figure A2.3: Photographs of vertical flame spread along rigid polyurethane foam. The foam sample is ignited at the base using a methanol wick, and flame pictures are recorded using a digital camera.

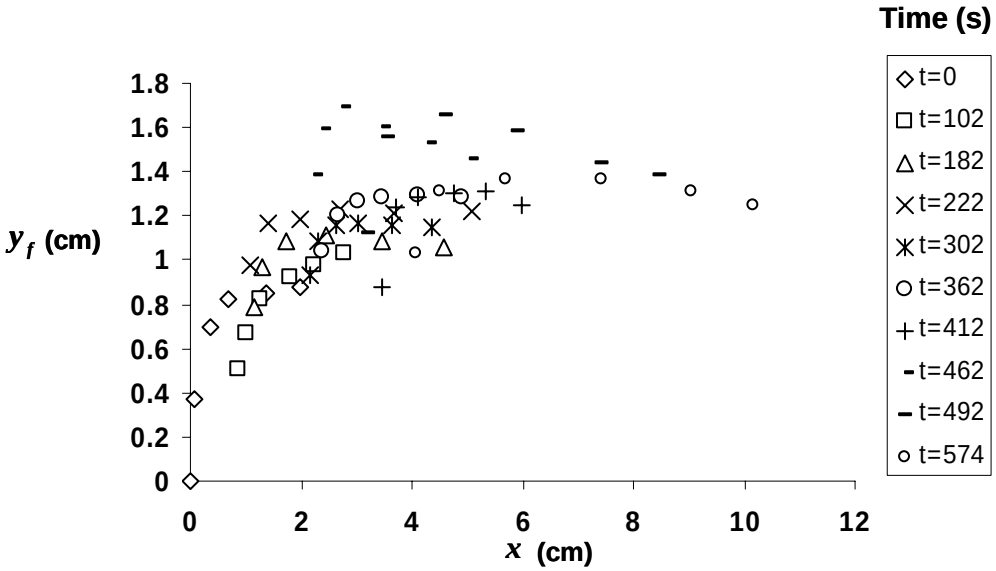

Figure A2.4: Standoff distance plotted as a function of the streamwise direction for rigid polyurethane foam.

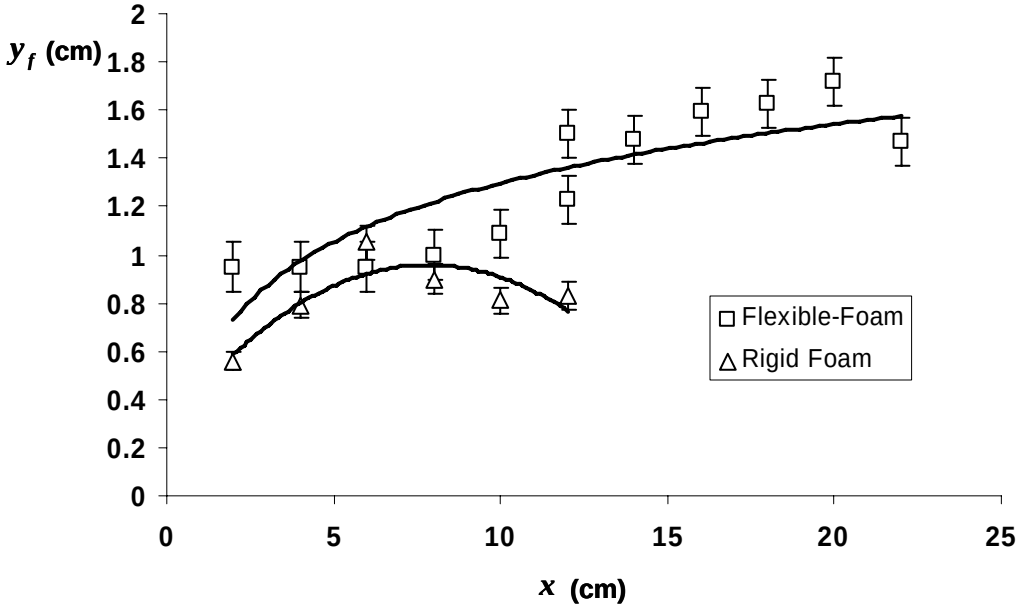

Figure A2.5: Difference in the measured standoff distance between rigid and flexible polyurethane foam. The two measurements are taken 30 s after ignition.

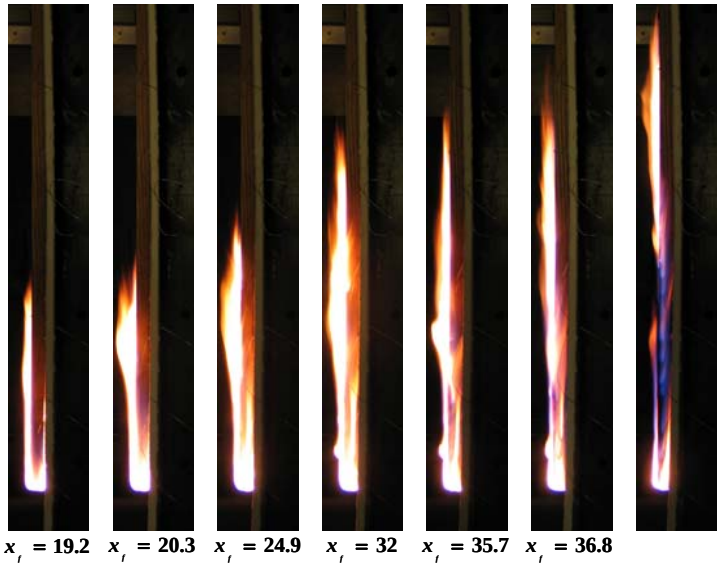

Figure A2.6: Photographs of vertical flame spread along Douglas fir wood. Flame heights are measured in cm. The wood samples are preheated in an oven at a constant temperature of 200 °C. Ignition is achieved using a gas burner. Charring of wood causes a reduction in the B-number as observed in Figure A2.6.

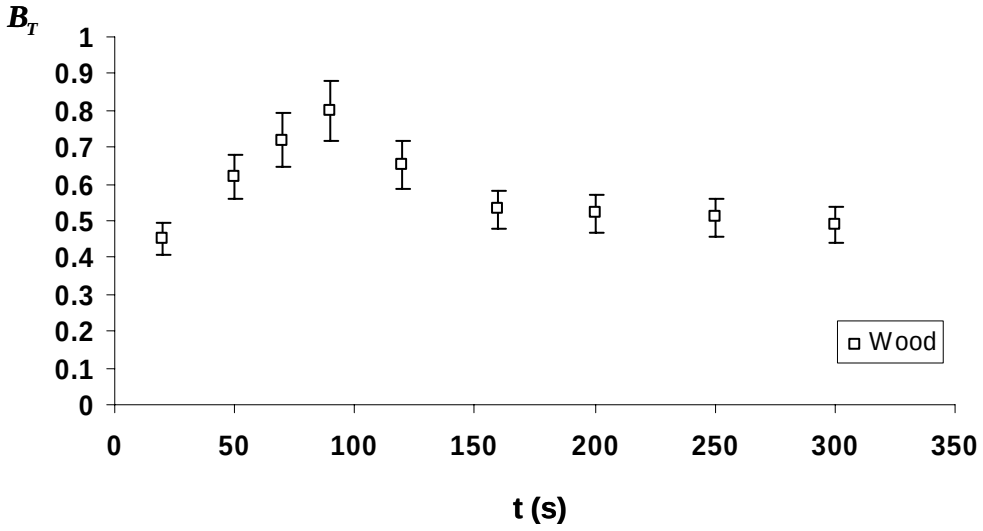

Figure A2.7: The average B-number (average between trailing and leading edge) plotted with respect to time for Douglas fir wood; the charring of wood acts as a retardant reducing the B-number with the progress of time.

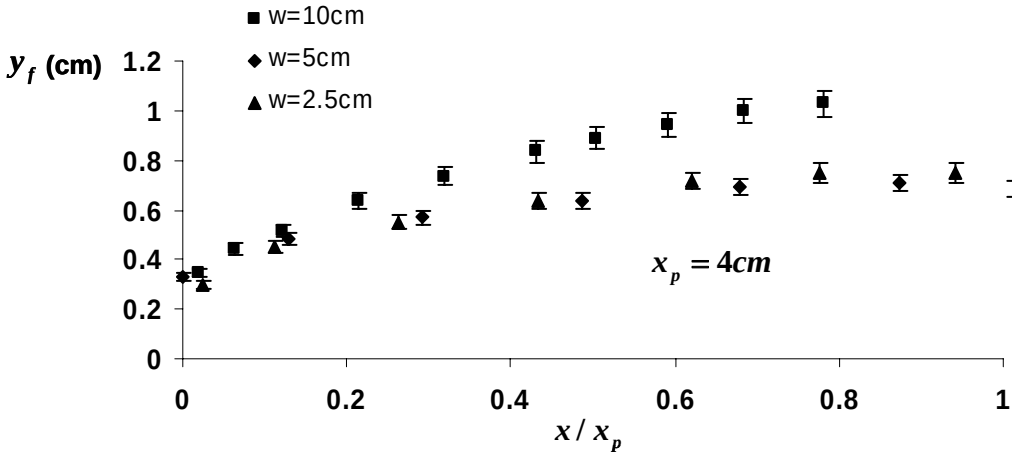

Figure A2.8: Flame standoff distance plotted as a function of the normalized x-axis for a methanol wick 8 cm long.

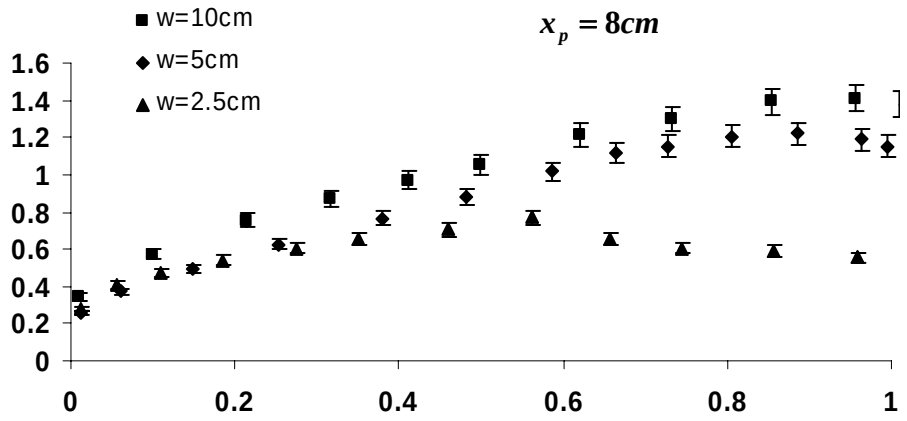

Figure A2.9: Flame standoff distance plotted as a function of the normalized x-axis for a methanol wick 4 cm long.

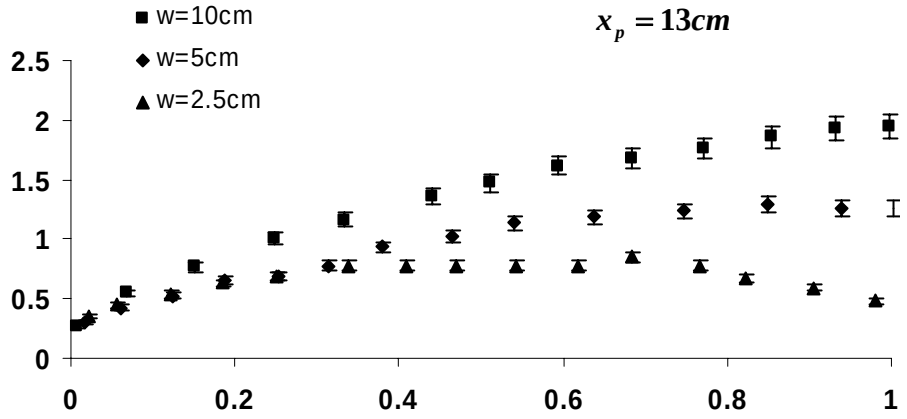

Figure A2.10: Flame standoff distance plotted as a function of the normalized x-axis for a methanol wick 13 cm long.